1971

Reactor frequency response based on pulsed neutron techniques

Donald Albert Moen
Iowa State University

Reactor frequency response based on pulsed neutron techniques

by

Donald Albert Moen

A Dissertation Submitted to the
Graduate Faculty in Partial Fulfillment of
The Requirements for the Degree of
DOCTOR OF PHILOSOPHY

Major Subject: Nuclear Engineering

Approved:

Signature was redacted for privacy.
In Charge of Major Work

Signature was redacted for privacy.
For the Major Department

Signature was redacted for privacy.
For the Graduate College

Iowa State University
Ames, Iowa

1971

TABLE OF CONTENTS

I. INTRODUCTION

To control a nuclear reactor properly, it is necessary to understand the reactor response to perturbations of its parameters. The study of reactor response has been an integral part of the developing reactor technology and is the topic of this thesis.

Reactor response is most often described by specifying the reactor transfer function. In general, the transfer function of some arbitrary device is defined to be the Laplace transformed output divided by the Laplace transformed input [34, 55]. When the device is a nuclear reactor, system output is usually taken to be neutron flux [54] and in this study will be specifically the prompt thermal flux. System input may be either a reactivity perturbation or a time dependent neutron source. Transfer functions obtained for the two cases are known respectively as the reactivity transfer function and the source transfer function.

The frequency response of a system is a concept closely related to the transfer function [37]. If the system transfer function is denoted by $G(s)$, then the frequency response is given by $G(j\omega)$. This relationship between $G(s)$ and $G(j\omega)$ is important because it means that if the frequency response can somehow be ascertained, the transfer function has, in effect, been determined.

An experiment to determine reactor frequency response might

be either a physical experiment performed on an actual reactor or an analytical "experiment" performed by introducing an appropriate driving function into a set of differential equations presumed to describe the reactor. This thesis describes an experiment of the first type performed on the Iowa State University UTR-10 reactor. Its primary purpose, however, is to draw comparisons with analytical experiments performed by Merritt [41], Betancourt [8], and Nodean [43]. For thoroughness, comparisons have also been drawn with solutions obtained using the WIGLE code [11].

II. REVIEW OF PREVIOUS WORK

When deducing frequency response analytically, it is first necessary to choose a theoretical model of the reactor. The simplest model in use is the "point kinetics" model [34] which, in some situations, may adequately represent a reactor. When the first transfer function measurements were made by Harrer et al. [24] in 1952 on CP-2, good agreement was obtained with the point kinetic equations at the low frequencies ($\leq$ 20 rad/sec) they investigated. However, as reactors have become larger and more complex (and as investigators have sought responses at higher frequencies), it has become necessary to include spatial effects when developing a reactor model [35, 56].

Several techniques for approximating the space-time dependent flux have been proposed; examples being given by Kaplan [31], Kaplan et al. [32], and Lewins [39]. Since the present study deals with the Iowa State University UTR-10, attention will at this point be focused on models relating specifically to this reactor.

A description of the UTR-10 may be found in Appendix A. For the present discussion, the most important feature of the UTR-10 is that it has two physically separate core tanks which are coupled in the sense that a fraction of the neutrons generated in one core must cause fissions in the other and vice-versa in order for criticality to be maintained. Any

model used to describe the URT-10 must include the coupled core feature if it is to achieve good accuracy.

Early work on coupled core models was done by Avery [3] and Baldwin [4]. Baldwin attempted to describe the Argonaut reactor by writing a separate diffusion equation in each core and including an interaction term with the source in each equation. Avery dealt with a system of N cores in which he wrote a point kinetics equation for each core and defined appropriate coupling parameters. Either of these models could be applied to the UTR-10. However, both are based on point reactor ideas and are thought to be less descriptive than later studies aimed directly at the UTR-10. They are mentioned here only for completeness.

In 1967, Carter and Danofsky [12, 13] modeled several tightly coupled, unreflected (other than the coupling medium), two core reactors which were all suggestive of a simplified UTR-10. Their model consisted of a modal analysis of the form $\phi(x,t) = \sum_{i=1}^{N} A_i(t)\psi_i(x)$. The space modes, $\psi_i(x)$, were Green's function modes obtained by solving the two group diffusion equations with sources fixed in various regions of the reactor and the time coefficients, $A_i(t)$, were obtained from a semi-direct variational principle. This basic modal technique can be attributed to Dougherty and Shen [17]. Carter and Danofsky extended the method to coupled core reactors and introduced coupling modes into the non-multiplying

region. Their primary objectives were to investigate use of the coupling modes and to study convergence of the solutions. However, they also obtained frequency response calculations which clearly demonstrated the space dependent nature of this function. The observed space dependence pointed out the inability of the point kinetics equations to describe a UTR-10 type reactor in detail and suggested that further work to deduce the space dependent frequency response of the actual UTR-10 would be useful. Analytical studies for this purpose were subsequently undertaken by Merritt [41], Betancourt [8], and Nodean [43].

Merritt based on his work on the Green's function modal analysis developed by Carter and Danofsky but modeled a reflected reactor. Using reactor parameters descriptive of the UTR-10, he introduced a sinusoidal perturbation into the absorption cross section and investigated the influence of different oscillator and detector locations on computed frequency response. His calculations yielded striking results in that at certain oscillator-detector combinations he found an anti-resonance or "sink" in the amplitude function at a frequency of about 2000 rad/sec. Although Merritt was able to suggest a plausible explanation for the sink, he was not able to prove its existence conclusively. It is conceivable that the sink could be the result of lack of convergence in the modal solutions or of inadequacies in the

basic two group model.

Resonance phenomena in nuclear systems are not without precedent [14, 25, 35, 47, 48]. Perez, Booth, Denning, and Harley [47], predicted similar sinks in a subcritical assembly and postulated essentially the same mechanism as Merritt. However, Perez and Uhrig [48] later expressed doubts about the reality of the sinks for reasons similar to those cited above. In the case of Merritt's sink, the question of its existence must remain open until it can be verified or disproved by independent means.

In parallel with Merritt's work, Betancourt developed a model of the URT-10 based on an application of the natural mode approximation (NMA) described by Foulke and Gyftopoulos [19]. Like Merritt, Betancourt introduced an oscillating absorber as the driving function. Also like Merritt, he predicted a sink in the amplitude of the space dependent frequency response. It should be noted, however, that the two methods are both modal approximations to solutions of the two-group equations and could conceivably suffer from similar deficiencies. Further, Betancourt's sink occurred at a frequency of approximately only 1000 rad/sec and was present only at a single oscillator-detector combination. Betancourt's results added credibility to the existence of the sink but still did not conclusively prove or disprove its reality.

Subsequent to the works of Merritt and Betancourt, Nodean cast the UTR-10 two group equations into a form which, for a localized perturbation, can be solved exactly by use of a Green's function technique. In situations where it applies, Nodean's method is considered to be an improvement over modal approximations because its accuracy is limited only by the extent to which the differential equations truly describe the physical reactor. Like Merritt and Betancourt, Nodean used an oscillating absorber as a driving function and computed space dependent frequency response. Unlike the previous investigators, he did not find sinks in the amplitude. He did, however, find an inflection point corresponding to Merritt's sink.

Actually, the presence of an inflection point is more compatible with Merritt's proposed "sink" mechanism than is the sink itself. Merritt found that a sink occurred with the oscillator in one core and the detector in the other. He suggested that the fast group perturbation from the oscillator core is thermalized in the detector core and at a frequency of about 2000 rad/sec (calculated from the perturbation transit time between cores) is 180 degrees out of phase with the slow group perturbation propagated to the detector core. This behavior would result in a partial cancellation effect and could account for a sink. But, for the sink to exist, the amplitude of the two perturbations would need to be very nearly the same. If there is a significant difference

between these amplitudes, the effect would be only an inflection point as predicted by Nodean.

Prior to the present investigation, Merritt, Betancourt, and Nodean had generated three different UTR-10 models which yielded three somewhat different sets of predictions. There was enough similarity to suggest strongly that a physically real phenomenon was responsible for the unusual behavior observed but its existence had not been conclusively proven. All three investigators recommended that an experiment be conducted to measure the URT-10 frequency response over the band in question. The goal of the present work was to design and perform the suggested experiment.

In addition to the frequency response sinks already discussed, a sink type of behavior has appeared in reactor noise formulations relating to the UTR-10. Hendrickson [25] experimentally observed a sink in the UTR-10 cross spectral density and Danofsky [14] has generated a mathematical model which predicts sinks under certain conditions in both the space-dependent auto-spectral-density function and the space-dependent cross-spectral-density function. While the sinks appearing in reactor noise studies bear a striking resemblance to those found in frequency response studies, there are also differences. A "unified" theory describing the extent to which these sinks are related would certainly

enhance understanding of the phenomenon. Such a study, however, is beyond the scope of the present work.

III. DESIGN OF THE EXPERIMENT

The theoretical models previously discussed all describe a critical UTR-10 driven by an oscillating absorber. Thus, the most obvious way of providing an experimental comparison would be to introduce a mechanical absorber oscillation into the critical UTR-10 and observe flux as a function of space and time. Mechanical oscillations can be implemented at low frequencies but become impractical at the frequencies of interest (up to 10^4 rad/sec). At high frequencies, a time-varying neutron source makes a more suitable driving function.

Given that a source-driving function is to be used, the experimenter must select the time dependence of the source. Perez and Uhrig [48] point out that the particular time dependence of the source is irrelevant as long as it can be Fourier analyzed. Conventionally, the choices are: 1) a neutron wave experiment wherein the source varies sinusoidally with time, and 2) a pulsed neutron experiment wherein the source approximates an impulse function, $\delta(t)$. Theoretically, the two techniques are substantially equivalent but both have experimental advantages and disadvantages depending on the type of experiment and the equipment available [48]. Sinusoidal variations concentrate the "power" of the disturbance into a single frequency but the impulse input is easier to apply to nuclear systems and introduces many frequencies simultaneously. For the present experiment,

the advantage of introducing many frequencies simultaneously plus the availability of a Kaman Nuclear model A-800 pulsed neutron generator dictated the use of a pulsed neutron experiment.

Since a source perturbation was used as the driving function, comparisons with the models must be made carefully because consideration must be given to possible differences between the source and reactivity transfer functions. Michael and Moore [42] show that in a pure moderator, an oscillating absorber experiment and a pulsed neutron experiment are theoretically equivalent. Since the two experiments are fundamentally the same, a phenomenon such as a sink which appears in one experiment can be anticipated in the other as well. But, the multiplying-medium, multiregion URT-10 is a far more complex system than a pure moderator and it would be dangerous to make quantitative comparisons between the two types of experiments without justification. For example, use of the point kinetics model leads to the conclusion that while the source and reactivity transfer functions should be similar at the frequencies of interest, the two functions may be different [50]. The important question, however, is whether or not the functions are different when based on the model actually being used. Conclusions relating to each of the models will be described later but first, it is convenient to consider a second difficulty.

With the pulsed neutron experiment, it was desirable to

operate the reactor in a subcritical configuration. Keeping the reactor subcritical avoided problems associated with power level increasing with time and also avoided excessive delayed neutron levels. Subcriticality did mean that the models had to be re-run with appropriate subcritical parameters before direct comparisons could be made.

In Section VII, it is shown that for Nodean's model [43] it is immaterial whether a source or an absorber perturbation is used. To compare experiment with this model, it was necessary only to re-run Nodean's computer code with parameters corresponding to the subcritical condition. But, to evaluate the meaning of the comparison, consideration must be given to the assumptions of the model. Nodean's model inherently contains the assumption that the perturbation is confined to a single plane in the reactor and in addition, the oscillator is in the thermal group. When the model was re-run, the source plane was located in the center of the south core. Therefore, the results generated can be viewed as assuming a plane thermal source in the center of the south core.

When the experiment was run, the pulsed neutron source was located in the south reflector 62 cm from the edge of the core tank (see Appendix A). Since the Kaman Nuclear source yields 14.3 Mev neutrons, it was qualitatively expected that the strongest thermal source would indeed be in the south

core where the water would have a strong moderating effect. The validity of the comparison, however, must be judged from the results obtained.

With Betancourt's model [8], it was possible to easily modify the method to describe response to a fast group source and furthermore, the source could have any desired spatial distribution. The technique did require the source to be a delta function in time. In the experiment, the 14.3 Mev source closely approximated a delta function in both time and space [29]. For Betancourt's model, however, the required source was not the 14.3 Mev source but rather the source corresponding to the 1.6 Mev fast group energy. It was thought reasonable to take the 1.6 Mev source as being a delta function in time [22, 42] but since the model allowed for a spatial distribution, the best comparison between experiment and theory should result if the 1.6 Mev source distribution is estimated as accurately as possible. The method of estimating the source distribution is shown in Appendix C and modifications to Betancourt's model are discussed in Section VI.

For Merritt's model [41] the relationship between source and reactivity transfer functions is not obvious and an investigation was considered to be beyond the scope of this study. Hence, no further work was attempted with this model and the only comparisons that may be drawn are of a

qualitative nature regarding the existence or non-existence of the sink.

Pulsed neutron experiments have been used extensively in conjunction with reactivity measurements [6] and Rotter [50] has reported utilizing a pulsed neutron source in conjunction with a modulated source to determine reactor transfer function. Using a pulsed neutron experiment alone to deduce a reactor transfer function is, however, a relatively new technique. The only known published work of this nature is that of Kaneko, Akino, Kyrokawa, and Sumita [30]. These investigators deduced frequency response for the Japanese SHE reactor (not a coupled core reactor) but published only magnitude curves and only to a frequency of about 10^3 rad/sec.

Note that the present study involves utilizing a relatively new experimental method to draw comparisons with theoretical models of questioned reliability. As a safeguard against major errors, it was desirable to make an additional comparison with a widely accepted model. Using the source distribution function described in Appendix C, it was possible to model the experiment with the finite difference scheme WIGLE [11]. The WIGLE code was used to generate time domain response curves which were then Fourier transformed numerically to yield frequency response. A modification of the numerical transform code FOURCO [5] was used to transform both WIGLE time response functions and the time

response functions obtained by experiment. The basic technique used to extract frequency response from a pulsed neutron experiment will next be described.

Reactor frequency response may be described by $G(j\omega) = \frac{\text{Output}(j\omega)}{\text{Input}\ (j\omega)}$. In the pulsed neutron experiment, the driving function may be considered to be an impulse, $\delta(t)$, so that Input $(j\omega) = 1$ and the frequency response becomes just the Fourier transform of the time response function. Theoretically, the frequency response for all frequencies from zero to infinity could be obtained by exciting the reactor with a single neutron burst, observing the flux as a function of time, and transforming the observed function. In practice, there are a number of difficulties which must be overcome.

Due to the stochastic nature of the neutron propagation and detection processes, the variance of the time function following a single burst would be far too large to provide adequate definition. The problem can be overcome by pulsing repetitively and letting detector output accumulate in a time analyzer until adequate statistics are obtained. This technique is common practice in pulsed neutron experiments [20, 21, 50, 51] and needs no further justification here.

The hypothesis that all frequencies from zero to infinity can be resolved, however, needs further examination. Frequency response at very high frequencies can in reality be determined

only if 1) the channel width of the time analyzer is made to approach zero, 2) the detector variance and dead time errors approach zero, and 3) the detector and instrumentation transfer functions are known for all frequencies. Obviously conditions 2 and 3 can not be met in practice. Condition 1 relates to the aliasing problem discussed by Blackman and Tukey [10]. In practice, the minimum usable channel width will be determined by equipment limitations and in this experiment was 50 microseconds. For a fixed channel width, Δt, the maximum frequency that could possibly be resolved is the Nyquist frequency given by $f_N = \frac{1}{2\Delta t}$ [10]. However, frequencies out to the Nyquist frequency can be resolved only if no frequency components of significant amplitude exist above this level. In the present experiment, there was no way of knowing a priori what the maximum resolvable frequency would be. When a possibility of aliasing was suspected, time data were accumulated at two different channel widths and the transforms were checked for convergence. As discussed in Section V, convergence was taken to mean that significant aliasing was not present.

One of the more difficult problems encountered was that statistical scatter in the time domain data resulted in excessive scatter in the frequency domain function. Such scatter was especially serious since it could completely mask any fine structure of the function such as Nodean's inflection

point. The method of overcoming scatter will be discussed in detail in Section V. Briefly, the data were smoothed prior to transformation and the success of the smoothing algorithm was judged from its ability to correctly transform test functions wherein artificial scatter had been introduced into a smooth function.

In summary, a pulsed neutron experiment was used to excite the UTR-10 in a subcritical configuration, frequency response functions were extracted through appropriate observations and data processing, and the previously discussed comparisons were made. Details of the procedures plus the results and conclusions will be presented later in the thesis. It should, however, be mentioned here that some means had to be provided to normalize theory to experiment. Characteristic behavior of a reactor during a pulsed neutron experiment will be described in Section IV. For present purposes, it is sufficient to say that normalization was accomplished by adjusting $\nu\Sigma_f$ in the model until the fundamental mode decay constant (or, for Nodean's model, an equivalent parameter) matched that observed in the north core. The reason for choosing to normalize to the north core will be discussed in Section VI.

IV. EXPERIMENTAL EQUIPMENT AND PROCEDURES

The pulsed neutron source used for the experiment was a Kaman Nuclear model A-800 sealed tube source yielding approximately 10^7 14.3 Mev neutrons per burst at a pulse width of approximately 3 microseconds. According to the manufacturer [29], each pulse is approximately Gaussian in time but for present pruposes, the pulse was taken to be an impulse function, $\delta(t)$. The accelerator-target module of this unit is approximately 4 inches in diameter by 14 inches long and can be installed in either of two possible locations within the UTR-10. These locations are 1) in the central reflector midway between the two cores, and 2) in the thermal column on the south face of the reactor. To create conditions compatible with a possible appearance of the sink, it was desired to drive primarily only a single core. Thus, the unit was installed in the thermal column with the source plane located as close as possible (62 cm) to the core boundary.

To provide neutron detection, N. Wood G-3-20 (special order) 3/8 inch diameter by 20 inches long $^{10}BF_3$ detectors were installed approximately in the center of each core tank and also in the center of the central reflector. These locations correspond to those investigated by Merritt [40], Betancourt [8], and Nodean [42]. Although only a single

detector was utilized at any one time, all three detectors remained in place throughout all data runs so as not to change reactivity or flux distribution. After processing by amplification and pulse shaping circuitry, the detector output was fed to a RIDL[1] model 3412B 400 channel analyzer operated in the time base mode. A block diagram of the circuitry is shown in Figure 1. The pulse inverter and amplifier circuit between the fast discriminator and the RIDL analyzer was necessary to achieve electronic compatability between these components.

One of the drawbacks of the system outlined here is the relatively long resolving time which was estimated by the method of Appendix E to be 1 microsecond. Since the slowest component in the system was the RIDL analyzer, further refinement of the preceding components would be of little value from a resolving time point of view. Ohanian and Diaz [43] point out that even though the standard resolving time corrections are made, long resolving times lead to significant errors in the observed time function if count rates are high enough for the corrections to be appreciable. In the present experiment, count rates in the south core were as high as 10^5 cps which resulted in a resolving time correction of approximately 10 percent. However, the most interesting phenomena were expected to occur in the north core and here,

[1]Radiation Instrument Development Laboratory.

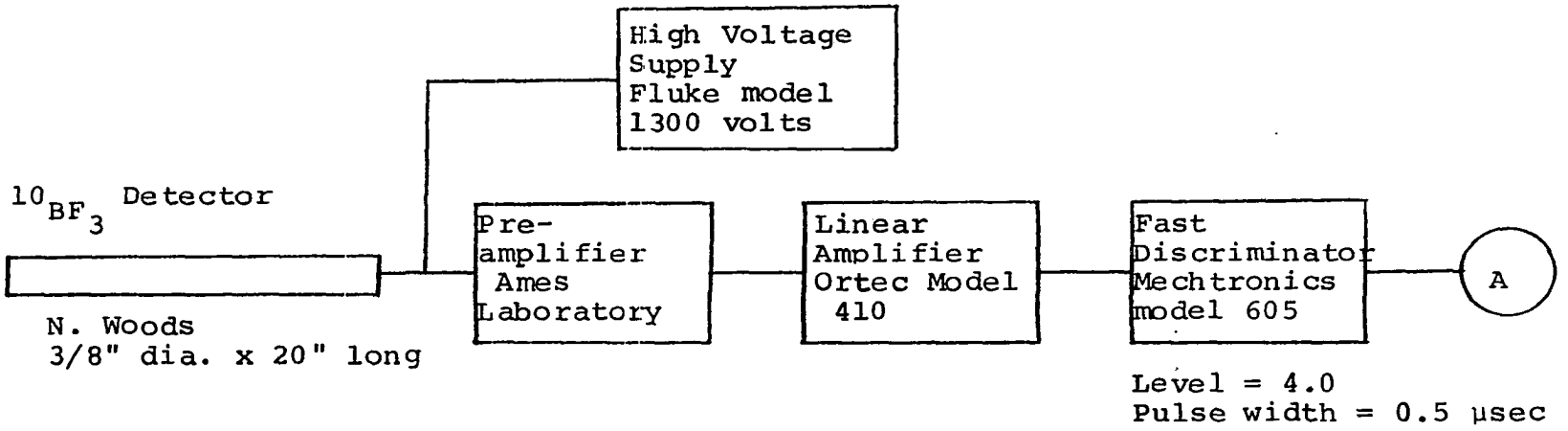

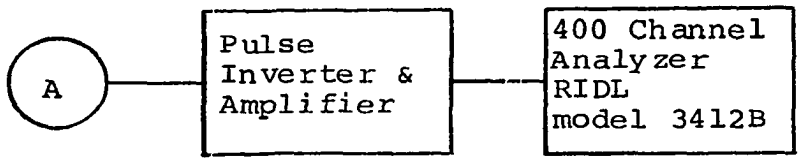

LINEAR AMPLIFIER SETTINGS:

Input Polarity = Neg.
Attenuation = 1
Coarse Gain = 3
Fine Gain = 1
Integration = Out
Differentiation = 0.1 μsec (both)
Pulse = Bipolar

Figure 1. Block diagram of counting system

count rates were sufficiently low (2×10^4 cps) that resolving time corrections were less than 2 percent. While the detection system described here is admittedly not the most sophisticated one possible, the components were all available and the system was adequate for the job to be done.

One unexpected difficulty was the high electronic noise level. When a detector was installed in one of the core tanks and the tanks were filled with water, the system began recording high count rates even with the detector high voltage turned off. The problem was traced to radio-frequency pickup from a local radio station and was overcome by operating at a sufficiently high discriminator level.

In addition to the electronics shown in Figure 1, it was necessary to provide a means of synchronizing the neutron generator with the time analyzer. However, it was expedient to consider pulsing rate requirements as well in the design of this equipment.

Figure 2 illustrates the thermal flux behavior following a neutron burst [38]. In the region labeled "higher harmonics", the time dependent prompt flux (at some fixed location) can be described by the series of exponentials $\phi(t) = A_1 e^{-\alpha_1 t} + A_2 e^{-\alpha_2 t} + \ldots A_n e^{-\alpha_n t}$ where $\alpha_1 < \alpha_2 < \alpha_3 \ldots$. In the region labeled "fundamental mode", all terms except the first have become negligible and the flux decays as $\phi(t) = A_1 e^{-\alpha t}$ where $\alpha = \alpha_1$. At large times, the fundamental prompt term also

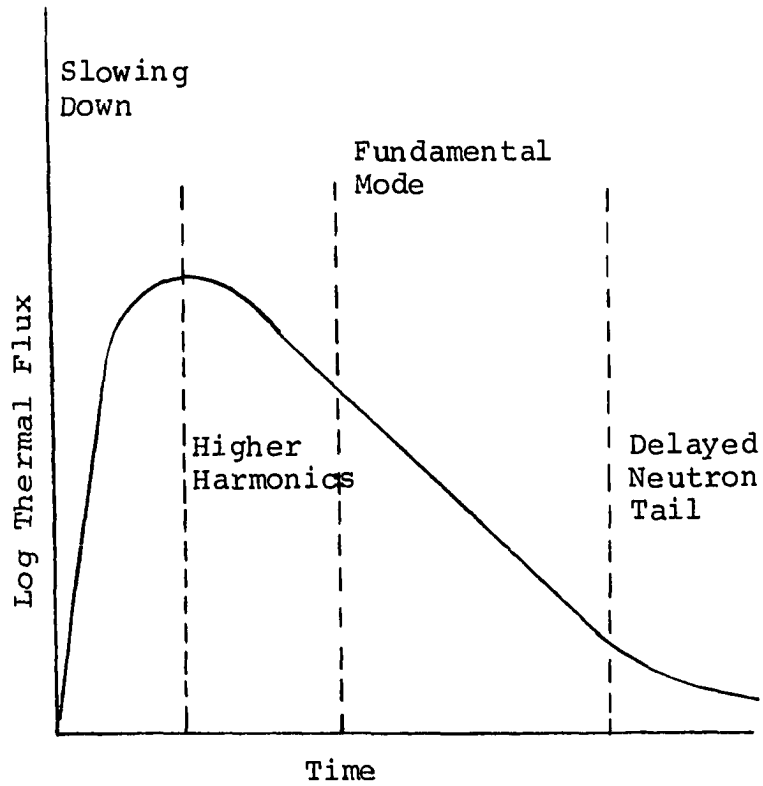

Figure 2. Reactor response to neutron burst

becomes negligible leaving only the delayed neutron tail. Delayed neutrons, however, make some contribution throughout the entire function. Since only the prompt response was desired, it was necessary to correct for delayed neutron influence.

Garelis and Russell [20, 21] have shown that if the pulsing rate, R, is sufficiently high, the delayed neutron contribution may be considered to be constant and simply subtracted from the total response. To allow correction by

this method, R should be much larger than the shortest precursor decay constant but much smaller than the fundamental mode decay constant. Garelis [20] suggests that the minimum pulse rate should be 10 pulses/sec. The Kaman Nuclear model A-800 is capable of a maximum pulsing rate of 10 pulses/sec. but only on a limited duty cycle. However, Garelis also shows that the effective pulse rate, R_{eff}, depends only on the sweep rate of the time channel analyzer (TCA). The effective pulse rate is given by $R_{eff} = R \times \frac{\text{Number of Sweeps}}{\text{Number of Bursts}}$ so that the experimenter can simulate a higher than actual pulse rate by making multiple analyzer sweeps per burst. Provided that sweeping continues after pulsing stops for a time long compared to the longest lived precursor mean life, there is no requirement that the pulses be of uniform strength.

In the present experiment, analyzer-generator synchronization was achieved by triggering the generator with a signal from the analyzer every tenth sweep. Most data were taken with a channel width of 100 microseconds (400 channels). Since the analyzer had a read-write time of 12.5 microseconds between channels, the effective pulsing rate became 22.2 pulses/sec. - a figure easily within range to justify assuming a constant delayed neutron background.

A block diagram of the synchronizing circuits is shown in Figure 3. The delay circuit was adjusted to provide a

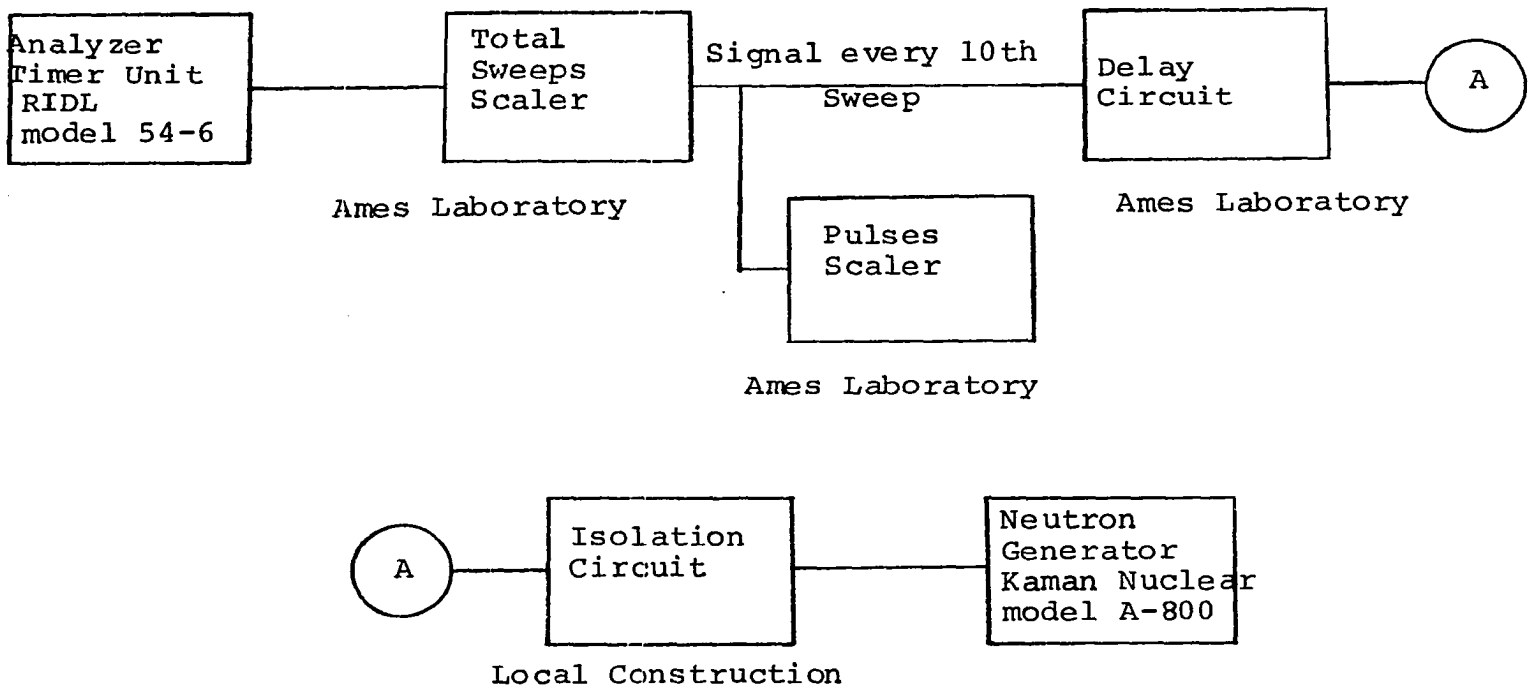

Figure 3. Block diagram of synchronization circuits

time delay of 4.5 microseconds which (to an accuracy of $\pm$ 1 microsecond) caused the beginning of the neutron burst to coincide with the opening of the analyzer data gate. During preliminary runs, the generator was found to produce an occasional spurious burst. The trouble was traced to an apparent loading of the scaling circuits by the generator. Installation of the isolation circuit shown in Figure 3 eliminated the problem.

After assembly and testing of the equipment, data runs were made with the reactor in two different subcritical configurations. The primary configuration was with all control and safety rods fully inserted (water at normal operating level) to make the reactor approximately \$3.00 subcritical. A set of data was also taken with safety rod one withdrawn to produce a subcriticality of approximately \$2.00. Inlet and outlet water temperatures were carefully monitored to insure constant reactivity throughout runs and also between runs.

Prior to a data run, water was pumped into the core, the start-up source removed, and the reactor background monitored until it stabilized. The reactor background referred to here is the detector response to radioactivity normally present in the core and is exclusive of the delayed neutron background discussed previously. When the reactor background had stabilized, the time analyzer and neutron generator were

started and allowed to run until the counts accumulated in memory were sufficient to provide adequate statistics. As a rule of thumb, a minimum of 10,000 counts in the peak channel will provide usable information but a peak of at least 20,000 counts is desirable. Depending upon the detector location in use, achieving desired levels required from 2000 to 10,000 pulses. After a sufficient number of pulses, the generator was stopped and the number of pulses recorded. The analyzer, however, was allowed to run at least an additional 5 minutes to justify [21] assuming a constant delayed neutron background. The total number of analyzer sweeps was also recorded. After a pulsed data run, a companion run was made under the same conditions as used for the pulsed run except that the neutron generator remained off. The total number of sweeps was again recorded so that data from this "background" run could be normalized to the total sweeps for the pulsed run and subtracted off. Again, the background referred to is the "reactor" background as opposed to the delayed neutron background.

In processing the data, it was assumed that the detector response to epithermal neutrons was negligible compared with the thermal neutron response. To check the validity of this assumption, a data run was made with a cadmium shield surrounding the detector. The epi-cadmium count rate was found to be down a factor of approximately 300 from the total count rate.

Further, when the epi-cadmium data were processed, the resulting transfer function was very similar to the thermal transfer function. Thus, the percentage error introduced by epithermal neutron response was thought to be acceptably small.

For both of the reactor configurations investigated, date were collected and processed for each detector location and appropriate comparisons made with theory. However, preliminary comparisons showed that other than the anticipated change in break frequency of the transfer function there was nothing fundamentally different between the two cases for either experiment or theory. The remainder of this thesis will be concerned primarily with the $3.00 subcritical (all rods in) configuration.

V. PROCESSING PULSED NEUTRON DATA

Once the data had been collected, the steps remaining to extract the frequency response were;

1) Correct for counting system dead time
2) Correct for reactor background
3) Correct for delayed neutron background
4) Fourier transform the resulting time function.

The first three tasks were easily carried out with a slightly modified version of the computer code GRIPE-II [33]. GRIPE-II is a computer program used for the determination of subcritical reactivity and the inverse reduced generation time, β/Λ, from experimental data taken in a pulsed reactor. In the present experiment, the degree of subcriticality and β/Λ were of only secondary interest but in the process of computing these parameters, GRIPE-II first performs operations 1), 2), and 3) listed above. Thus, at an appropriate place in GRIPE-II, a WRITE statement was inserted to punch the corrected data on cards for later Fourier transformation.

GRIPE-II assumes a constant system dead time which is read in as data and makes the dead time correction via the standard formula. Correcting for reactor background is merely a matter of computing the arithmetic average of the background points, normalizing to the total sweeps used in the pulsed data run, and subtracting. Correcting for delayed neutron background, however, is more difficult. The problem

encountered is one of deciding where the delayed neutron tail really starts. GRIPE-II makes the decision by trying different starting places and choosing the one which minimizes the variance of the delayed neutron background.

As shown in Figure 2, the later portion of the prompt neutron time response becomes a single negative exponential characterized by the decay constant, α. At an intermediate step in its processing, GRIPE-II computes the best α to describe the data. To get the best fit, GRIPE-II initially utilizes the first and last points of the exponential range as specified by a user's guess and then iteratively works in from both ends of the range until it decides the best α has been obtained. Let α_n be the α from the nth iteration and $\sigma^2_{\alpha_n}$ be an estimate of its variance. With the routine as originally received from Kaufman [33], α_n was presumed to be the best fit when 1) $|\alpha_{n+1}-\alpha_n| < \sigma_{\alpha n}$ and 2) $\sigma^2_{\alpha_{n+1}} > \sigma^2_{\alpha n}$. Although a precise estimate of reactivity was not of great importance in the experiment, an accurate value of α was needed for later use in the transformation routine. It was noted, however, that in the north core only, the value of the statistic χ^2 for the exponential fit seemed unusually large. At David's suggestion [16], a third test was implemented so that iteration for α would continue until $(\frac{\chi^2}{N} - 1) \leq 2\sigma_{\chi^2}$ where N is the number of points in the fit. Since counting data follow a Poisson distribution, σ_{χ^2} could be computed from

the properties of this function. In the south core and central reflector, the third test was satisfied at almost the same time as Kaufman's tests but in the north core, its use did result in improved χ^2 values.

After computing α, GRIPE-II goes on to compute reactivity via both the extrapolated area ratio method [23] and the Garelis-Russell method [21].

Fourier transformation was accomplished with the computer code FOURCO [5] which is based on an analogy between the Fourier transform integral and the convolution integral. However, when GRIPE-II corrected data from the central reflector and north core were transformed by FOURCO, the frequency functions were found to contain excessive scatter at frequencies beyond about 1000 rad/sec. An example of the unmodified FOURCO transform is shown in Figure 4. The phase curve has not been shown because the scatter was too excessive to he handled without modification of the computer plotting routine. It should be noted, however, that the onset of phase scatter occurred approximately one decade lower in frequency than the onset of magnitude scatter.

In studying causes of the scatter, the first step was to experiment with FOURCO using scatter-free time data sets generated from exact mathematical functions. The functions chosen for this purpose were 1) $10^6 \times e^{-160t}$ and 2) $6.25 \times 10^5 (e^{-130t} - e^{-145t})$. Hereafter these functions will

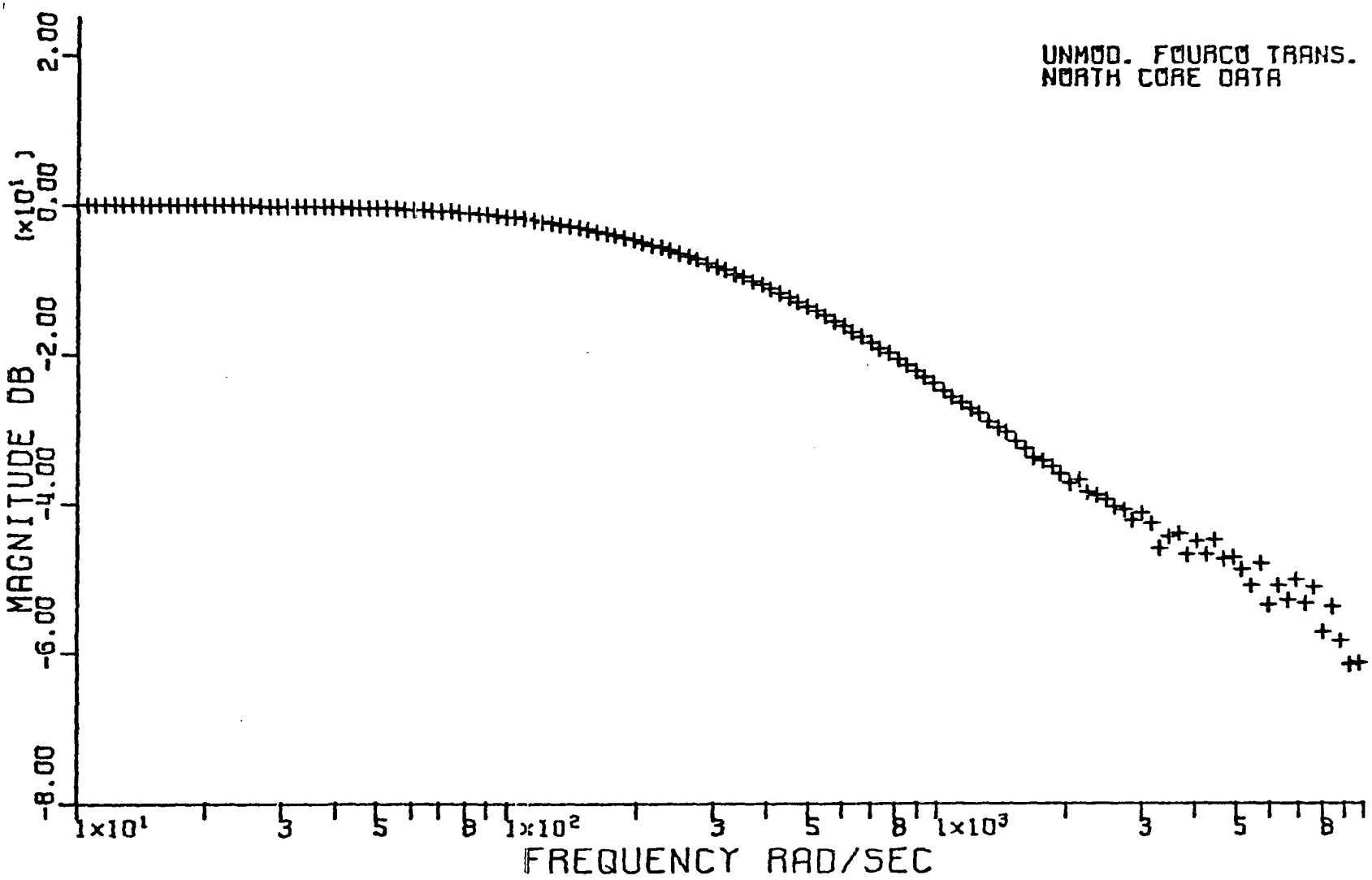

Figure 4. Illustration of frequency domain scatter

be referred to as test problem one and test problem two respectively. Test problem one was chosen because of its simplicity and test problem two was chosen because while it was simple enough to be analyzed easily, it did resemble the pulsed neutron time function observed in the north core where the frequency scatter was most severe.

Through working with these functions, it was found that some frequency scatter was being introduced by truncation of the function at "channel" 400. Because all functions of interest in this application become pure negative exponentials at large time values, it was easy to continue the integration analytically from any specified channel within the exponential range to infinity. This modification (to be referred to as "analytic continuation") was introduced into FOURCO and is described in detail in Appendix B. With analytic continuation, FOURCO was able to transform the test problems to a frequency of 10,000 rad/sec with essentially zero scatter. As an illustration of FOURCO operation, the transform of test problem one has been shown as Figures 5 and 6. When applied to experimental data, however, analytic continuation did little good. Such a result was not surprising since by channel 400 the experimental function had become so small that extending the limit of integration to infinity would make little additional contribution to the integral.

Although analytic continuation did not completely solve

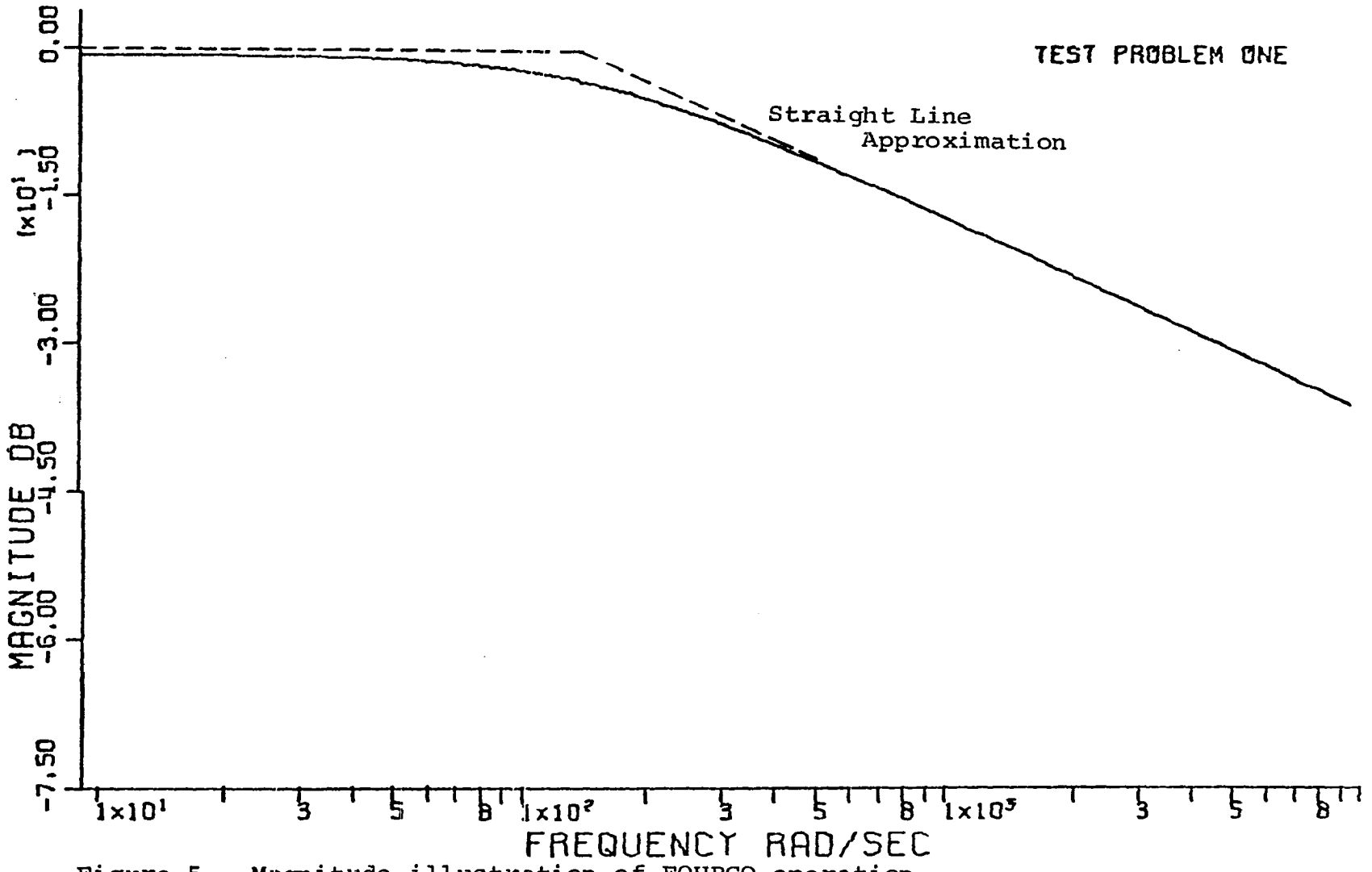

Figure 5. Magnitude illustration of FOURCO operation

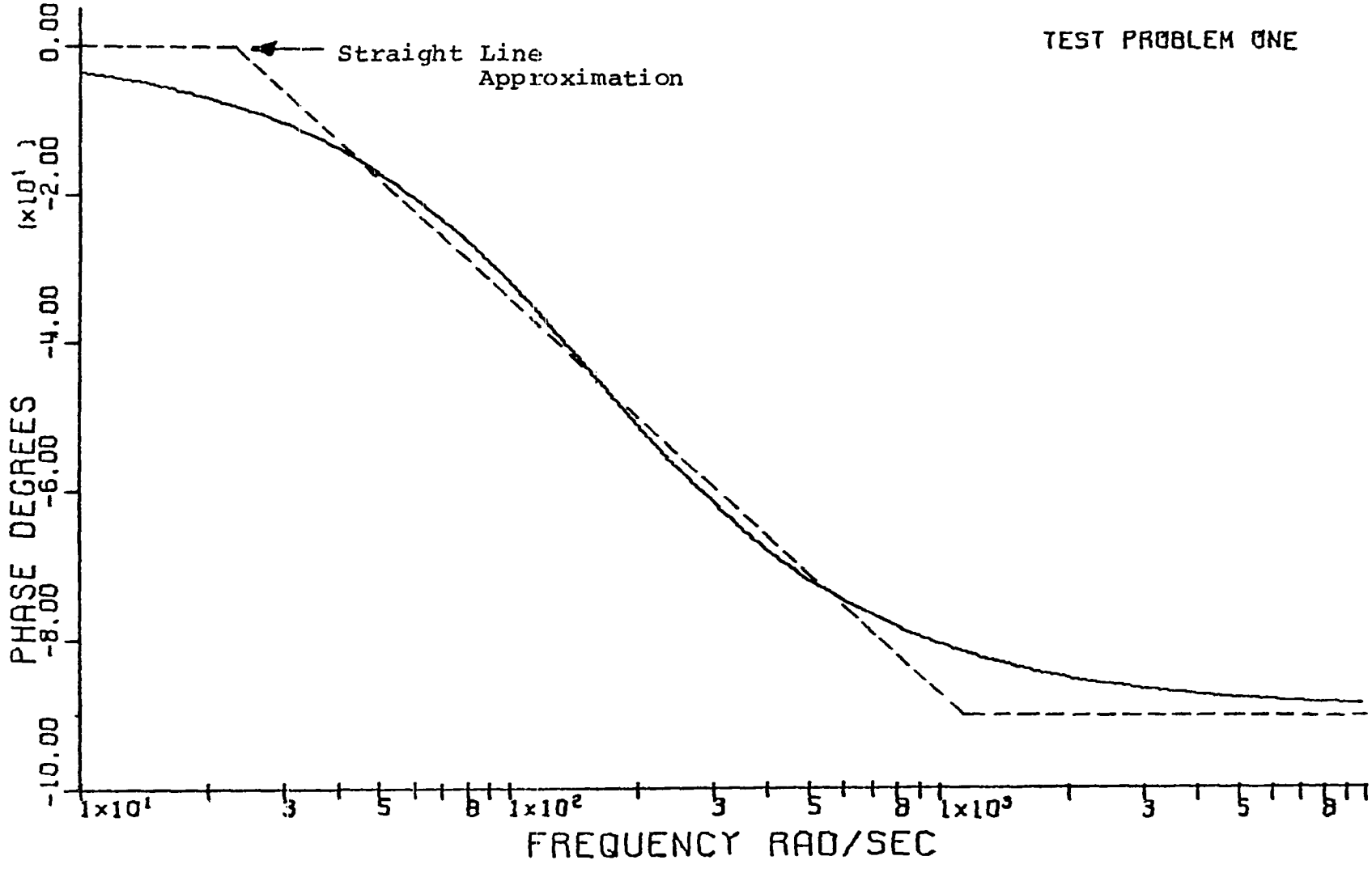

Figure 6. Phase illustration of FOURCO operation

the scatter problem, it did prove to be a useful feature. With analytic continuation, numerical transformation could be discontinued at any point within the exponential region and the transformation completed analytically. For most FOURCO processing, the transition to analytic continuation was made at channel 200. This procedure decreased computer time and also avoided numerical operations on the later points of the time function which tended to have a high degree of scatter.

After observing that FOURCO was able to transform smooth functions correctly, it was concluded that the frequency scatter was due to statistical scatter in the time domain function. The question of whether the FOURCO algorithm might be especially sensitive to statistical scatter was then raised. To check out that possibility, a routine named FORSIM was written which performed the transformation directly from the defining integral, $F(\omega) = \int_{-\infty}^{+\infty} f(t)e^{-j\omega t}dt$, using Simpson's rule integration of the real and imaginary parts. FORSIM, however, was found to be equally sensitive to scatter, have greater inherent error (determined using the test problems), and require far more computer time. The important deduction was that there was nothing specific to FOURCO which caused the frequency scatter to appear.

Having made the foregoing conclusion, it became necessary to consider the problem of how to construct a smoothing

algorithm to extract as much information as possible from the existing data. The basic question of whether to smooth before or after transformation was never satisfactorily answered on theoretical grounds but in this case, there was a definite practical advantage to presmoothing. From theory, it was expected that the time domain scatter would be approximately Gaussian with variance equal to the mean [46]. The advantage of time domain smoothing was that the scatter could be modeled and artificially introduced into the test problems. This procedure yielded a data set which contained scatter representative of the experiment but for which the correct transform was known. Performance of a smoothing algorithm could thus be evaluated from its ability to yield the correct transform of the scattered test problem.

Scatter was introduced into both of the test problems using subroutine GAUSS [28]. However, FOURCO was able to transform test problem one satisfactorily even with the scatter. For test problem two, transforming the scattered function produced frequency scatter strongly resembling that found with north core data. This result coincides with the observation that frequency scatter was not a problem in the south core. A comparison of Figures 12, 13, and 14 shows the relative shapes of the south core, central reflector, and north core time functions respectively. After an extremely rapid rise, the south core function remains high at early

times as does the pure exponential. In contrast, the central reflector and north core functions rise slowly as does the second test function. From the fundamental nature of the Fourier transform [57], the high frequency portion of the transform will be influenced primarily by the most rapidly varying part of the time function. For all of the time functions considered here, the most rapid change occurs at early times and hence, behavior of the function at early times has a strong influence on the transform at high frequencies. Note also that the relative error due to statistical time scatter decreases as the magnitude of the function increases. With a slowly rising function, the relative error is apparently sufficient to produce intolerable frequency scatter. For a function that is high valued at early times, the relative error is small enough for FOURCO to operate normally to 10,000 rad/sec even with the statistical scatter. Since test problem two approximately modeled the north core situation, development work on the smoothing algorithm was carried out using this function. Operation of the algorithm was later double-checked using a north core WIGLE solution on on which artificial scatter had also been introduced.

Although several approaches to smoothing were considered, the ultimate result was a computer code named SMODAT-IX which performs a second degree (parabolic) local least squares smoothing. SMODAT-IX is constructed so that the user can

choose from 11, 21, or 31 points per parabola with the point to be adjusted centered in the range. The user can also choose to make multiple passes with SMODAT-IX. By experimenting with the test problems, optimum performance was found to result from two passes with 21 points per parabola. Using 31 points per fit provided more smoothing but tended to distort the frequency function. Further discussion of SMODAT-IX is provided in Appendix D.

Figures 7, 8, 9, and 10 illustrate the operation of SMODAT-IX using 1) test problem two and 2) the north core WIGLE test problem. Only amplitude curves have been shown but the phase curves displayed a similar result. Because the WIGLE solution is larger at early times, the frequency function contains less scatter as would be expected in view of the foregoing conclusions. By similar reasoning, the observation that neither of these test problems produces frequency scatter of severity identical to that found in the experiment becomes quite plausible.

In applying FOURCO to corrected and smoothed pulsed neutron data, it is necessary to insure that aliasing is not causing an erroneous solution [10]. Consider a function f(t) which is sampled at equally spaced intervals Δt. The condition referred to as aliasing results when Δt is too large to permit observation of fine structure due to high frequency components. Blackman and Tukey [10] show that for a given Δt,

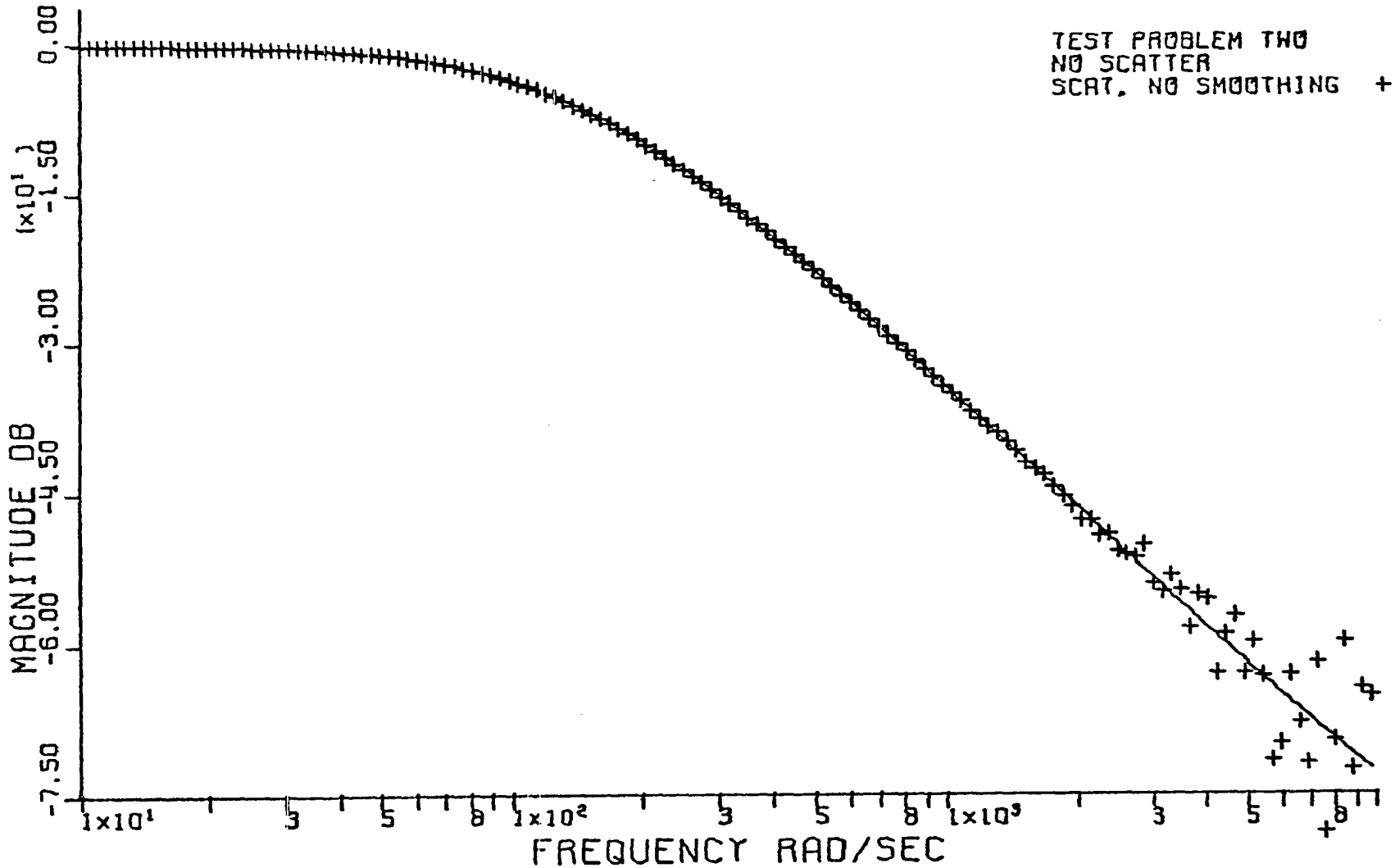

Figure 7. Illustration of time scatter effects using test problem 2

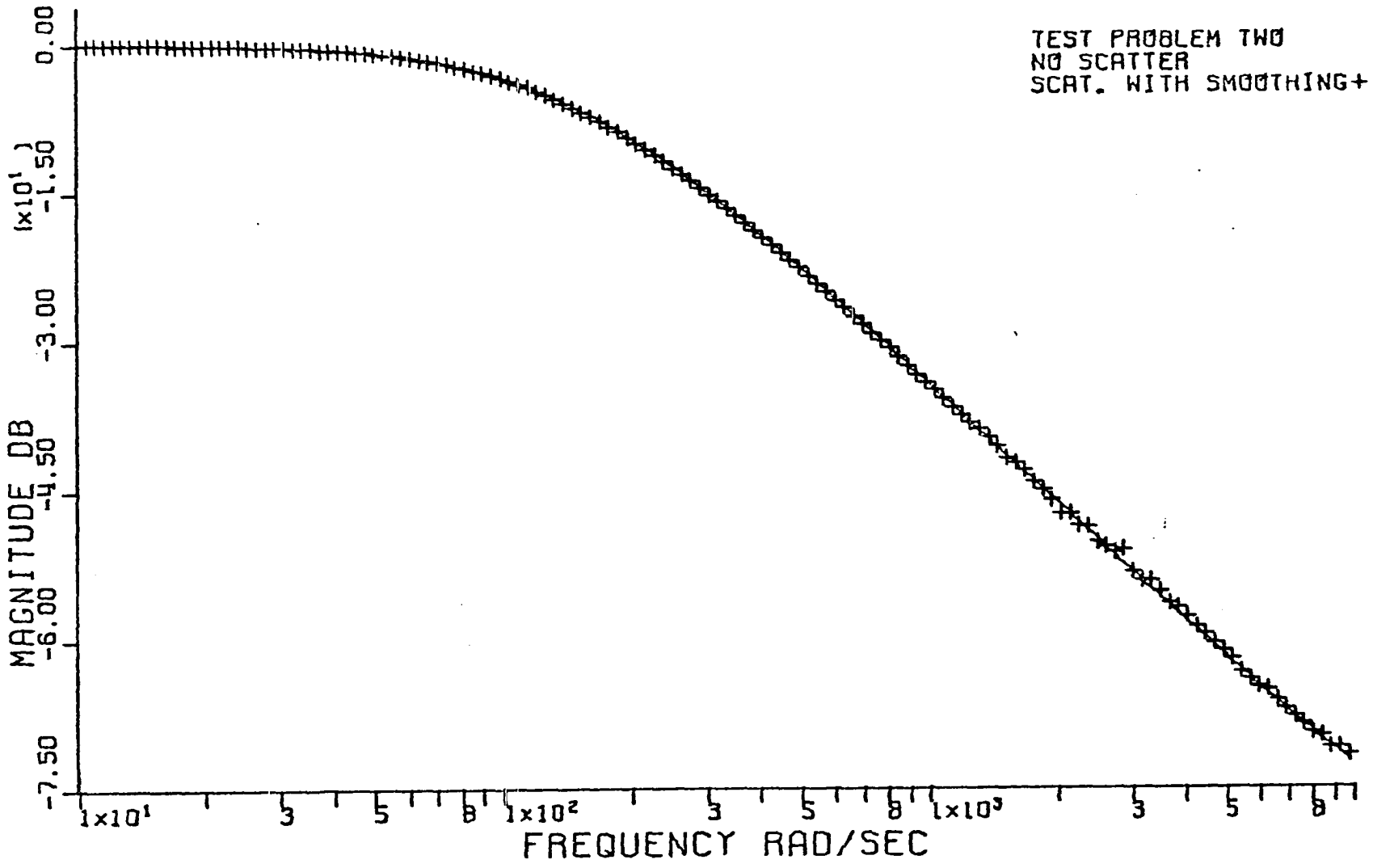

Figure 8. Illustration of smoothing using test problem 2

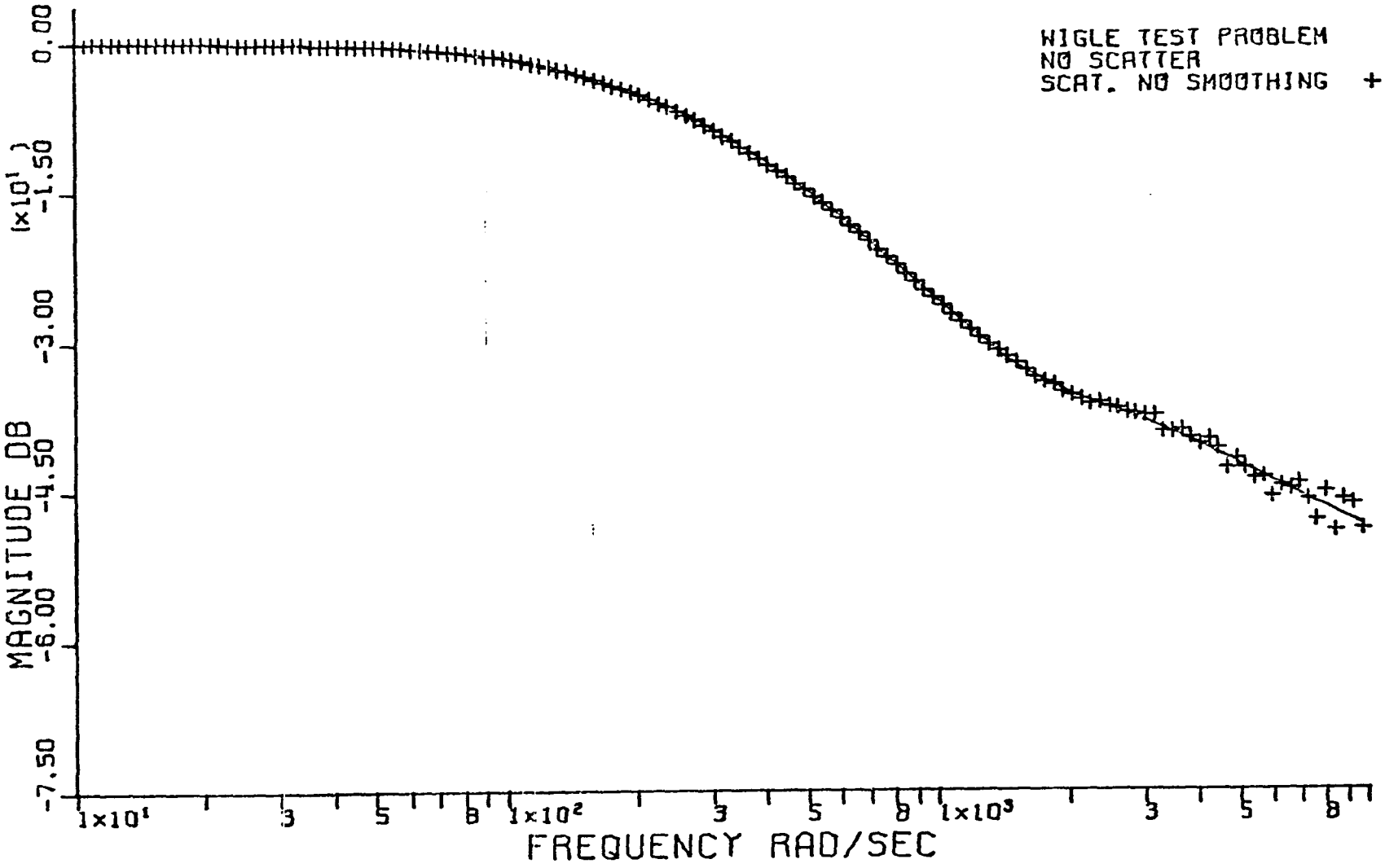

Figure 9. Illustration of time scatter effects using WIGLE test problem

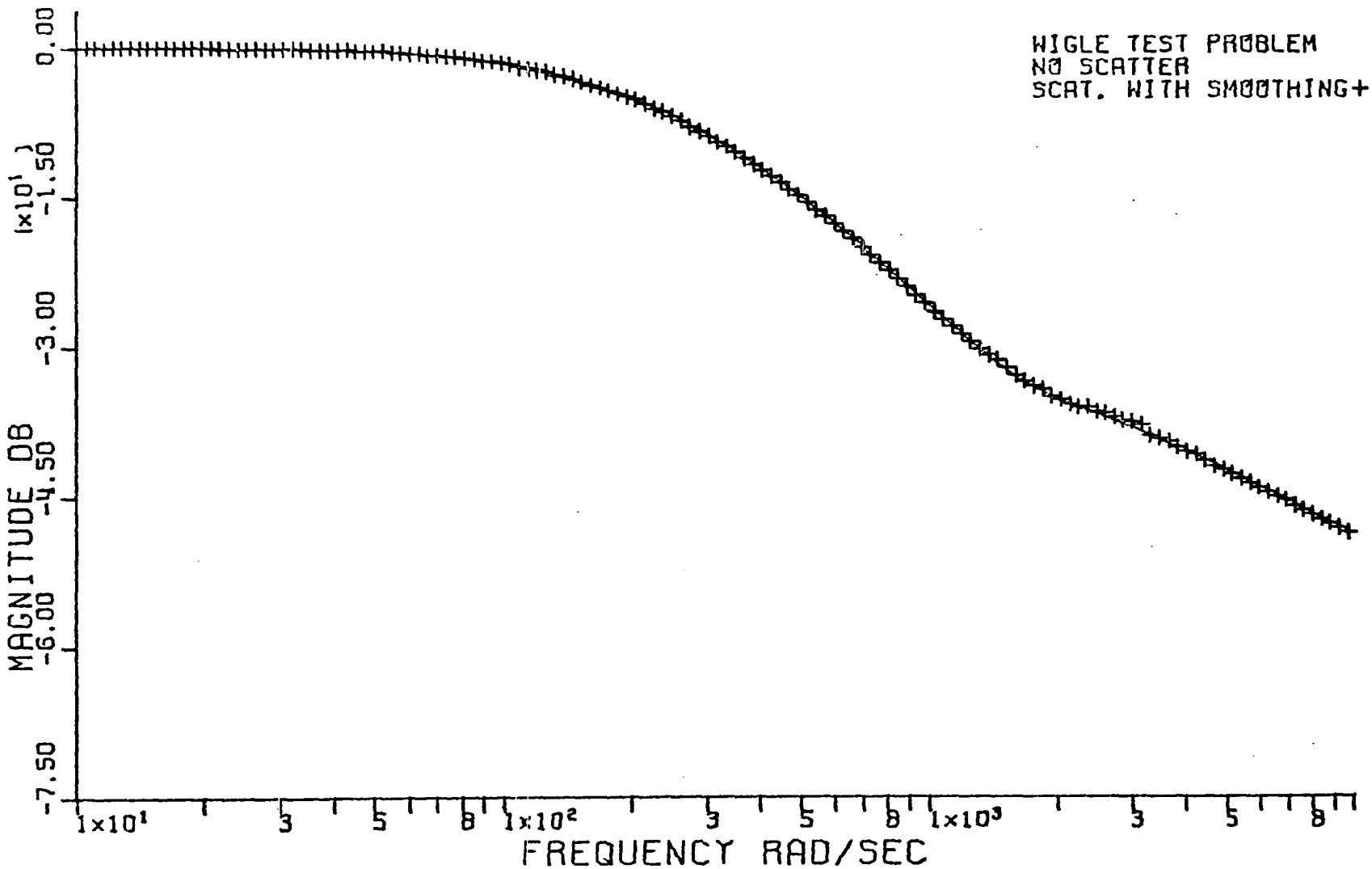

Figure 10. Illustration of smoothing using WIGLE test problem

the maximum resolvable frequency is the Nyquist frequency, $f_N = \frac{1}{2\Delta t}$, provided that there are no higher frequency components of significant amplitude present. If higher frequency components are present, the computed frequency function may be meaningless and the situation must be corrected either by filtering out the high frequencies or by reducing the sampling interval. The most practical way to check for the presence of aliasing is to process two or more data sets from experiments which are identical except for different sampling intervals [27]. If the solutions converge, aliasing is highly unlikely.

Since the most rapidly varying time function would be expected to contain the highest frequency components, the test for aliasing was performed in the south core. Except for the aliasing check, all data runs were made with the time analyzer channel width set at 100 microseconds. Due to equipment limitations, channel widths of less than 50 microseconds were not possible. A 50 microsecond width, however, was useable and a south core data run at this setting was used as the aliasing check. Convergence was judged to be satisfactory.

The above method does assume the true frequency function to be well behaved in the sense that it does not contain any large lobes at very high frequencies. But, there is nothing in either the physical situation or in any of the mathematical

models to suggest the presence of such lobes. The most explicit prediction is that of the simple point kinetics model which says that after the break frequency ($\omega_b = \beta/\ell$) the amplitude function should "roll off" at a constant 20 db per decade. The possibility of aliasing having significantly influenced the FOURCO transforms is thought to be remote.

As further support for the absence of aliasing, a simplified calculation using the point kinetics equations predicted that at the "sink" frequency of 2000 rad/sec, errors due to aliasing would be completely negligible.

VI. COMPARISON OF THE NATURAL MODE APPROXIMATION WITH EXPERIMENT

As previously discussed, the natural mode approximation was first applied to the UTR-10 by Betancourt [8]. In the present investigation, Betancourt's analysis was used as a starting point but was modified to achieve compatibility with the pulsed neutron experiment. To facilitate describing the modifications, a review of the basic method will be presented next. The following discussion applies to a one dimensional reactor without feedback. Under subcritical or low power conditions, it applies directly to the UTR-10 provided a transverse buckling term is used to account for leakage in the y and z directions.

In the framework of G group diffusion theory with I groups of delayed neutrons, the space-time dependent behavior of a reactor may be described by the matrix relation [19]

$$\frac{\partial \underline{\psi}(x,t)}{\partial t} = [H(x,t)]\underline{\psi}(x,t) + \underline{S}(x,t) \qquad (1)$$

where

$$\underline{\psi}(x,t) = \text{col}[\underline{N},\underline{C}]$$

$$\underline{N} = \text{col}[N^1(x,t),\ N^2(x,t),\ldots N^G(x,t)]$$

$$\underline{C} = \text{col}[C^1(x,t),\ C^2(x,t),\ldots C^I(x,t)]\ .$$

The gth neutron group density is denoted by $N^g(x,t)$ and the ith precursor density by $C^i(x,t)$. The K x K matrix operator $[H(x,t)]$ consists of all production and destruction operators and K = G+I. The column vector $\underline{S}(x,t)$ contains all external sources.

One method of finding an approximate solution to Equation (1) is to expand the solution vector $\underline{\psi}(x,t)$ into a finite series of the form

$$\underline{\psi}(x,t) = \sum_{m=1}^{M} \sum_{k=1}^{K} A_{mk}(t)\underline{\psi}_{mk}(x). \tag{2}$$

The space modes $\underline{\psi}_{mk}(x)$ are defined to be the eigenvectors of the eigenvalue problem

$$[H_0(x)]\underline{\psi}_{mk}(x) = \omega_{mk}\underline{\psi}_{mk}(x) \tag{3}$$

where $[H_0(x)]$ is defined by a steady state reference condition

$$[H_0(x)]\underline{\psi}_0(x) + \underline{S}_0(x) = 0. \tag{4}$$

After determining the space modes from Equation (3), the problem becomes one of finding the appropriate time functions $A_{mk}(t)$. In doing so, the eigenvectors of the adjoint equation

$$[H_0^*(x)]\underline{\psi}_{mk}^*(x) = \omega_{mk}^*\underline{\psi}_{mk}^*(x) \tag{5}$$

form a convenient set of weighting vectors. The linear operator $[H_0^*(x)]$ is the adjoint of the operator $[H_0(x)]$ and

is defined by the equation

$$\langle \underline{\psi}^*_{nj}(x),\ [H_0(x)]\ \underline{\psi}_{mk}(x)\rangle = \langle \underline{\psi}_{mk}(x),\ [H^*_0(x)]\underline{\psi}^*_{nj}(x)\rangle. \quad (6)^1$$

It is considered that both $\underline{\psi}_{mk}(x)$ and $\underline{\psi}^*_{nj}(x)$ have the same boundary conditions. The eigenvalues are assumed to be distinct and it thus follows [8], that the eigenvectors of the $[H_0(x)]$ operator in combination with the eigenvectors of the adjoint operator have the orthogonality property

$$\langle \underline{\psi}^*_{nj}(x),\ \underline{\psi}_{mk}(x)\rangle = 0 \quad \text{for} \quad \omega_{mk} \neq \omega^*_{nj}\ . \qquad (7)$$

Further, it will be assumed that $\langle \underline{\psi}^*_{mk}(x), \underline{\psi}_{mk}(x)\rangle \neq 0$ which implies that the set of eigenvalues $\{\omega^*_{mk}\}$ is the same as the set $\{\omega_{mk}\}$.

It will also be convenient to decompose the operator $[H(x,t)]$ into

$$[H(x,t)] = [H_0(x)] + [H_1(x,t)] \qquad (8)$$

where $[H_1(x,t)]$ is the perturbation matrix operator. Equation (1) may then be re-written as

$$\frac{\partial \underline{\psi}(x,t)}{\partial t} = [H_0(x)]\underline{\psi}(x,t) + [H_1(x,t)]\,\underline{\psi}(x,t) + \underline{S}(x,t) \qquad (9)$$

Substituting Equation (2) into Equation (9), multiplying by $\underline{\psi}^*_{nj}(x)$, and subsequently integrating over the reactor yields

---

[1] In this paper, the bracket notation will be used to represent the inner product

$$\langle \underline{x}, \underline{y}\rangle = \int_{\text{reactor}} \underline{x}^T \underline{y}\ \underline{dr}\ .$$

the set of ordinary differential equations

$$\sum_{m=1}^{M}\sum_{k=1}^{K}\frac{dA_{mk}(t)}{dt}\langle\underline{\psi}^*_{nj}(x),\ \underline{\psi}_{mk}(x)\rangle$$

$$=\sum_{m=1}^{M}\sum_{k=1}^{K}\{A_{mk}(t)\langle\underline{\psi}^*_{nj}(x),\ [H_0(x)]\underline{\psi}_{mk}(x)\rangle$$

$$+A_{mk}(t)\ \langle\underline{\psi}^*_{nj}(x),\ [H_1(x,t)]\underline{\psi}_{mk}(x)\rangle\}$$

$$+\langle\underline{\psi}^*_{nj}(x),\ \underline{S}(x,t)\rangle \qquad (10)$$

where

$$n = 1,2,\ldots,M$$

$$j = 1,2,\ldots,K\ .$$

Since there are M x K linearly independent weighting vectors, $\underline{\psi}^*_{nj}(x)$, there are M x K coupled differential equations in the set. Utilizing the orthogonality property, the set of equations reduces to

$$\frac{dA_{mk}(t)}{dt}=\omega_{mk}A_{mk}(t)+\sum_{n=1}^{M}\sum_{j=1}^{K}\frac{\langle\underline{\psi}^*_{mk}(x),\ [H_1(x)]\underline{\psi}_{nj}(x)\rangle A_{nj}(t)}{\langle\underline{\psi}^*_{mk}(x),\ \underline{\psi}_{mk}(x)\rangle}$$

$$+\frac{\langle\underline{\psi}^*_{mk}(x),\ \underline{S}(x,t)\rangle}{\langle\underline{\psi}^*_{mk}(x),\ \underline{\psi}_{mk}(x)\rangle}\ . \qquad (11)$$

By defining

$$S_{mk}(t)=\frac{\langle\underline{\psi}^*_{mk}(x),\ \underline{S}(x,t)\rangle}{\langle\underline{\psi}^*_{mk}(x),\ \underline{\psi}_{mk}(x)\rangle}\ , \qquad (12)$$

the set may be expressed by the matrix equation

$$\frac{d\underline{A}(t)}{dt} = \text{diag}[\omega]\underline{A}(t) + [P]\underline{A}(t) + \underline{S}(t) \qquad (13)$$

where

$$\underline{A}(t) = \text{col}[A_{11}(t),\ A_{21}(t),\ldots\ A_{MK}(t)]$$

$$\underline{S}(t) = \text{col}[S_{11}(t),\ S_{21}(t),\ldots\ S_{MK}(t)]$$

$\text{diag}[\omega]$ = an M x K by M x K diagonal matrix with elements ω_{mk}

$$P_{\mu\gamma} = \frac{\langle \underline{\psi}^*_{mk}(x),\ [H_1(x)]\underline{\psi}_{nj}(x)\rangle}{\langle \underline{\psi}^*_{mk}(x),\ \underline{\psi}_{mk}(x)\rangle}$$

where

$\mu = (m-1)K+k$ for $m = 1,2,\ldots M$; $k = 1,2,\ldots K$

$\gamma = (n-1)K+j$ for $n = 1,2,\ldots M$; $j = 1,2,\ldots K$.

Equation (13) is known as the Mth order natural mode approximation (NMA).

In Betancourt's study, there were no external sources so that and the equation he used was

$$\frac{d\underline{A}(t)}{dt} = \text{diag}[\omega]\underline{A}(t) + [P]\underline{A}(t) \ . \qquad (14)$$

Using two group theory with one group of delayed neutrons, Betancourt formed the $[H_0(x)]$ operator for the UTR-10 as shown in Appendix A. It should be noted that the reference

condition (criticality in this case) was achieved by the conventional reactor statics method of adjusting $\nu\Sigma_f$. For a two group model with one group of delayed neutrons, Foulke and Gyftopoulos [19] show that the eigenvalues ω_{m1}, ω_{m2}, and ω_{m3} are associated with delayed neutrons, prompt thermal neutrons, and prompt epithermal neutrons respectively. In his investigation, Betancourt was interested in the prompt response only and further, it was known that the prompt epithermal modes were not important except at oscillator frequencies above 10^4 rad/sec. Thus, he chose to utilize only the prompt thermal modes and in effect used an expansion of the form

$$\underline{\psi}(x,t) = \sum_{m=1}^{M} A_{m2}(t)\underline{\psi}_{m2}(x)$$

To implement his solutions, Betancourt wrote computer programs to solve the equations

$$[H_0(x)]\underline{\psi}_{mk}(x) = \omega_{mk}\underline{\psi}_{mk}(x)$$

and

$$[H_0^*(x)]\underline{\psi}^*_{mk}(x) = \omega_{mk}\underline{\psi}^*_{mk}(x)$$

for the eigenvalues and eigenvectors. He then defined the perturbation matrix, [P], in terms of a plane oscillating thermal absorber and manipulated in such a way as to solve for the elements of $\underline{A}$ expressed in the frequency domain.

Consider next how the Mth order NMA might be made to

describe a pulsed neutron experiment. In a pulsed neutron experiment, none of the reactor production or destruction operators deviate from the reference condition so that the perturbation matrix reduces to the null matrix and Equation (13) becomes

$$\frac{d\underline{A}(t)}{dt} = \text{diag}[\omega]\underline{A}(t) + \underline{S}(t) \quad . \tag{15}$$

Obviously, $\underline{S}(t)$ must now be non-zero but the elements of $\underline{S}(t)$ can easily be computed from Equation (12) provided $\underline{S}(x,t)$ is known.

The space-time source vector may be written

$$\underline{S}(x,t) = \text{col}[S^1(x,t), S^2(x,t), S^3(x,t)] \tag{16}$$

where the components represent 1) the fast group source, 2) the slow group source, and 3) the precursor source respectively. The third component, $S^3(x,t)$ is obviously zero and since all source neutrons are born at 14.3 Mev, $S^2(x,t)$ is also taken to be zero. For $S^1(x,t)$, the appropriate function is the space-time slowing down source at the 1.6 Mev fast group energy. In keeping with the work of Masters and Cady [40], it was assumed that the time dependence of this source could be expressed as

$$S^1(x,t) = S^1(x)\delta(t).$$

The space dependence, $S^1(x)$, can be estimated by the method of Appendix C and the source vector expressed by

$$\underline{S}(x,t) = \{\mathrm{col}[S^1(x),\ 0,\ 0]\}\delta(t)\ . \tag{17}$$

Equation (17) can then be substituted into Equation (12) to yield

$$\underline{S}(t) = \mathrm{col}[S_{11}, S_{12}, \ldots S_{MK}]\delta(t) \tag{18}$$

where $S_{11}, S_{12}, \ldots S_{MK}$ are constants. Following Schultz and Melsa [52], the solution to Equation (15) can be written as

$$\underline{A}(t) = [\Phi(t)]\underline{A}(0) + \int_0^t [\Phi(t-\tau)]\underline{S}(\tau)\,d\tau \tag{19}$$

where $[\Phi(t)]$ is known as the "state transition matrix" and is given by

$$[\Phi(t)] = e^{\underline{A}(t)t} = \begin{bmatrix} e^{\omega_{11}t} & & 0 \\ & \ddots & \\ 0 & & e^{\omega_{MK}t} \end{bmatrix}$$

In the experiment, the reactor and delayed neutron backgrounds were subtracted off to leave only the prompt response. Since the prompt flux is zero at time zero, Equation (19) can be made to describe the experiment only if $\underline{A}(0) = \underline{0}$. Therefore, Equation (19) becomes

$$\underline{A}(t) = \int_0^t [\Phi(t-\tau)]\underline{S}(\tau)\,d\tau\ . \tag{20}$$

Substituting Equation (18) into Equation (20) and utilizing the properties of the delta function, yields

$$\underline{A}(t) = [\Phi(t)]\ \mathrm{col}[S_{11}, S_{12}, \ldots S_{MK}] \tag{21}$$

or

$$A_{mk}(t) = S_{mk} e^{\omega_{mk} t}$$

Foulke and Gyftopoulos [19] show that all eigenvalues are negative and that the eigenvalues corresponding to the delayed neutron modes are numerically small. The delayed neutron contribution to the total neutron density will thus appear to be a constant in relation to the prompt mode contributions. In conjunction with setting $\underline{A}(0) = \underline{0}$, the experimental subtraction of delayed neutron background can be modeled by ignoring the delayed neutron modes. Further, the prompt epithermal eigenvalues are numerically very large [19] and provide only an extremely rapid transient at very early times. Thus, as in Betancourt's work, the prompt epithermal modes were also ignored and the pulsed neutron experiment was assumed to be described by the expansion

$$\underline{\psi}(x,t) = \sum_{m=1}^{M} S_{m2} e^{\omega_{m2} t}\ \underline{\psi}_{m2}(x). \tag{22}$$

The above discussion assumes that the source is a single delta function neutron burst and implies that a series of such bursts will yield the same result when superimposed. Gozani [23] discusses reactor response to a series of delta

function bursts and concludes that "the basic feature of the system response to a single burst is preserved". If Gozani's description is introduced into the NMA, it turns out that for a series of P bursts the right side of Equation (22) is simply multiplied by the scale factor P provided P is a large number. The 2000 pulse minimum used in the experiment is sufficiently large and the scale factor is completely irrelevant because only flux shapes are of interest. In fact, when the fluxes are actually computed, an arbitrary scale factor is introduced to yield convenient magnitudes.

Equation (22) provides the basis for modeling pulsed neutron time functions via the NMA. At this point, however, it is relatively easy to also extract the frequency response directly. For this purpose, a sinusoidal time dependence of the source is postulated and Equation (18) re-written as

$$\underline{S}(t) = \text{col}[S_{11}, S_{12}, \ldots S_{MK}]e^{j\omega t} . \tag{23}$$

Equation (15) now becomes

$$\frac{d\underline{A}(t)}{dt} = \text{diag}[\omega]\underline{A}(t) + \hat{\underline{S}}e^{j\omega t} \tag{24}$$

where

$$\hat{\underline{S}} = \text{col}[S_{11}, S_{12}, \ldots S_{MK}].$$

Since the equations are linear, each mode will also oscillate with frequency ω. The vector $\underline{A}(t)$ may thus be written as $\underline{A}(t) = \hat{\underline{A}}e^{j\omega t}$. Performing the differentiation and dividing

out the common $e^{j\omega t}$ in Equation (24) produces

$$j\omega\hat{\underline{A}} = \text{diag}[\omega]\hat{A} + \hat{S} \ . \tag{25}$$

Solving Equation (25) for $\hat{\underline{A}}$ yields

$$\hat{A} = \{j\omega I - \text{diag}[\omega]\}^{-1} \hat{\underline{S}} \ . \tag{26}$$

Finally,

$$\hat{A}_{mk} = \frac{S_{mk}}{j\omega - \omega_{mk}} \ .$$

As before, prompt epithermal and delayed neutron modes are ignored and the frequency domain description becomes

$$\underline{\psi}(x,\omega) = \sum_{m=1}^{M} \frac{S_{m2}}{j\omega - \omega_{m2}} \psi_{m2}(x) \ . \tag{27}$$

To implement the computation described in the foregoing paragraphs, a computer program was written for the IBM 360/65 which incoroprated as many of Betancourt's original routines as possible. Except for minor modifications to improve efficiency, the routines used to compute the eigenvalues, the eigenvectors, and the adjoint eigenvectors were Betancourt's routines. His basic numerical integration scheme for evaluating $\langle \underline{\psi}^*_{mn}(x), \underline{\psi}_{mn}(x) \rangle$ was also retained but was expanded to accept a numerical source function $S^1(x)$ (see Appendix C) and calculate the S_{mk} as well. All numerical

integrations were performed using a 4th order polynomial in conjunction with the trapezoidal rule. New routines, implementing Equations (22) and (27), were written to obtain respectively the time and frequency response.

In order for the NMA to properly describe the reactor, it is necessary for the reference operator $[H_0(x)]$ to correctly represent the existing reactor state. Within the framework of ordinary two group diffusion theory, however, it is impossible to describe sufficient detail to achieve that objective without some sort of normalization. The conventional procedure is to ficticiously adjust $\nu\Sigma_f$ until the desired reference response is obtained. In Betancourt's work, $\nu\Sigma_f$ was adjusted to achieve criticality. In the present study, the subcritical reactor was modeled by adjusting $\nu\Sigma_f$ until the fundamental mode decay constant (ω_{12} in the model) matched that observed experimentally (α). One problem did arise in that the experimental α was not constant throughout the reactor but rather displayed a weak but definite space dependence similar to that pointed out by Ohanian and Diaz [44]. Note that the NMA has no mechanism for describing a space dependent α. Since the most interesting phenomena were anticipated in the north core, $\nu\Sigma_f$ was adjusted until ω_{12} matched the north core α. For the rods in configuration, this α was found to be 157.98.

When describing a reactor with a modal analysis, the

appropriate number of modes to use must be determined. The usual criterion for making this decision is to run solutions with different numbers of modes and look for convergence. Betancourt used a maximum of 9 modes but did note evidence of convergence difficulty in certain situations.

For the present study, solutions were run using 6, 7, 8, 9, 10, and 11 modes. In the south core and central reflector, all modal solutions were in good agreement. The only effect of adding modes was to shift the solution slightly towards the true function at very early times (less than about 1 millisecond). In the north core, agreement of all solutions was excellent at times greater than 1 millisecond. At early times, however, there was a pronounced lack of convergence as evidenced by Figure 11. The cause of this difficulty is not certain but two possibilities are: 1) the number of modes used was not sufficient, and 2) the eigenvalues of the higher order modes were not known with sufficient accuracy. Note that in Figure 11 the true function must start at zero. The first explanation is thought unlikely since the higher order modes seem to be actually diverging from a function which goes to zero at zero time. The second explanation, on the other hand, is thought to be correct. It was noted that for the higher order modes, significant changes in the coefficient S_{m2} could result from very small changes in the eigenvalue. For example, a 0.08

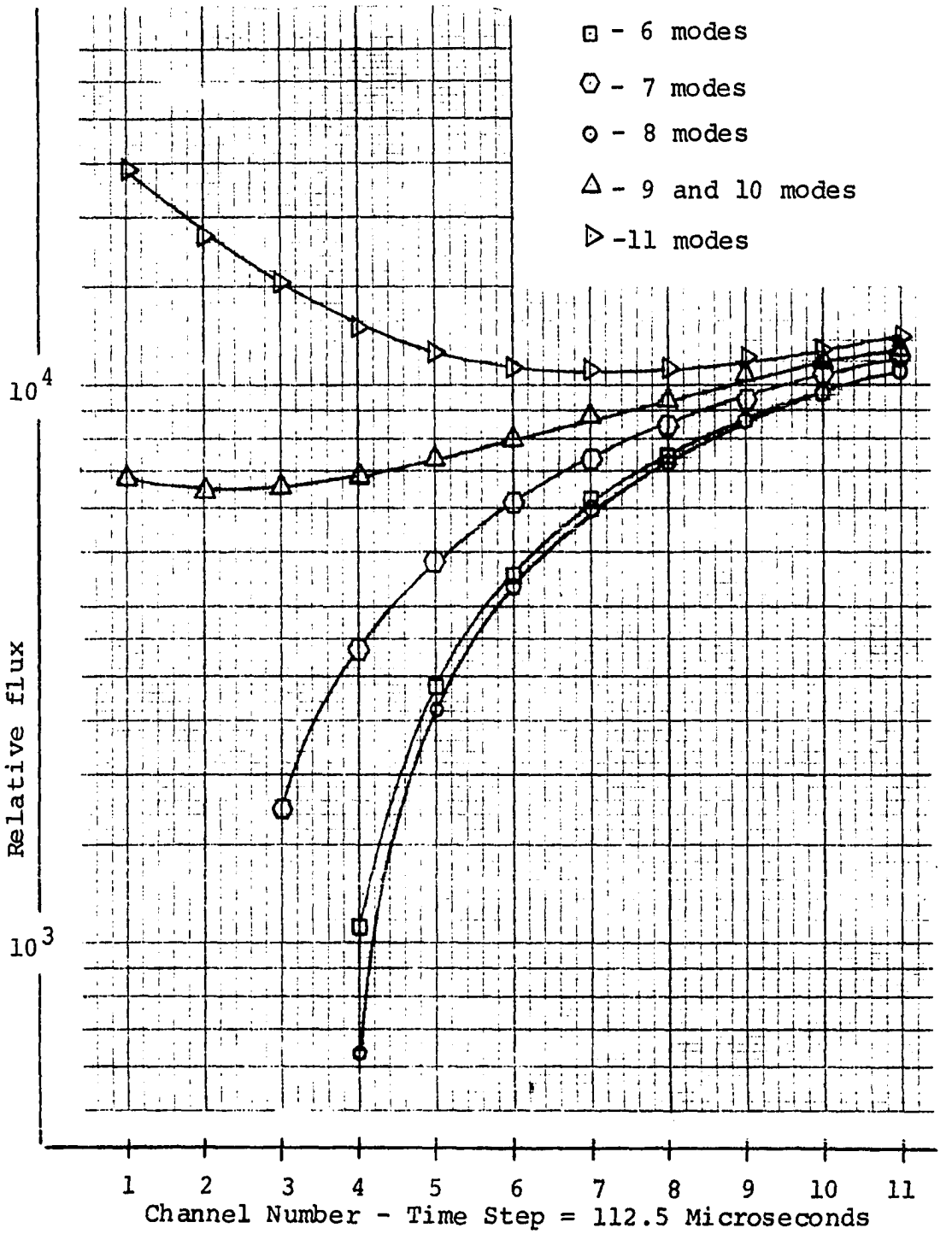

Figure 11. Illustration of north core, rods in, NMA convergence

per cent change in ω_{82} (rods in configuration) was observed to change S_{82} by a factor of more than 100. At best, ω_{82} was known to an accuracy of 0.008 per cent and there is some evidence that a change in the eigenvalue of less than this amount may significantly change the S_{m2}. Since the higher order eigenvalues are numerically large (see Table 1), these terms die out quickly and have little influence at times greater than 1 millisecond.

Although the convergence problem is certainly important, a thorough study would involve investigating the convergence criterion used in Betancourt's eigenvalue routine and was not attempted because of time limitations. Rather, a 7 mode analysis was judged to provide the best available approximation and all NMA calculations to be subsequently presented are hence based on a 7 mode expansion. It is interesting to note that Betancourt also encountered convergence difficulty in the north core and that he also chose to use a 7 mode analysis to describe this location.

Figures 12, 13, and 14 show the NMA time solutions compared with the experimental. It should be pointed out that the apparent "knee" in the north core NMA curve just after time zero is meaningless. It results from the insertion of ficticious numbers into the first two "channels" to avoid confusing the plotting routine with the negative numbers actually generated by the NMA. As might be expected from the

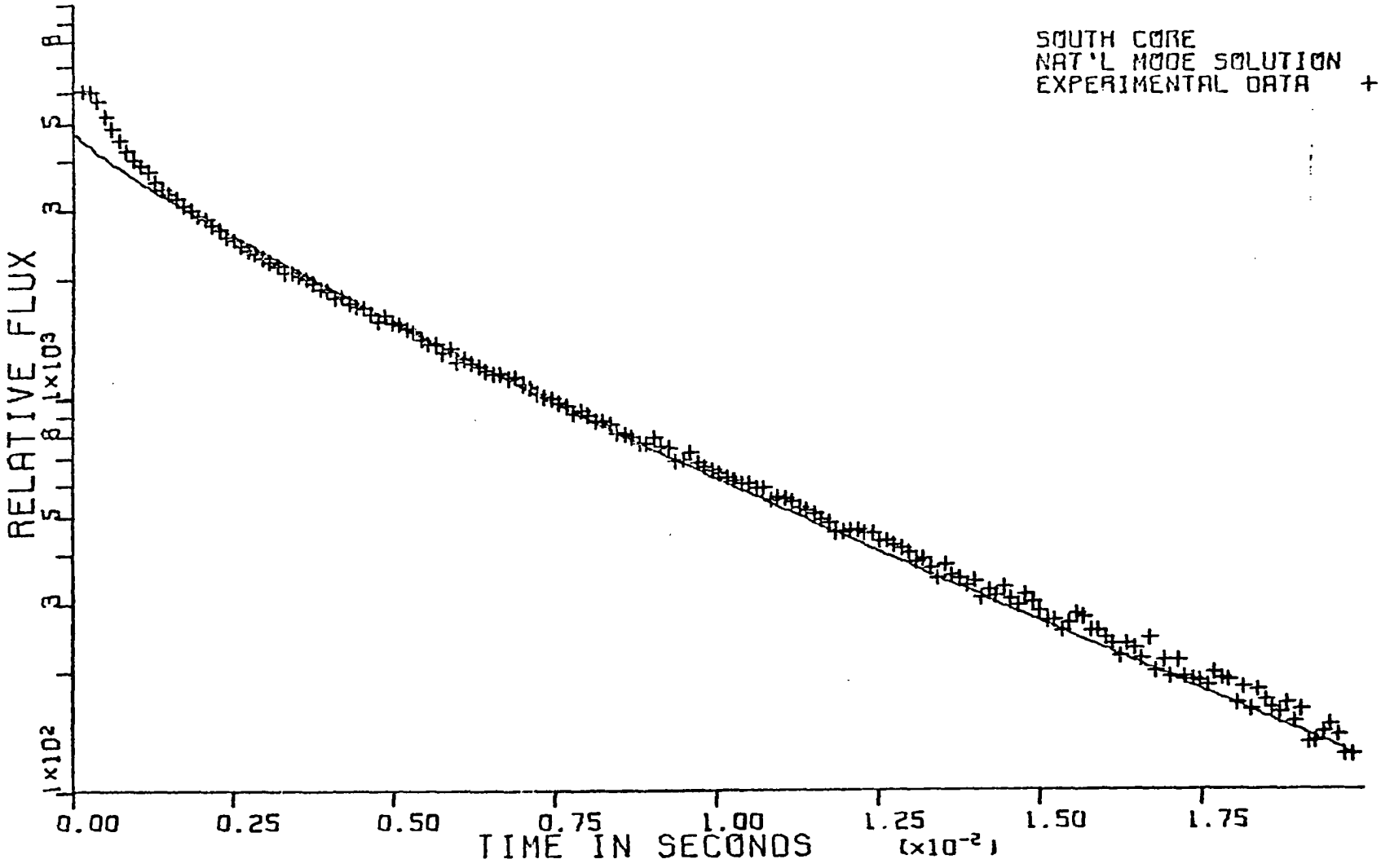

Figure 12. South core time response after burst

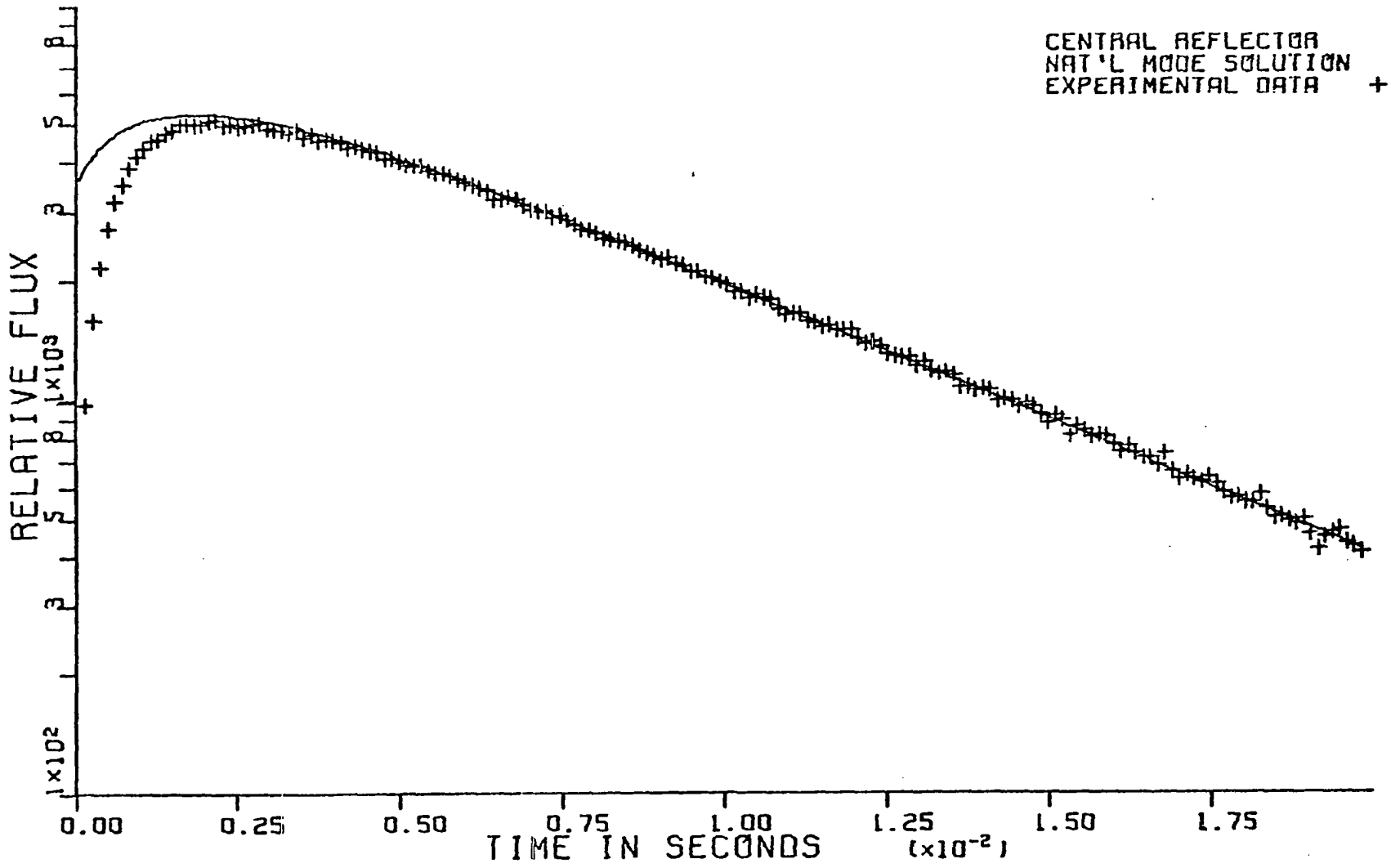

Figure 13. Central reflector time response after burst

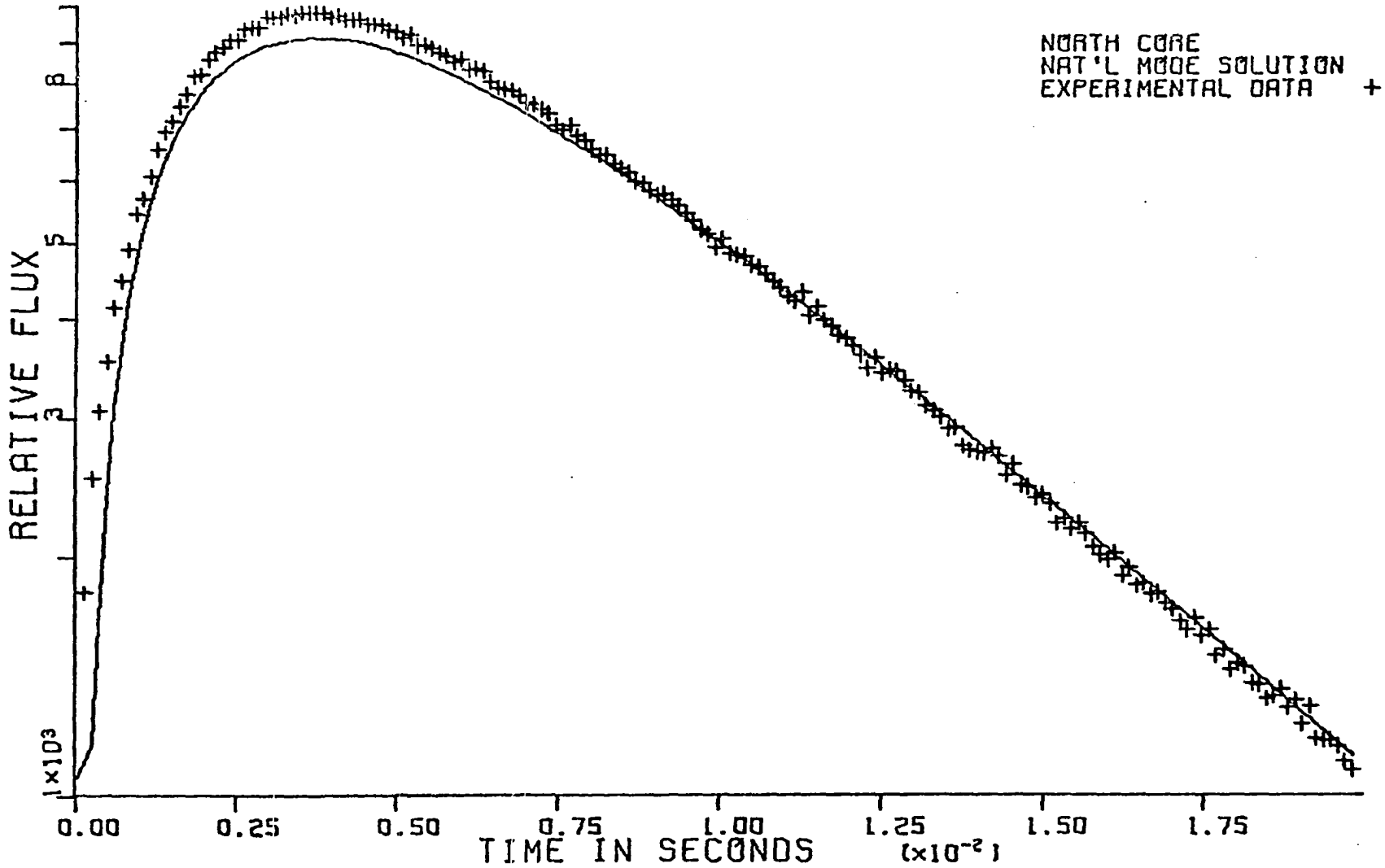

Figure 14. North core time response after burst

convergence problem discussed above, the NMA is unable to provide a good fit at early times. Therefore, it would be anticipated that the NMA frequency response would be in error at high frequencies. Examination of Figures 15-20 confirms these suspicions. The NMA accurately predicts the 3 db down point but begins to depart from the experiment at approximately 1000 rad/sec for the magnitude and at about 200 rad/sec for the phase. It should also be pointed out that all magnitude curves have been normalized to 0 db at 10 rad/sec.

It is interesting to note that the experiment does show a broad inflection point in the magnitude curve and a corresponding upswing in phase at about 2000 rad/sec. In contrast, the NMA shows little evidence of either and certainly no evidence of a sink. Betancourt's sink, however, occurred in the north reflector and the results displayed here are similar to those observed by Betancourt for the three locations under consideration.

In summary, the NMA in its present form is unable to predict either magnitude or phase of the frequency response accurately at frequencies above 1000 rad/sec. The immediate problem is thought to be a numerical problem with the algorithms rather than a basic deficiency of the NMA. Yet, the NMA does not provide a mechanism for describing a space dependent α and is limited in accuracy by the approximations inherent

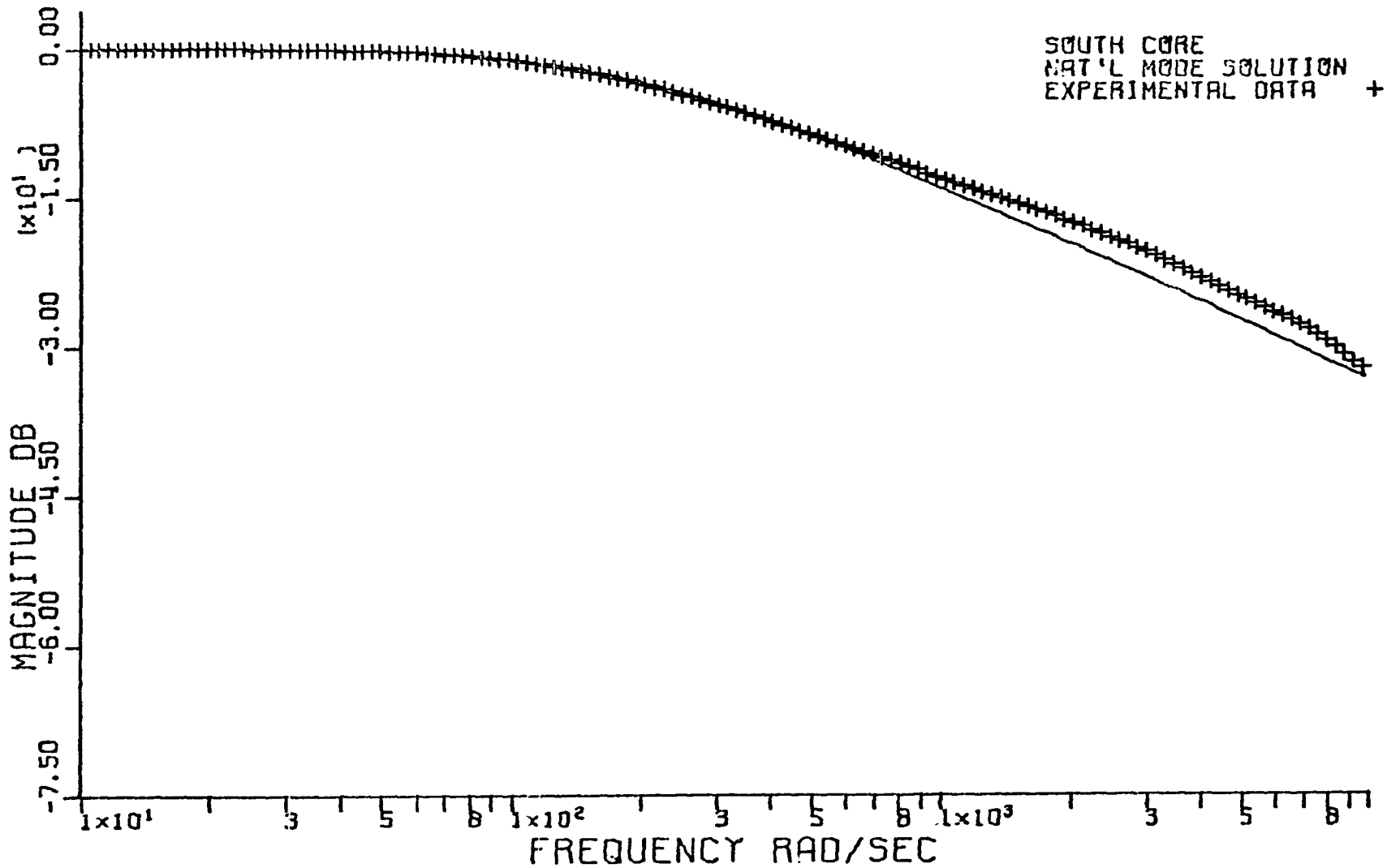

Figure 15. Magnitude of south core frequency response

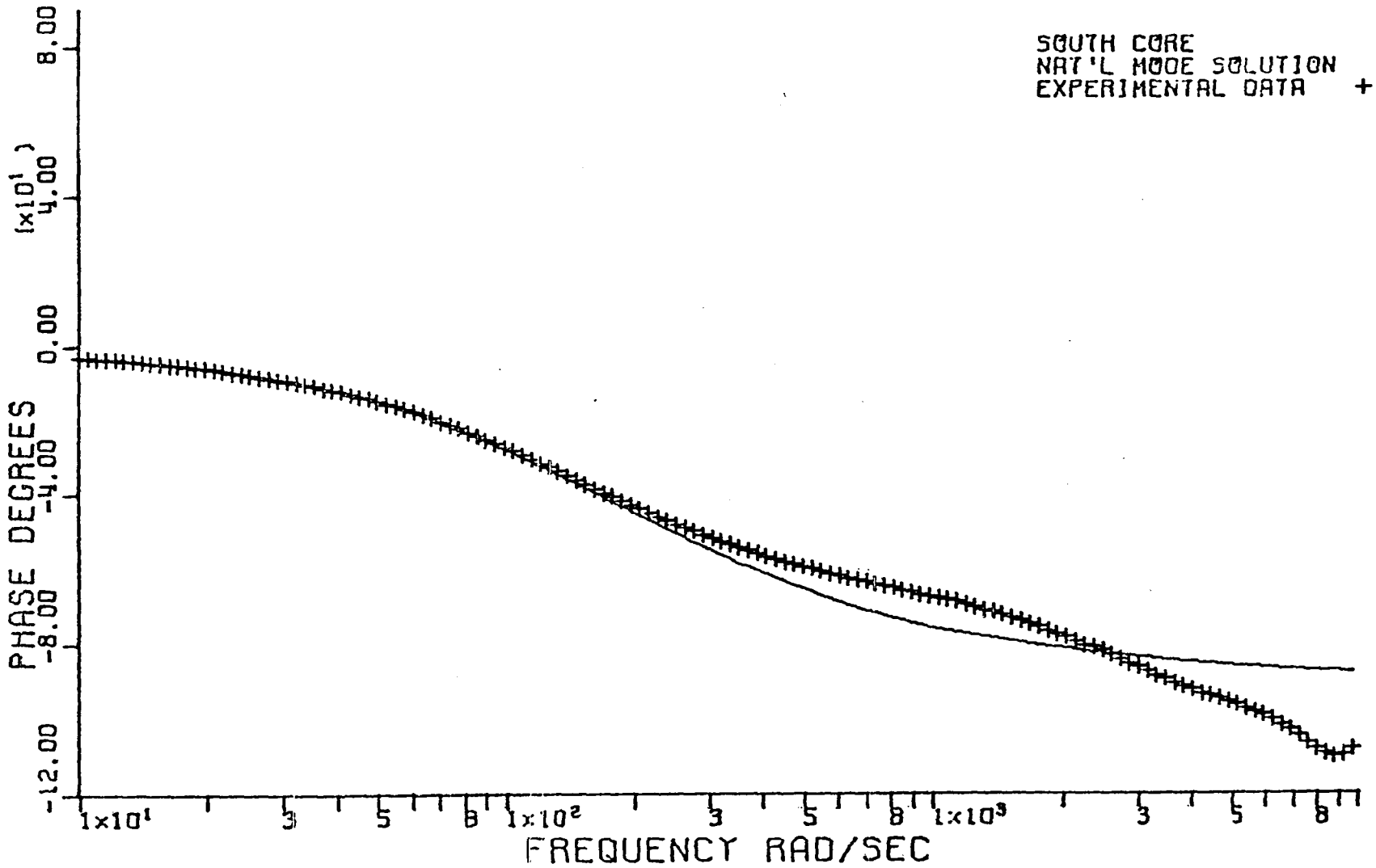

Figure 16. Phase of south core frequency response

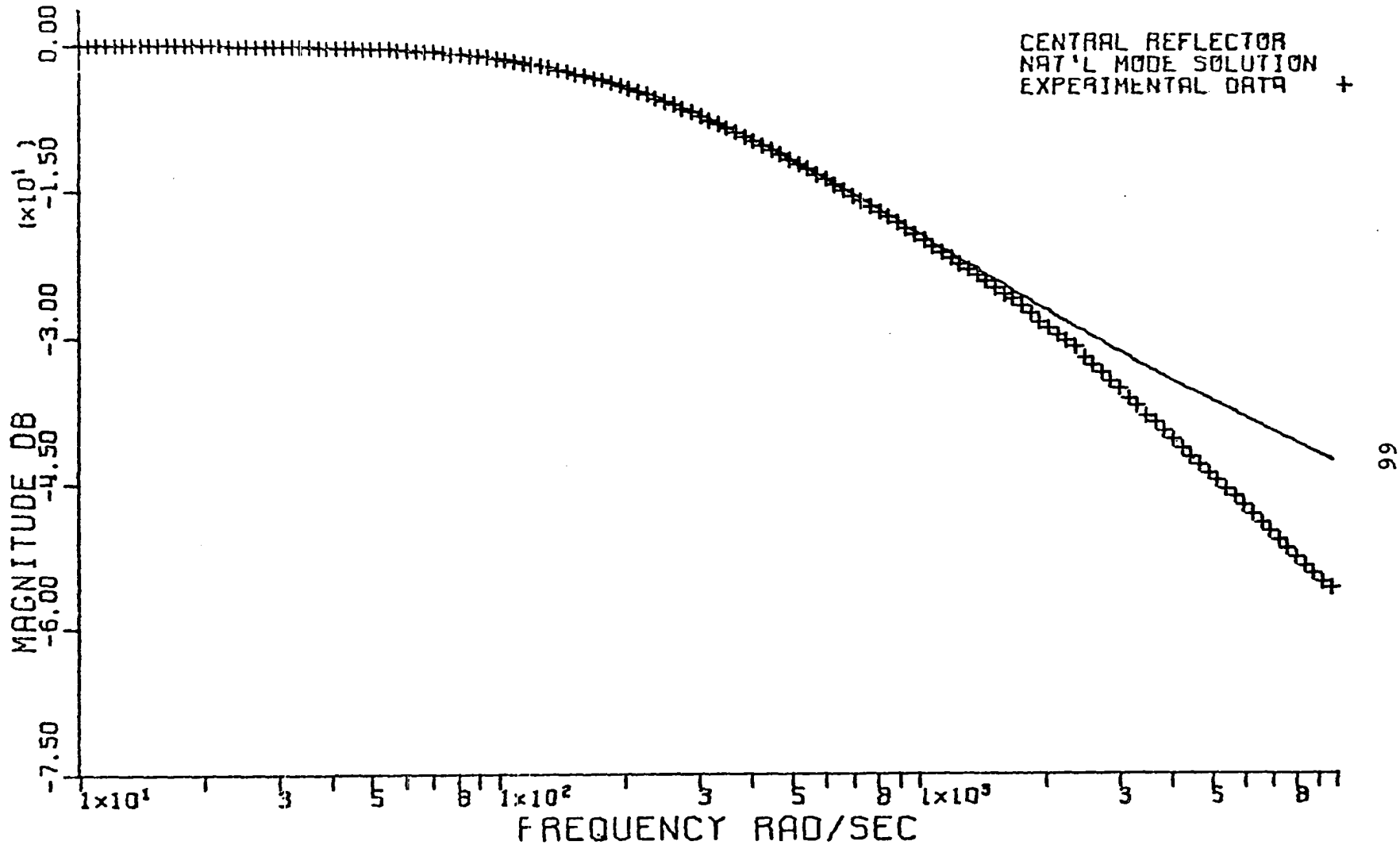

Figure 17. Magnitude of central reflector frequency response

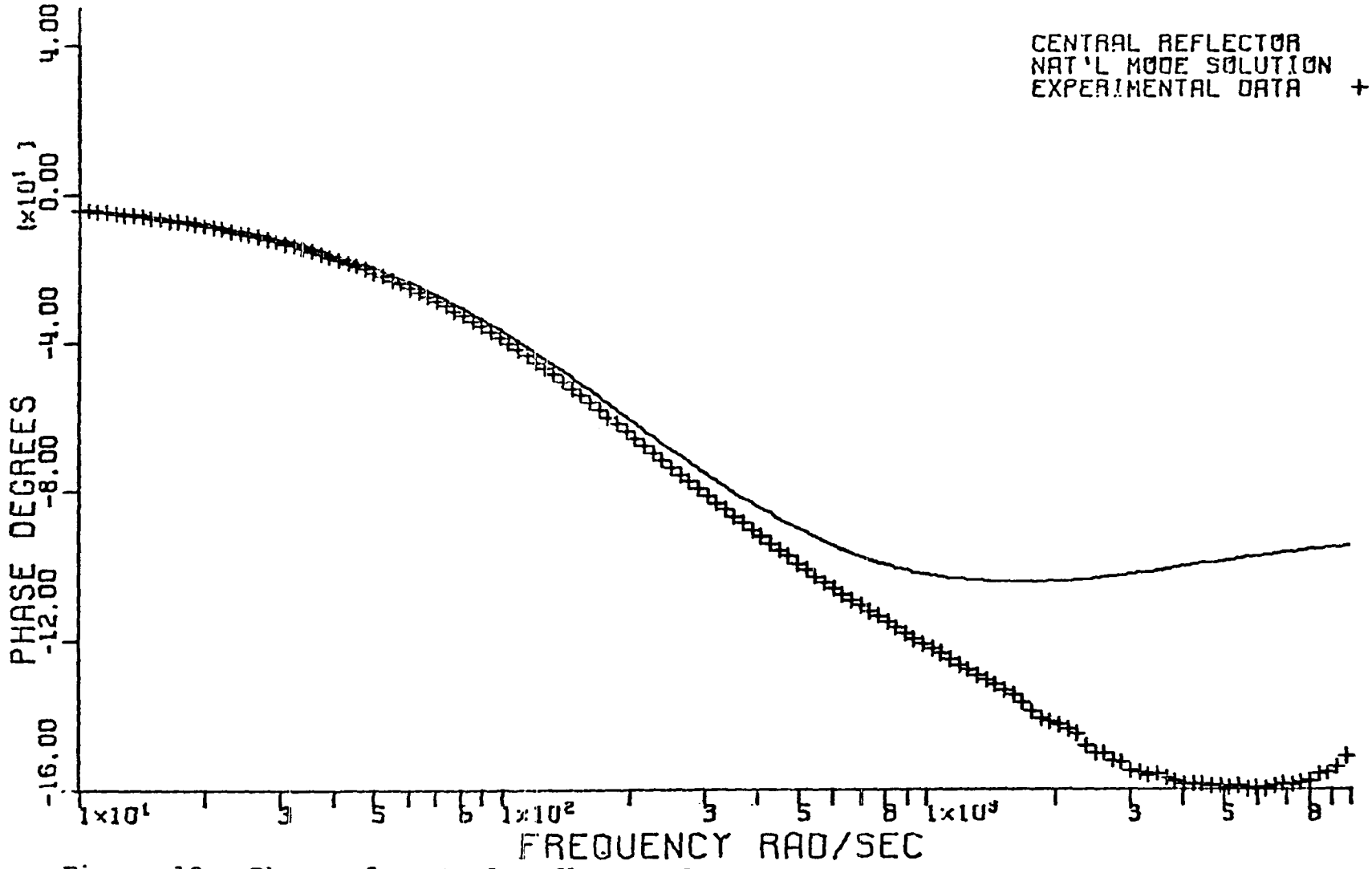

Figure 18. Phase of central reflector frequency response

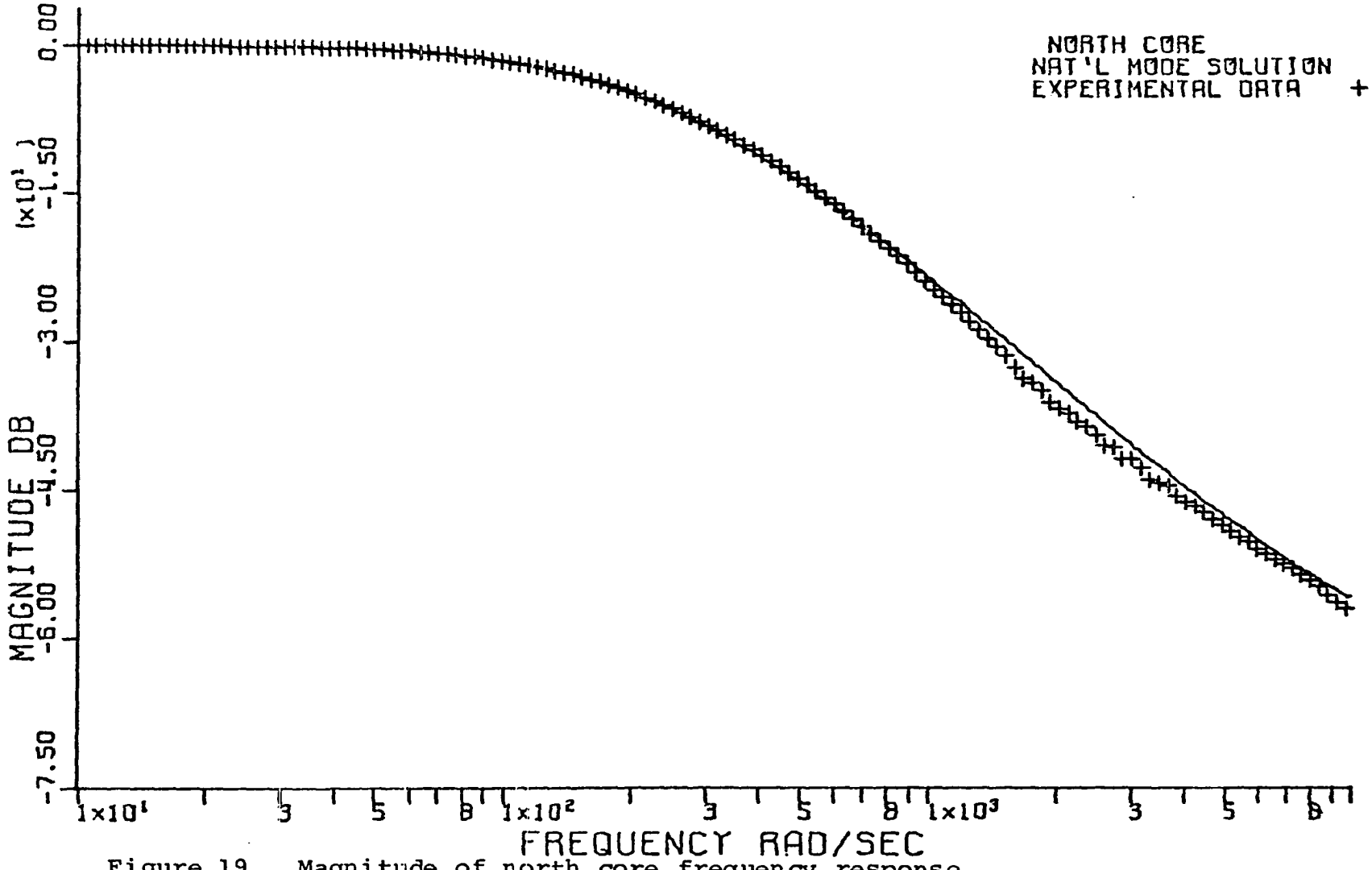

Figure 19. Magnitude of north core frequency response

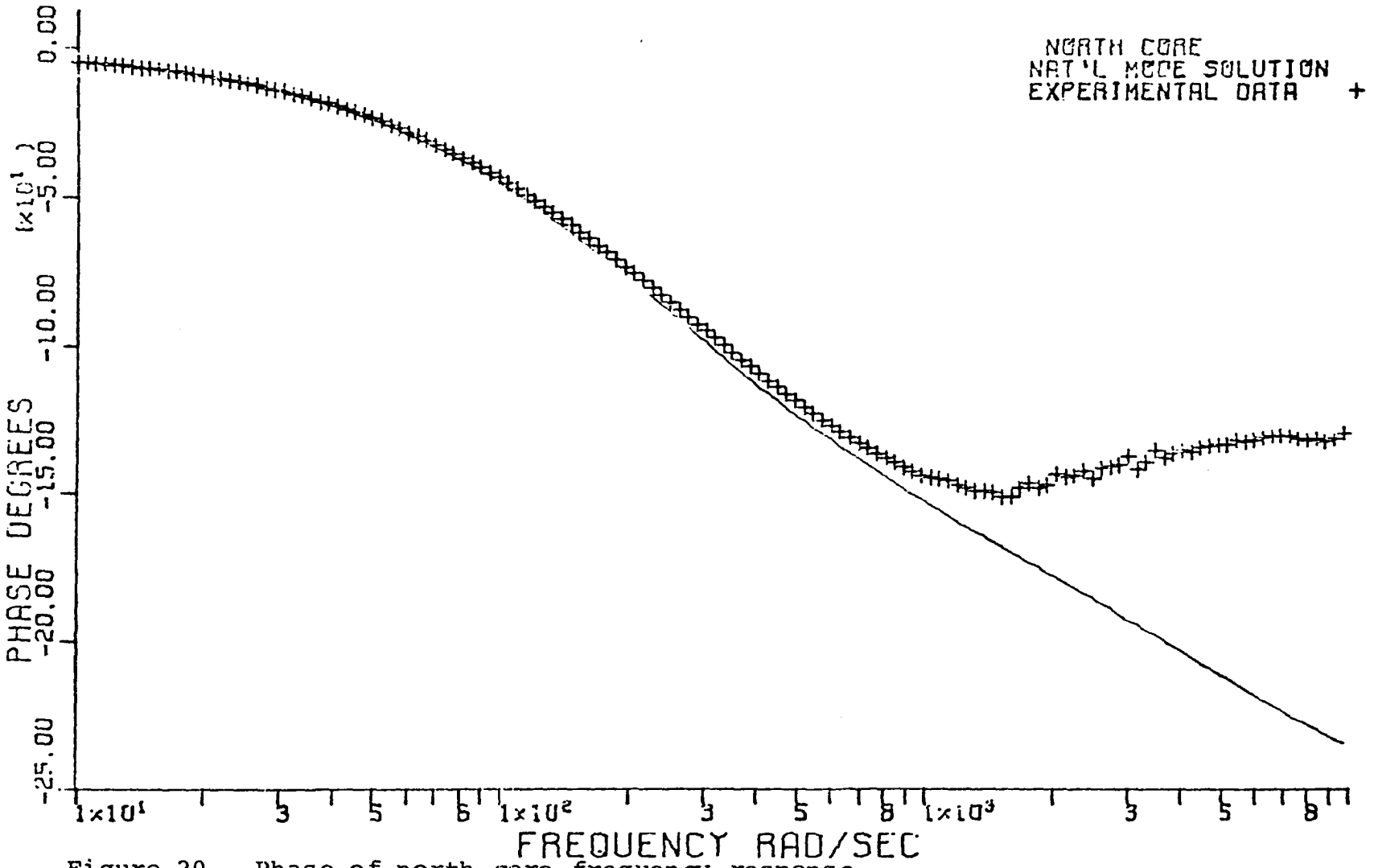

Figure 20. Phase of north core frequency response

in two group diffusion theory. The upper frequency limit of accurate NMA calculation can likely be extended by improving the algorithms but what the maximum might practically be is not shown.

The following tables have been included to document numbers considered pertinent to the NMA comparisons. Table 1 compares the eigenvalues from the present calculation with Betancourt's critical reactor eigenvalues. Although the foregoing curves all apply to the rods-in case, the rod 1 out eigenvalues have been included in the table for completeness. Table 2 lists the experimental α values and their

Table 1. Eigenvalues of the NMA

Mode Number	Critical Eigenvalue ($\nu\Sigma_f$=0.110552)	Rod 1 In Eigenvalue ($\nu\Sigma_f$=0.11958)	Rod 1 Out Eigenvalue ($\nu\Sigma_f$=0.12015)
1	-43.7942	-157.9830	-132.2364
2	-383.8615	-428.1709	-412.2364
3	-814.6350	-621.5652	-620.5391
4	-881.2175	-761.8359	-752.5293
5	-1143.015	-979.2634	-987.7058
6	-1368.782	-1296.382	-1285.288
7	-1652.127	-1558.829	-1553.641
8	-1990.517	-1898.523	-1894.113
9	-2339.455	-2365.787	-2352.262
10	-	-2701.523	-2700.420
11	-	-3240.467	-

standard deviations for several normal data runs. These values are taken directly from the GRIPE-II printouts.

Table 2. Experimental alpha values and standard deviations

Run Identifier	Rod 1 Position	Location	Alpha	Standard Deviation
3	In	South Core	+163.55	0.611
1	In	Center	+157.01	0.474
9	In	North Core	+159.11	1.075
5	In	North Core	+155.33	1.069
7	In	North Core	+156.25	0.560
14	Out	South Core	+137.07	0.925
16	Out	Center	+126.31	0.528
18	Out	North Core	+132.02	0.912

Of the three runs representing the north core "rods-in" configuration, run 7 utilized the largest number of pulses (10,000) and hence is statistically the most accurate as evidenced by the standard deviation. Figures 12-20 were based on runs 1, 3, and 7.

It is of considerable interest to note the relationship between the time domain α and the frequency domain "break frequency" which for purposes of this thesis will be defined as the 3 db down point. This relationship will be of greatest interest in Section VIII but since it is best understood in terms of the natural mode picture of the reactor, the

discussion will be presented next.

With the NMA description, prompt thermal flux can be written as an expansion of the form

$$\phi(x,t) = S_{12}e^{\omega_{12}t}\,\psi_{12}^{2}(x) + S_{22}2^{\omega_{22}t}\,\psi_{22}^{2}(x)$$

$$+\ldots\ S_{M2}e^{\omega_{M2}}\,\psi_{M2}^{2}(x).$$

At a fixed location in the reactor,

$$\phi(t) = A_1e^{\omega_{12}t} + A_2e^{\omega_{22}t} +\ldots A_me^{\omega_{m2}t} +\ldots\ A_Me^{\omega_{M2}t} \qquad (28)$$

where

$$A_m = S_{m2}\psi_{m2}^{2}\ .$$

In the frequency domain, this expression becomes

$$\phi(\omega) = \frac{A_1}{j\omega-\omega_{12}} + \frac{A_2}{j\omega-\omega_{22}} +\ldots\ \frac{A_m}{j\omega-\omega_{m2}} +\ldots\ \frac{A_M}{j\omega-\omega_{M2}} \qquad (29)$$

Note that ω_{12} is equal to $-\alpha$ and that the ω_{m2} become larger in magnitude as m increases. For the trivial case of a one term expansion, the break frequency (a true break frequency in this case) would obviously be $\omega_b = -\omega_{12} = \alpha$. In a more realistic M term expansion, the first term will still dominate $\phi(\omega)$ at low frequencies and hence ω_b (the 3 db down point) will still be approximately equal to α. The other terms in Equation (29) will make contributions of decreasing significance as m increases. Thus, the influence of these terms

can be qualitatively illustrated using the simple two term example

$$\phi(\omega) = \frac{A_1}{j\omega-\omega_{12}} + \frac{A_2}{j\omega-\omega_{22}} \quad . \tag{30}$$

Setting $\omega_1 = -\omega_{12}$ and $\omega_2 = -\omega_{22}$ for convenience and rearranging yields

$$\phi(\omega) = \frac{(A_1\omega_2+A_2\omega_1)+j\omega(A_1+A_2)}{(j\omega+\omega_1)(j\omega+\omega_2)} \quad . \tag{31}$$

Since A_1 and A_2 depend on the space dependent ψ^2 function, the manner in which the second term of Equation (30) influences $\phi(\omega)$ is also space dependent. When appropriate parameters from the NMA calculation are substituted into Equation (31), $\phi(\omega)$ is given in the south core, central reflector, and north core respectively by

$$\phi_s(\omega) = 1.02 \times 10^{-6} \frac{(j\omega+295)}{(j\omega+158)(j\omega+428)} \tag{31s}$$

$$\phi_c(\omega) = 8.23 \times 10^{-7} \frac{(j\omega+455)}{(j\omega+158)(j\omega+428)} \tag{31c}$$

$$\phi_n(\omega) = 1.70 \times 10^{-8} \frac{(j\omega+8420)}{(j\omega+158)(j\omega+428)} \quad . \tag{31n}$$

Consider first the central reflector. Here, the zero at $\omega = 455$ approximately cancels the pole at $\omega = 428$. In fact, it can easily be shown that if all NMA parameters were known with zero error, the cancellation would be exact.

Therefore, in the central reflector, the break frequency should be very nearly equal to the fundamental mode decay constant, α.

In the north core, the zero at $\omega = 8420$ is at too high a frequency to influence ω_b but the pole at $\omega = 428$ is sufficiently close to the first pole to shift ω_b slightly towards lower frequency. Consequently, the north core ω_b should be close to α but on the low side.

In the south core, the pole at $\omega = 428$ will still influence ω_b but the zero at $\omega = 295$ will over-ride and cause ω_b to shift towards higher frequency. The south core ω_b should thus be close to α but on the high side.

Table 3 shows clearly that the foregoing relationships do hold for both experimental results and the NMA model. It

Table 3. Experimental and NMA 3 db down points

Location	Rod 1 Position	Alpha	NMA 3 db Down Point	Experimental 3 db Down Point
South Core	In	164	176	172 (Run 3)
Center	In	157	151	150 (Run 1)
North Core	In	156	142	143 (Run 7)
South Core	Out	137	146	146 (Run 14)
Center	Out	126	128	126 (Run 16)
North Core	Out	132	122	126 (Run 18)

is interesting to note that while the NMA is not capable of predicting the α space dependence, it does correctly predict the trend of the ω_b space dependence.

VII. COMPARISON OF NODEAN'S MODEL WITH EXPERIMENT

Nodean's computations [42], like those of Betancourt [8], were based on two group diffusion theory with one group of delayed neutrons. However, Nodean first illustrated his method of solution with the simple case of a single region slab reactor utilizing one group diffusion theory with one group of delayed neutrons. A portion of that discussion will be reproduced here, both for reader convenience and to show that the method is valid for source as well as absorber perturbations.

For the simple model postulated above, the basic diffusion equations are

$$D\frac{d^2}{dx^2}\phi(x,t) - \Sigma_a\phi(x,t)+\nu\Sigma_f(1-\beta)e^{-B^2\tau}\phi(x,t) + C(x,t)e^{-B^2\tau} = \frac{1}{V}\frac{\partial\phi(x,t)}{t} \tag{32a}$$

$$\nu\Sigma_f\beta\phi(x,t) - \lambda C(x,t) = \frac{\partial C(x,t)}{\partial t} \tag{32b}$$

where the symbols have their standard meanings. Note that in the steady state condition the time derivatives become zero. Nodean assumed a small perturbation, $\Delta\Sigma_a(x,t)$, in the absorption cross section so that

$$\Sigma_a(x,t) = \Sigma_{a0} + \Delta\Sigma_a(x,t) \tag{33a}$$

where Σ_{a0} is the constant steady state value. The flux and precursor density will then undergo perturbations given by

$$\phi(x,t) = \phi_0(x) + \Delta\phi(x,t) \tag{33b}$$

$$C(x,t) = C_0(x) + \Delta C(x,t) \tag{33c}$$

where $\phi_0(x)$ and $C_0(x)$ represent the steady state flux and precursor density distributions. Substituting Equations (33) into Equations (32), noting that the steady state parts of the equations sum to zero, and assuming the product $\Delta\Sigma_a\Delta\phi$ is negligibly small, leads to the resultant equations

$$D\frac{d^2}{dx^2}\Delta\phi(x,t) - \Sigma_{a0}\Delta\phi(x,t) + \Delta\Sigma_a(x,t)\phi_0(x) + \nu\Sigma_f(1-\beta)e^{-B^2\tau}\Delta\phi(x,t) + \lambda e^{-B^2\tau}\Delta C(x,t) = \frac{1}{V}\frac{\partial\Delta\phi(x,t)}{\partial t} \tag{34a}$$

$$\nu\Sigma_f\beta\Delta\phi(x,t) - \lambda\Delta C(x,t) = \frac{\partial\Delta C(x,t)}{\partial t}\ . \tag{34b}$$

Nodean assumed the absorber perturbation to be sinusoidal in time but confined to a single plane in the reactor at $x = x'$. Mathematically, these features can be expressed by

$$\Delta\Sigma_a(x,t) = \delta(x-x')\left|\overline{\Delta\Sigma}_a\right|e^{j\omega t}. \tag{35a}$$

Since the equations have been linearized by ignoring $\Delta\Sigma_a\Delta\phi$, the flux and precursor density will also oscillate with frequency ω so that

$$\Delta\phi(x,t) = \Delta\hat{\phi}(x,\omega)e^{j\omega t} \tag{35b}$$

and

$$\Delta C(x,t) = \Delta\hat{C}(x,\omega)e^{j\omega t} \tag{35c}$$

where $\Delta\hat{\phi}$ and $\Delta\hat{C}$ are the complex amplitudes.

After substituting Equations (35) into Equations (34) and dividing out the common $e^{j\omega t}$, the equations become

$$D\frac{d^2}{dx^2}\Delta\hat{\phi}(x,\omega) - \Sigma_{a0}\Delta\hat{\phi}(x,\omega)+\delta(x-x')|\Delta\bar{\Sigma}_a|\phi_0(x)$$

$$+ \nu\Sigma_f(1-\beta)e^{-B^2\tau}\Delta\hat{\phi}(x,\omega) + \lambda\Delta\hat{C}(x,\omega)e^{-B^2\tau}$$

$$= \frac{j\omega}{V}\Delta\hat{\phi}(x,\omega) \tag{36a}$$

$$\nu\Sigma_f\beta\Delta\hat{\phi}(x,\omega) - \lambda\Delta\hat{C}(x,\omega) = j\omega\Delta\hat{C}(x,\omega) \tag{36b}$$

Solving Equation (36b) for $\Delta\hat{C}(x,\omega)$ and substituting into Equation (36a) yields

$$\frac{d^2}{dx^2}\Delta\hat{\phi}(x,\omega) + B_m^2\Delta\hat{\phi}(x,\omega) + \frac{|\Delta\bar{\Sigma}_a|\phi_0(x)}{D}\delta(x-x') = 0 \tag{37}$$

where

$$B_m^2 = \frac{1}{D}\left[-\Sigma_{a0}+\nu\Sigma_f(1-\beta)e^{-B^2\tau} + \frac{\lambda\nu\Sigma_f\beta e^{-B^2\tau}}{\lambda+j\omega} \quad \frac{j\omega}{V}\right] .$$

Equation (37) is of the form

$$Ly(x) + \Phi(x) = 0 \tag{38}$$

where L is the linear, self-adjoint, differential operator

$$L = \frac{d}{dx}\left(p\frac{d}{dx}\right)+q = p\frac{d^2}{dx^2} + \frac{dp}{dx}\frac{d}{dx} + q$$

and $\Phi(x)$ is a driving function. In the present problem,

$$\Phi(x) = \frac{|\Delta\bar{\Sigma}_a|}{D}\phi_0(x)\delta(x-x') \quad . \tag{39}$$

Following Hildebrand [26], the solution to Equation (38) can be expressed as

$$y(x) = \int_a^b G(x,\varepsilon)\Phi(\varepsilon)d\varepsilon \quad . \tag{40}$$

The function $G(x,\varepsilon)$ is called the Green's function, and for a given number ε, is given by $G_1(x)$ for $x<\varepsilon$ and by $G_2(x)$ for $x>\varepsilon$. The Green's function satisfies the following conditions:

1) $G(x,\varepsilon)$ satisfies the equation $LG = 0$; that is, $LG_1 = 0$ when $x<\varepsilon$ and $LG_2 = 0$ when $x>\varepsilon$.

2) $G(x,\varepsilon)$ satisfies prescribed boundary conditions; that is $G_1(a) = 0$ and $G_2(b) = 0$.

3) $G(x,\varepsilon)$ is continuous at $x = \varepsilon$; that is $G_1(\varepsilon) = G_2(\varepsilon)$.

4) The first derivative of $G(x,\varepsilon)$ has a discontinuity of magnitude

$\frac{-1}{p(\varepsilon)}$ at $x = \varepsilon$; that is, $\frac{dG_2(\varepsilon)}{dx} - \frac{dG_1(\varepsilon)}{dx} = \frac{-1}{p(\varepsilon)}$.

Substituting Equation (39) into (40) and setting $y(x) = \phi(x,\omega)$ yields

$$\phi(x,\omega) = \frac{|\Delta\bar{\Sigma}_a|}{D} \int_a^b G(x,\varepsilon)\phi_0(\varepsilon)\delta(\varepsilon-x')d\varepsilon.$$

Utilizing the delta function properties,

$$\phi(x,\omega) = \frac{|\Delta\bar{\Sigma}_a|}{D} \phi_0(x)G(x,x') \tag{41}$$

and the problem has now been reduced to one of determining $G(x,x')$ from the 4 conditions on the Green's function listed above.

From the first condition,

$$\frac{d^2G}{dx^2} + B_m{}^2G = 0 . \tag{42}$$

By the usual techniques for solving differential equations, the solution to Equation (42) is recognized to be

$$G_1(x) = A_1e^{jB_mx} + A_2e^{-jB_mx} \qquad \text{for } x < x'$$

$$G_2(x) = A_3e^{jB_mx} + A_{4e}^{-jB_mx} \qquad \text{for } x > x'.$$

The remaining conditions lead to 4 simultaneous algebraic equations from which the A_i may be found and thus the solution for $\hat{\Delta\phi}(x,\omega)$ is

$$\Delta\hat{\phi}(x,\omega) = \frac{|\Delta\bar{\Sigma}_a|\phi_0(x)}{D} [A_1e^{jB_mx} + A_2e^{-jB_mx}] \quad \text{for } x < x'$$

$$\Delta\hat{\phi}(x,\omega) = \frac{|\Delta\bar{\Sigma}_a|\phi_0(x)}{D} [A_3e^{jB_mx} + A_4e^{-jB_mx}] \quad \text{for } x > x'.$$

Although the mathematical manipulations become considerably more complex, the Green's function approach outlined above can also be carried through for the two group model of the multi-region UTR-10. Nodean did exactly that with the perturbation being applied to the slow group absorption cross section. Transverse buckling terms were included to account for leakage in the y and z directions.

Since the pulsed neutron experiment is directly equivalent [48] to an oscillating source experiment, it is convenient to demonstrate the applicability of the model to the present experiment by showing that it is immaterial whether the perturbation is considered to be an absorber perturbation or a source perturbation. The simple one region, one group model will also be used for this purpose.

If an external source term is postulated, Equations (32) become

$$D\frac{d^2}{dx^2}\phi(x,t) - \Sigma_a\phi(x,t) + \nu\Sigma_f(1-\beta)e^{-B^2\tau} + C(x,t)e^{-B^2\tau} + S(x,t) = \frac{1}{V}\frac{\partial\phi(x,t)}{\partial t} \tag{43a}$$

$$\nu\Sigma_f\beta\phi(x,t) - \lambda C(x,t) = \frac{\partial C(x,t)}{\partial t} \cdot \tag{43b}$$

If a source perturbation of the form

$$S(x,t) = S_0 + \Delta S(x,t) \tag{44a}$$

is introduced, the flux and precursor density can again be

written as

$$\phi(x,t) = \phi_0 + \Delta\phi(x,t) \tag{44b}$$

and

$$C(x,t) = C_0 + \Delta C(x,t) \ . \tag{44c}$$

Substituting Equations (44) into Equations (43) and realizing that the steady state terms sum to zero yields

$$D\frac{d^2}{dx^2}\Delta\phi(x,t) - \Sigma_a\Delta\phi(x,t) + \nu\Sigma_f(1-\beta)e^{-B^2\tau}\Delta\phi(x,t)$$

$$+ \lambda e^{-B^2\tau}\Delta C(x,t) + \Delta S(x,t) = \frac{1}{V}\frac{\partial\Delta\phi(x,t)}{\partial t} \tag{45a}$$

$$\nu\Sigma_f\beta\Delta\phi(x,t) - \lambda\Delta C(x,t) = \frac{\partial C(x,t)}{\partial t} \ . \tag{45b}$$

Taking the source perturbation to be

$$\Delta S(x,t) = \delta(x-x')|\Delta\bar{S}|e^{j\omega t} \ , \tag{46a}$$

the flux and precursor density again become

$$\Delta\phi(x,t) = \Delta\hat{\phi}(x,\omega)e^{j\omega t} \tag{46b}$$

and

$$\Delta C(x,t) = \Delta\hat{C}(x,\omega)e^{j\omega t} \ . \tag{46c}$$

Note that for the source perturbation, it is not necessary to ignore second order terms like $\Delta\Sigma_a\Delta\phi$ to linearize the equations. Hence, the following equations will remain valid even for large amplitude source perturbations whereas the previous absorber perturbations were implied to be small.

When Equations (46) are substituted into Equations (45) and manipulated in the same manner as their absorber perturbation counterparts, the result is

$$\frac{d^2}{dx^2}\Delta\phi(x,\omega) + B_m^2\Delta\phi(x,\omega) + \frac{|\Delta\bar{S}|}{D}\delta(x-x') = 0 \qquad (47)$$

Solving Equation (47) via the Green's function technique yields

$$\Delta\hat{\phi}(x,\omega) = \frac{|\Delta\bar{S}|}{D}G(x,x'). \qquad (48)$$

Comparing Equation (48) with Equation (41) shows that the only difference in form is through the flux $\phi_0(x)$ which appears in Equation (41). But, at a fixed x, $\phi_0(x)$ becomes a constant multiplying a perturbation magnitude which is arbitrary in the first place. Thus, the perturbation introduced with Nodean's existing computer codes might equally well represent an absorber perturbation or a source perturbation. In fact, considering it to be a source perturbation does not imply the small amplitude restriction that must hold for an absorber perturbation.

To model the present subcritical experiment with Nodean's model, $\nu\Sigma_f$ was taken to be the value found from the NMA calculation, the remaining reactor parameters were taken to be those of Appendix A, and frequency response was computed at a total of 41 selected frequencies ranging from 10 to 10,000 rad/sec.

These frequencies were chosen with maximum density in the vicinity of 2000 rad/sec to provide best definition in the region of the anticipated inflection point. Two aspects of the calculation which deserve further comment here are: 1) the manner of dealing with delayed neutrons, and 2) the choice of $\nu\Sigma_f$.

Except for minor modifications to expand the number of frequency points and provide for punched output, Nodean's programs were not changed. Consequently, the computed frequency response contains the delayed neutron response as well as the prompt. For practical purposes, however, the delayed neutron influence is negligible above 10 rad/sec so that comparisons between model and experiment are still valid. This claim can be substantiated with the following argument.

In the time domain, the delayed neutrons make only a slowly varying contribution to the flux. Therefore, in the frequency domain the contribution will appear only at low frequencies [57]. The appropriate question to ask becomes, "Is 10 rad/sec a sufficiently high frequency to be outside the range of delayed neutron influence?" The answer can most easily be found through the point kinetics model which should actually be quite accurate at these low frequencies. Within the framework of the point kinetics equations using one group of delayed neutrons, frequency response can be expressed as

$$G(j\omega) = \frac{K(j\omega+\lambda)}{j\omega(j\omega+\beta/\ell)} \quad . \tag{49}$$

At high frequencies, Equation (49) becomes

$$G(j\omega) = \frac{K}{j\omega+\beta/\ell}$$

and thus the delayed neutron contribution has to enter through the factor $\frac{j\omega+\lambda}{j\omega}$. The accepted value for λ is 0.08 and by a frequer y of 10 rad/sec, $\frac{j\omega+\lambda}{j\omega}$ has been reduced to an excellent approximation of unity. The delayed neutron contribution is therefore negligible over the frequency range of interest.

As in the NMA calculation, Nodean's model must be normalized to the experiment if meaningful results are to be obtained. Since the NMA and Nodean's method are based on the same differential equations, assuming $\nu\Sigma_f$ to be the NMA value was a logical first choice. It was necessary, however, to provide a check on this assumption. Since Nodean's method calculates a response in the frequency domain only, it was not possible to compare fundamental decay constants as was done with the NMA. Instead, the break frequencies as defined in Section VI were compared between model and experiment. As discussed in Section VI, the break frequency is expected to be space dependent and all locations should be considered.

Table 4 displays this comparison and shows that the

choice of $\nu\Sigma_f$ was indeed correct. Finding the best agreement in the north core coincides with having normalized to the north core initially. Table 4 also shows that while Nodean's model (like the NMA) does not predict the ω_b space dependence exactly, the trends are certainly correct.

Table 4. Experimental and Nodean's method 3 db down points

Location	Rod 1 Position	Nodean's Method ω_b	Experimental ω_b
South Core	In	196	172 (Run 3)
Center	In	158	150 (Run 1)
North Core	In	146	143 (Run 7)
South Core	Out	158	146 (Run 14)
Center	Out	135	126 (Run 16)
North Core	Out	124	126 (Run 18)

Figures 21-26 show the Nodean's method calculation for the UTR-10 compared with experimental results (rods-in configuration). Nodean's method curves begin to depart from the experimental at lower frequencies than do the NMA curves. The difference could be due to the fact that the NMA calculation models the spatial distribution of the slowing down source whereas Nodean's method assumes a localized thermal source. However, the departure from experiment for Nodean's method is of an entirely different nature than the NMA departure. Nodean's solution is not limited by the early time convergence

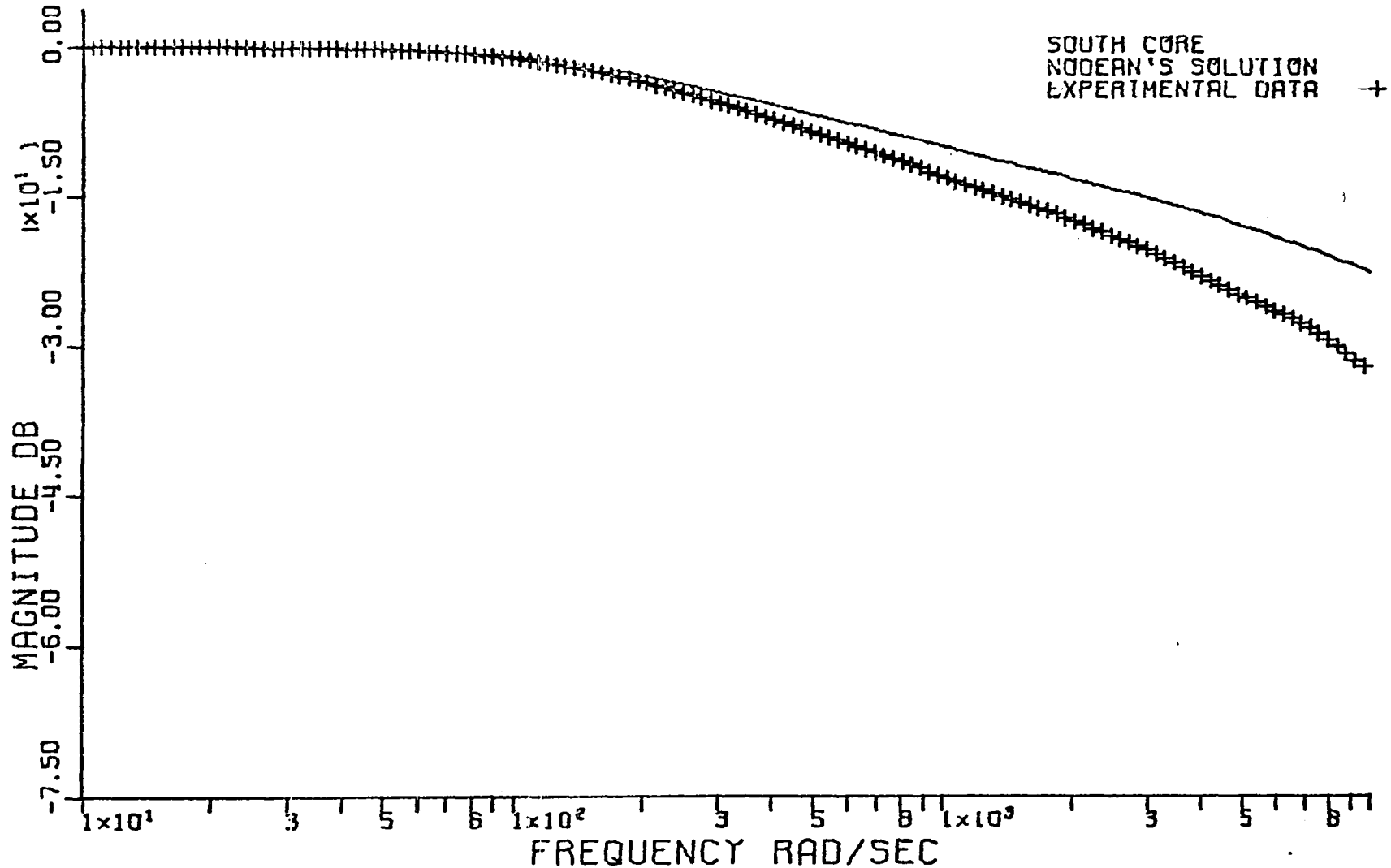

Figure 21. Magnitude of south core frequency response

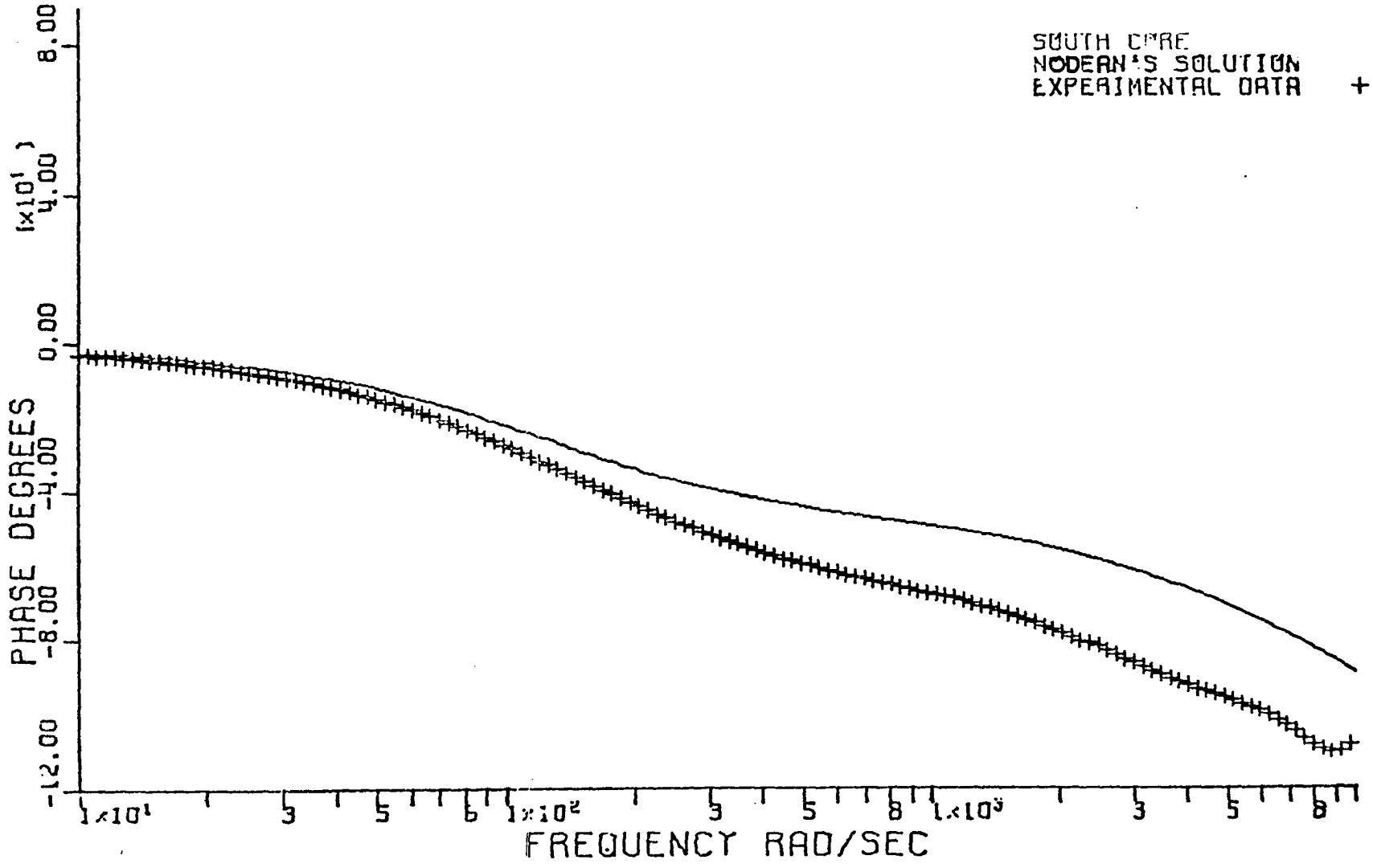

Figure 22. Phase of south core frequency response

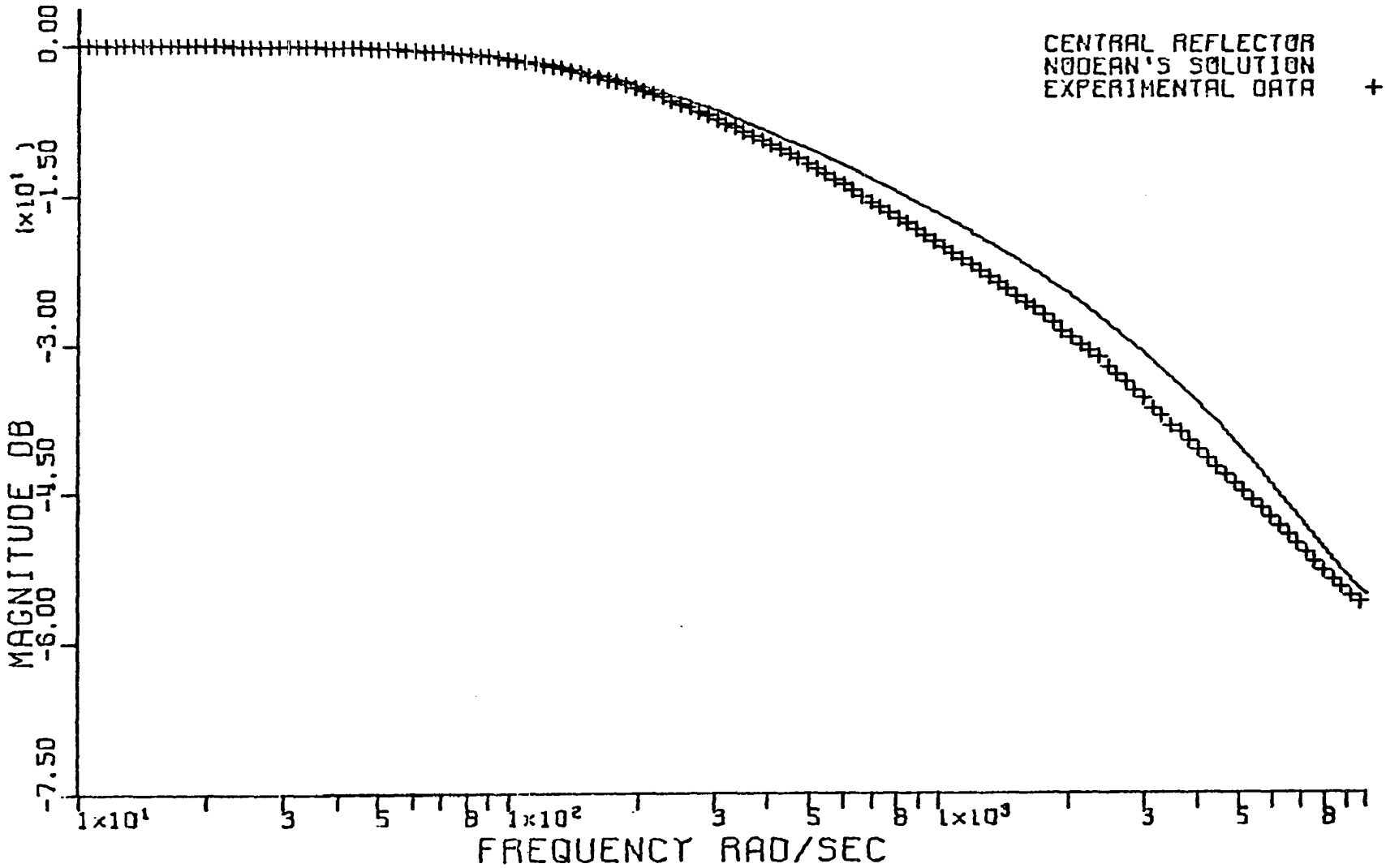

Figure 23. Magnitude of central reflector frequency response

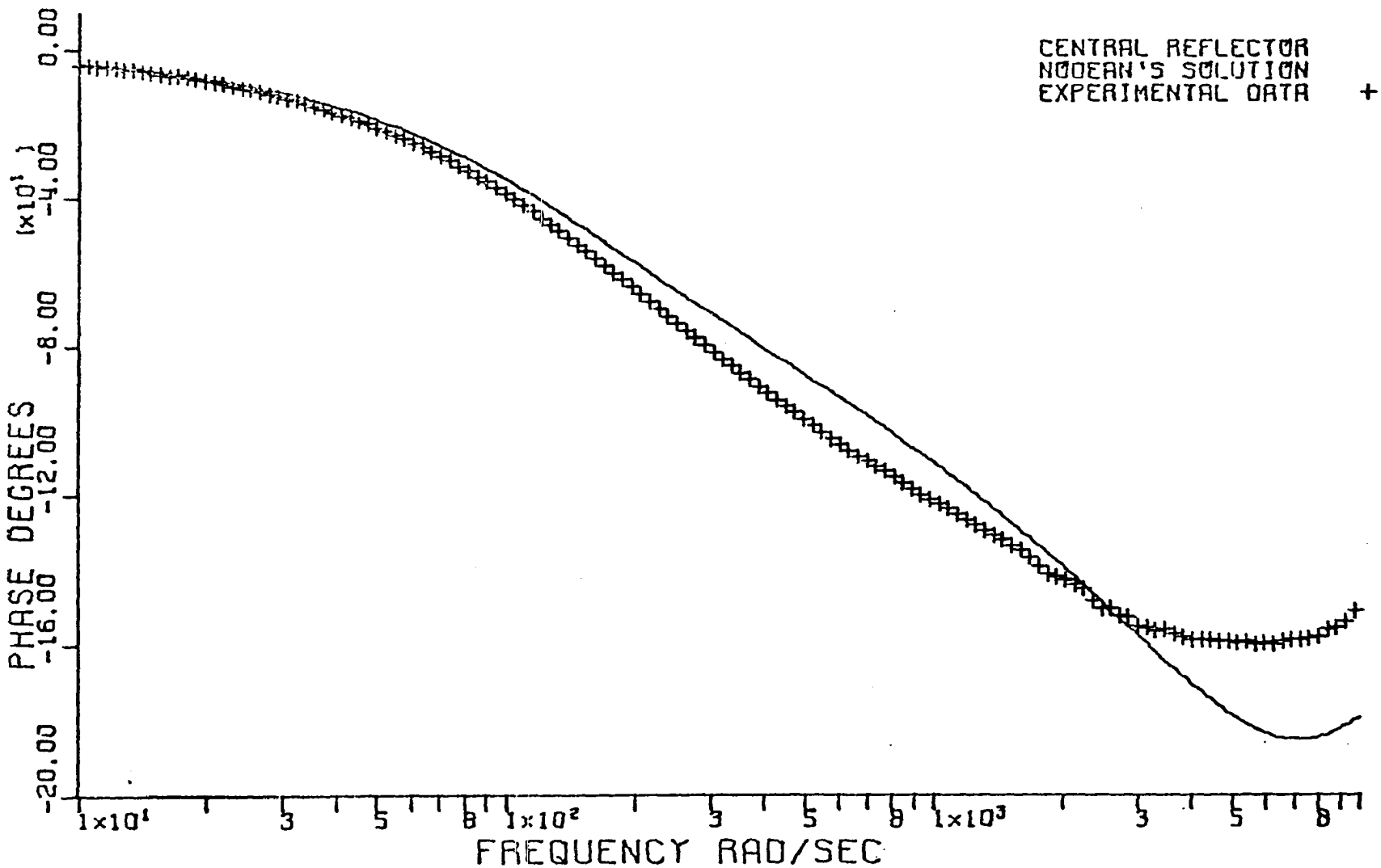

Figure 24. Phase of central reflector frequency response

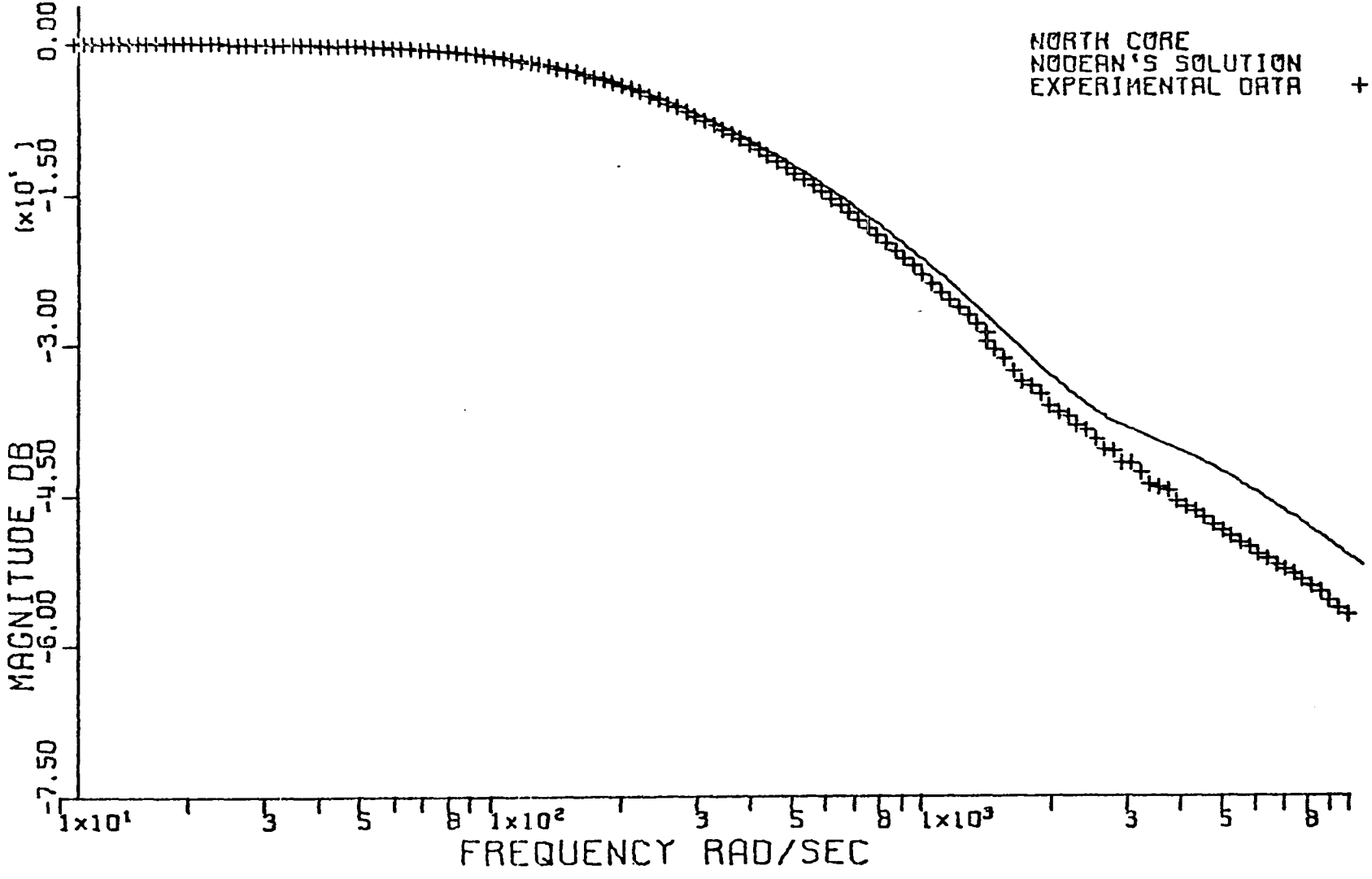

Figure 25. Magnitude of north core frequency response

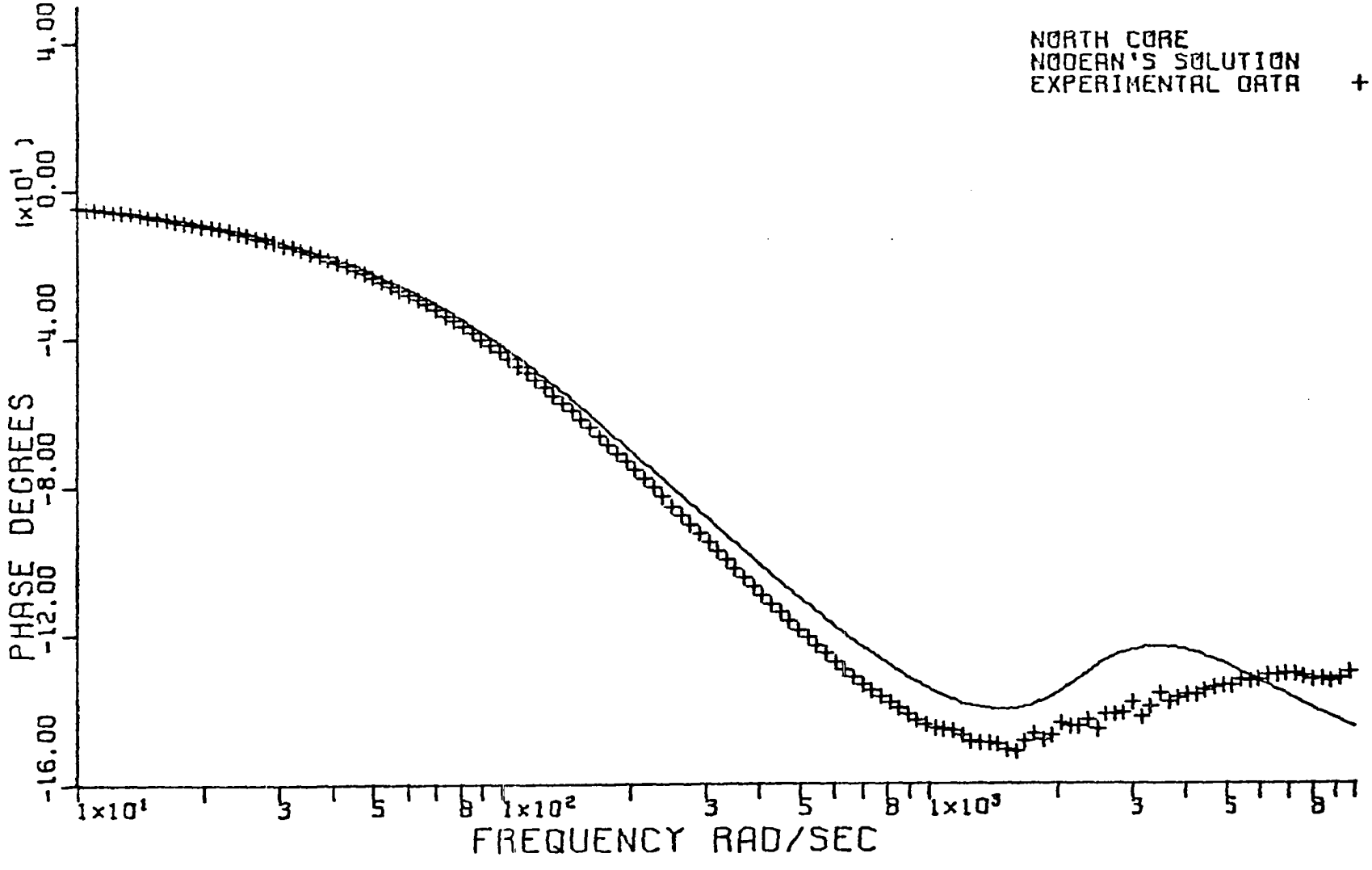

Figure 26. Phase of north core frequency response

problem of the NMA and in all cases, Nodean's method correctly predicts curve shapes at high frequencies whereas the NMA does not. In the north core, for example, both the inflection point in the magnitude curve and the upswing in the phase are predicted by Nodean's model. It is true that numerical values of the functions are not in complete agreement with experiment, but nevertheless, the trends are correct.

VIII. COMPARISON OF WIGLE SOLUTIONS WITH EXPERIMENT

WIGLE [11] is a finite difference scheme for solving the two group diffusion equations in a one dimensional, multi-region reactor. The user may elect to use from 0 to 6 groups of delayed neutrons. WIGLE was originally written for the Philco 2000 computer but has been modified at Iowa State University to the extent necessary to run on the IBM 360/65 computer.

Through use of the source function described by Appendix C, it was possible to model the present pulsed neutron experiment with WIGLE. An additional modification which allowed the thermal flux time functions at locations of interest to be punched on cards was introduced. Fourier transformation was then accomplished using routine FOURCO [5] in the same way as when processing experimental data except that smoothing was not necessary since the WIGLE output does not contain scatter. WIGLE output was normally punched every 100 microseconds but to provide an aliasing check for FOURCO, a special run was made with output every 50 microseconds. Aliasing was not a problem.

When running WIGLE, the user must supply the reactor parameters, select the number of delayed neutron groups, choose the size of the space and time grids, and numerically define

the space-time source. Up to 10 spatial regions may be defined within the reactor and although the mesh size, Δx, must remain constant within a given region, it may vary between regions. Similarly, the time step, Δt, may be changed at pre-selected times so that smaller steps may be used during periods of anticipated rapid change.

The reactor parameters were again chosen as described in Appendix A and as in the NMA calculation, normalization to experiment was accomplished by adjusting $\nu\Sigma_f$ to match fundamental decay constants between model and experiment. Since WIGLE is based on the same differential equations as the previous models, it might be expected that $\nu\Sigma_f$ would remain unchanged. This thinking would probably be true if WIGLE were run with one group of delayed neutrons. In the present problem, however, the zero delayed group option was selected since prompt response was being modeled. When used in this mode, WIGLE takes the delayed neutron fraction, β, to be zero and thus increases the slow flux coefficient in the fast group equation as well as driving the precursor density to zero (see Appendix A). To compensate, $\nu\Sigma_f$ must be correspondingly decreased. WIGLE solutions were run for the rods-in configuration only and the correct $\nu\Sigma_f$ for this case was found to be 0.11823. In the WIGLE code, the "transfer" or removal cross section is input separately to each neutron group so that the transverse buckling corrections described in Appendix A could

easily be made by appropriately adjusting the input cross sections.

Referring to Figure A.1, the UTR-10 was subdivided into the following 7 spatial regions:

Region 1 - x = 0 to x = 90 cm

Region 2 - x = 90 to x = 105 cm

Region 3 - x = 105 to x = 120 cm

Region 4 - x = 120 to x = 165 cm

Region 5 - x = 165 to x = 180 cm

Region 6 - x = 180 to x = 195 cm

Region 7 - x = 195 to x = 285 cm.

Regions 3 and 5 are the core tanks, but all other regions are pure reflector. The reflector was thus subdivided so that a relatively large Δx (15 cm) could be used in regions 1 and 7 where the flux was expected to vary slowly with x. In all other regions, Δx was taken to be 1 cm.

Since the flux changes rapidly at early times, the initial Δt was chosen to be 1 microsecond. As time increases, however, the flux does not change as quickly and in the interest of computation efficiency, it is desirable to increase Δt. Table 5 shows the schedule of time steps used for normal runs. The single exception to this schedule occurred in the aliasing check where the time step obviously could not be increased to more than 50 microseconds. Convergence of the two solutions,

Table 5. Time steps used in WIGLE calculation

Time (sec)	Δt (sec)
0 to 2×10^{-5}	1×10^{-6}
2×10^{-5} to 10^{-4}	5×10^{-6}
10^{-4} to 10^{-3}	20×10^{-6}
greater than 10^{-3}	100×10^{-6}

however, served to justify use of the larger time step.

In using WIGLE, both the space and time dependence of the source must be specified. As in the NMA calculation, the source space dependence was assumed to be that of Appendix C. For WIGLE, however, the source time function was assumed to be a rectangular pulse 3 microseconds wide.

Figures 27, 28, and 29 show respectively the WIGLE solutions compared with experimental results in the south core, central reflector, and north core. Although the WIGLE solution fits the experiment extremely well in the central reflector, it contains significant early time errors in both of the multiplying regions - the most obvious being in the north core. The reasons for these errors have not been thoroughly investigated but within the WIGLE framework, about all that could be done would be to reduce the space and time mesh sizes. If such manipulation failed to improve the comparison, the logical conclusion would be that two group diffusion theory

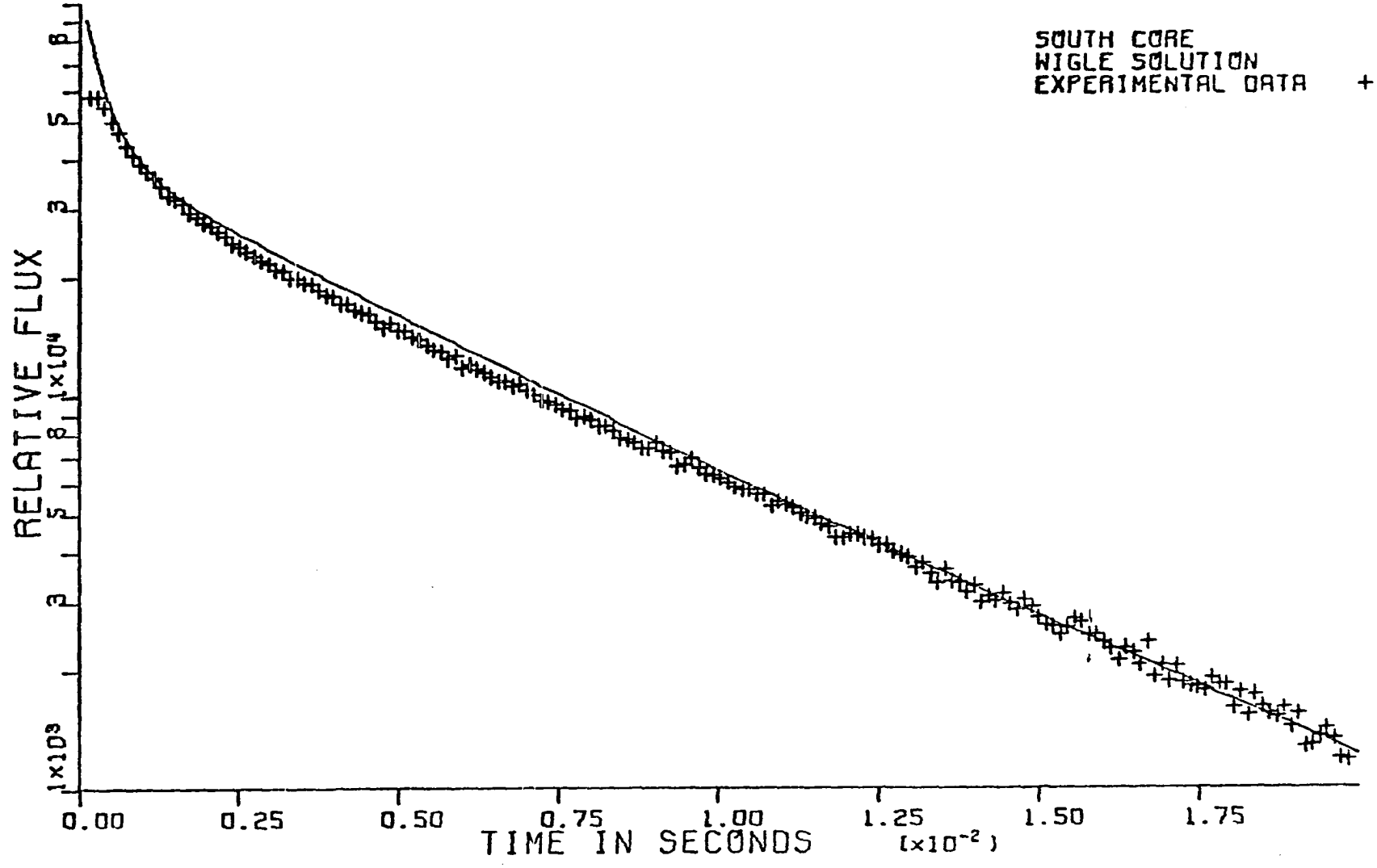

Figure 27. South core time response after burst

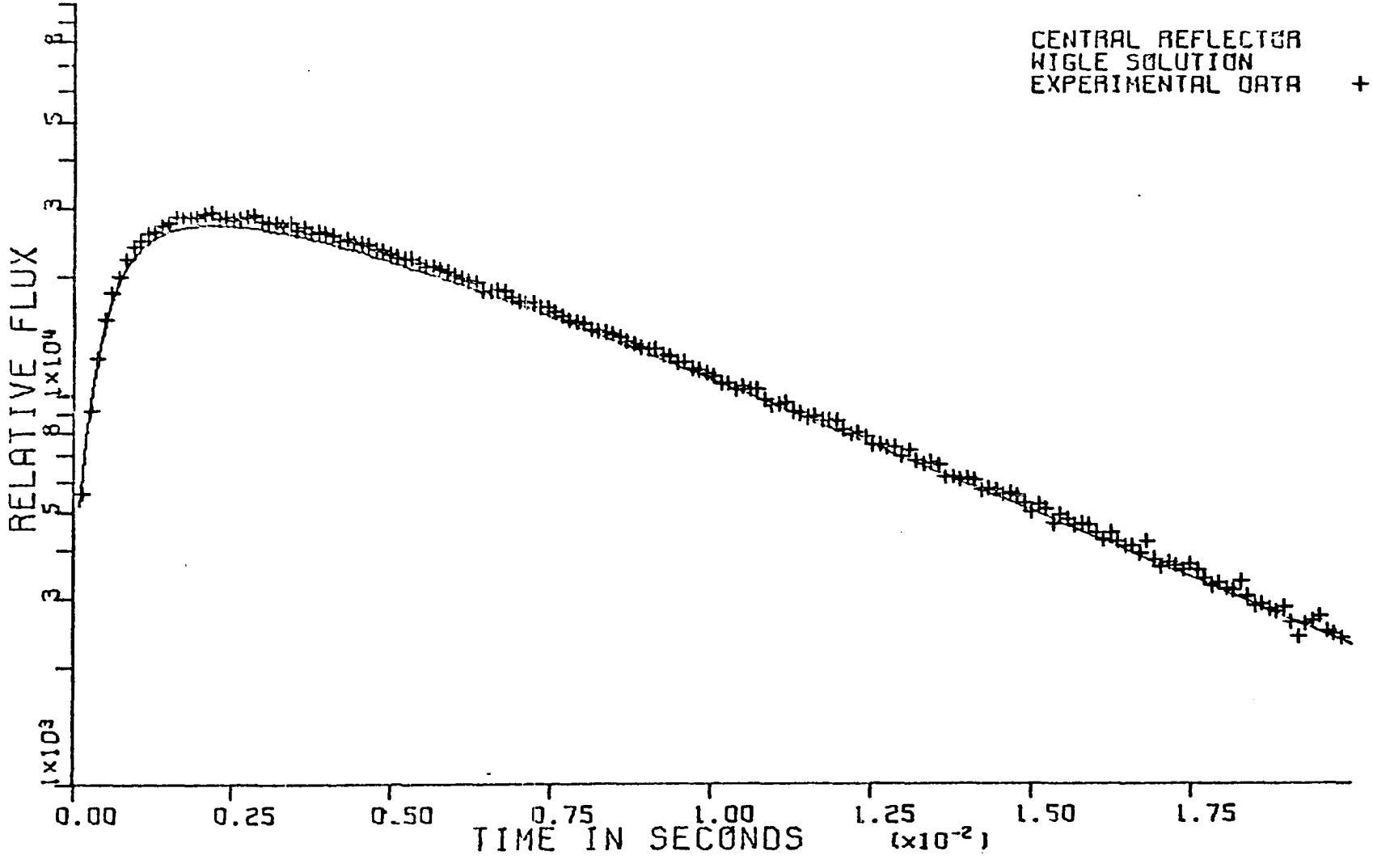

Figure 28. Central reflector time response after burst

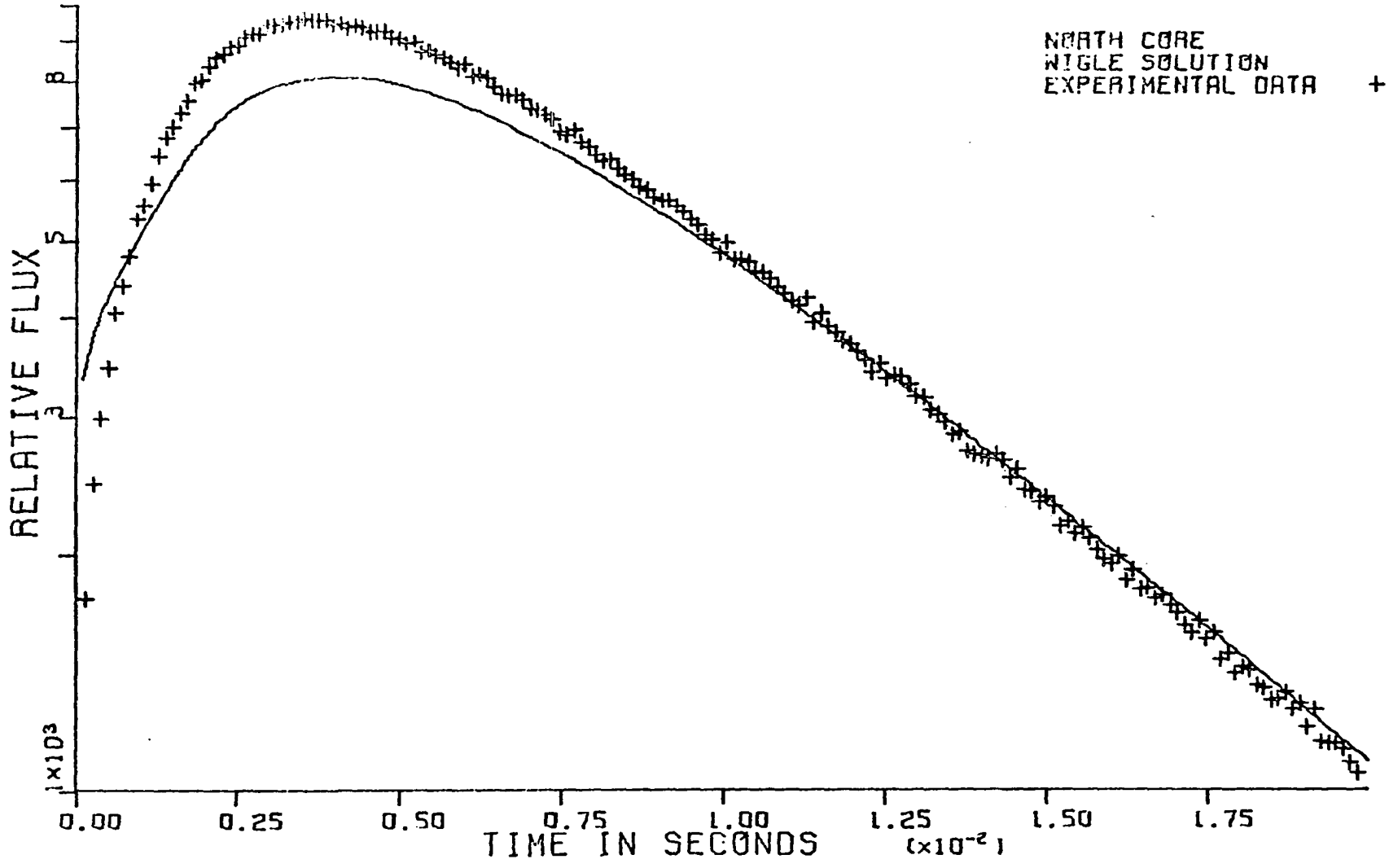

Figure 29. North core time response after burst

is simply inadequate to provide sufficient description. It should be pointed out that previous experience with WIGLE at Iowa State University suggests that the mesh sizes chosen should be adequate [15]. Further, significant reductions in these sizes would sharply increase the cost of running WIGLE.

The frequency response curves generated from the WIGLE solutions are compared with experiment in Figures 30-35. As would be expected from the time domain comparisons, agreement is best in the central reflector and poorest in the north core. Even in the north core, however, agreement is good to at least 1000 rad/sec for the magnitude curve and to approximately 500 rad/sec for the phase. Further, both the magnitude inflection point and the phase upswing do appear (although exaggerated) in the WIGLE results as well as the experimental. These characteristics are thought due to the fact that WIGLE, like the NMA, accounts for the spatial dependence of the source but unlike the NMA, is not plagued by early time convergence problem.

It is interesting to note that although WIGLE did not predict the fundamental decay constant space dependence (all WIGLE α's were the same), the break frequency space dependence again compares favorably with experiment. This comparison is shown in Table 6.

Table 6. Experimental and WIGLE 3 db down points

Location	WIGLE ω_b sec^{-1}	Experiment ω_b sec^{-1}
South Core	178	172
Center	153	150
North Core	139	143

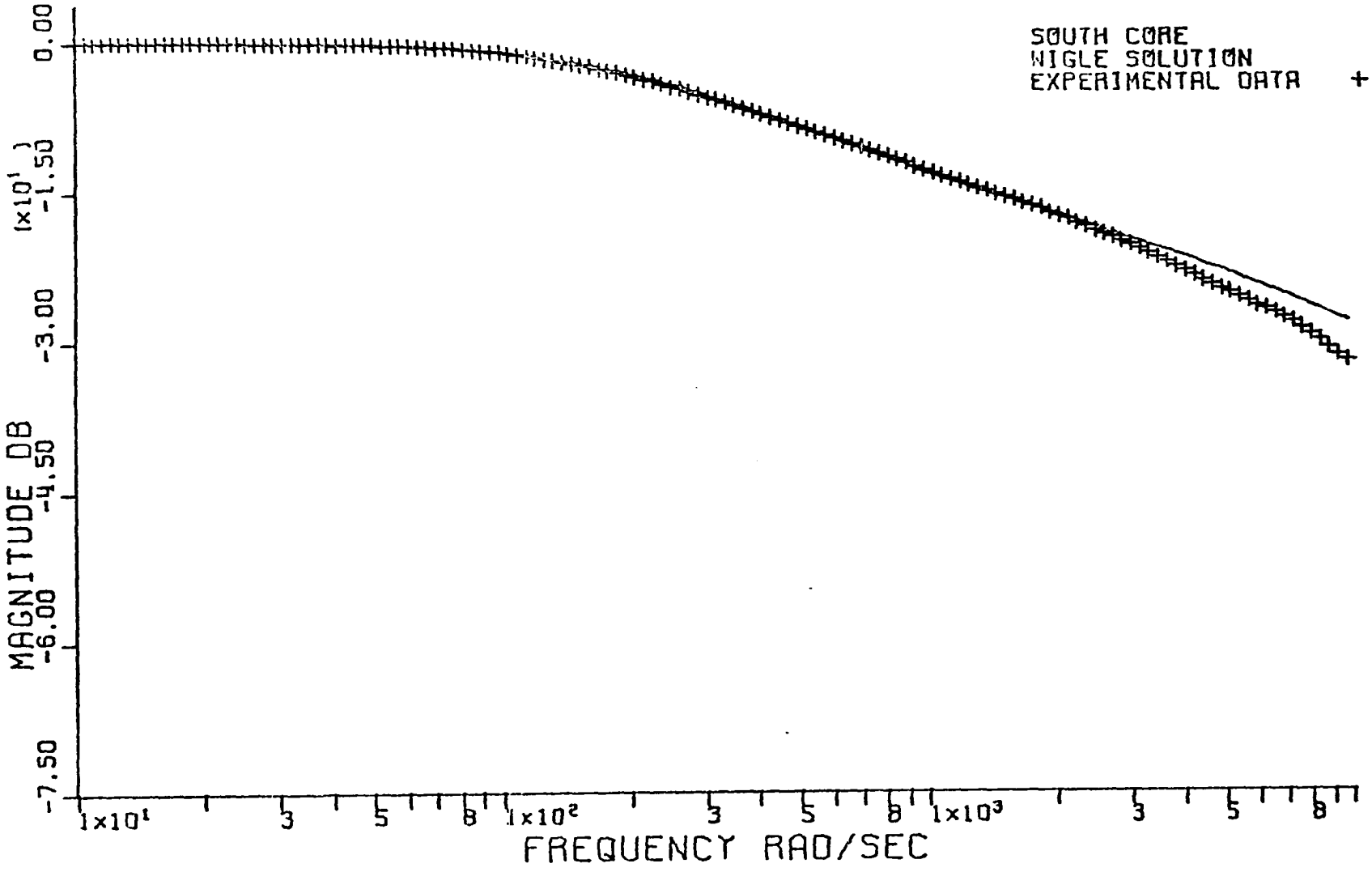

Figure 30. Magnitude of south core frequency response

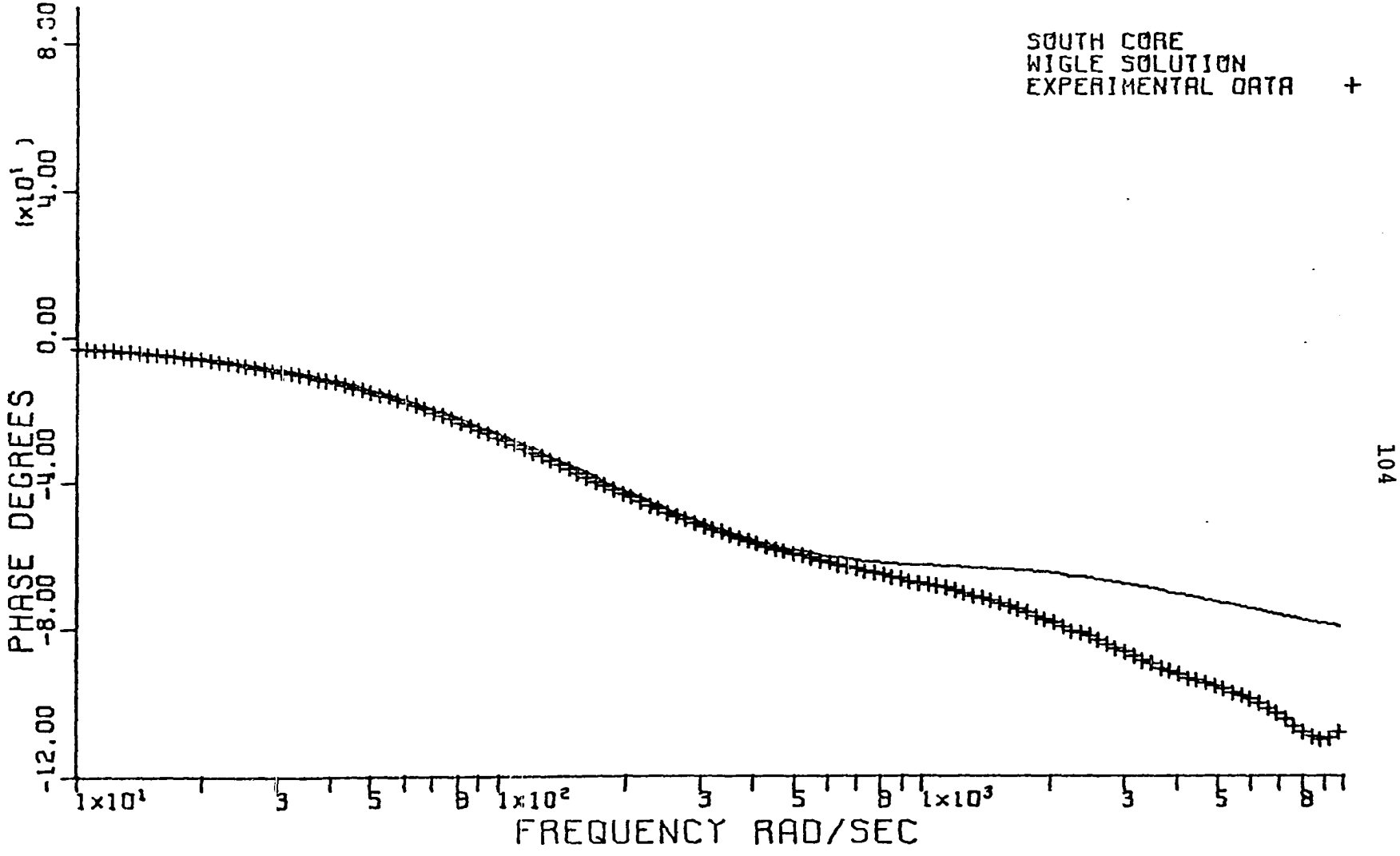

Figure 31. Phase of south core frequency response

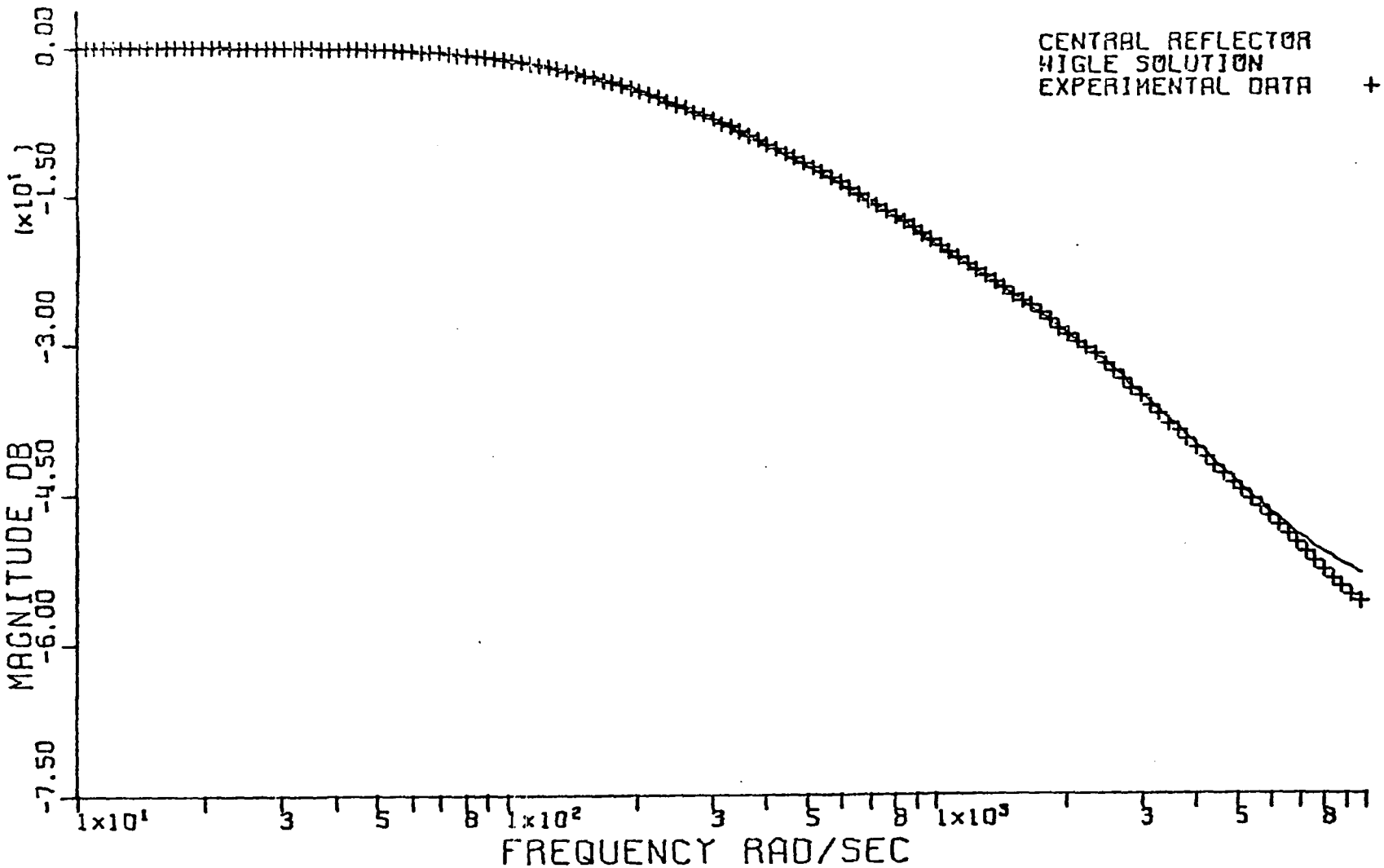

Figure 32. Magnitude of central reflector frequency response

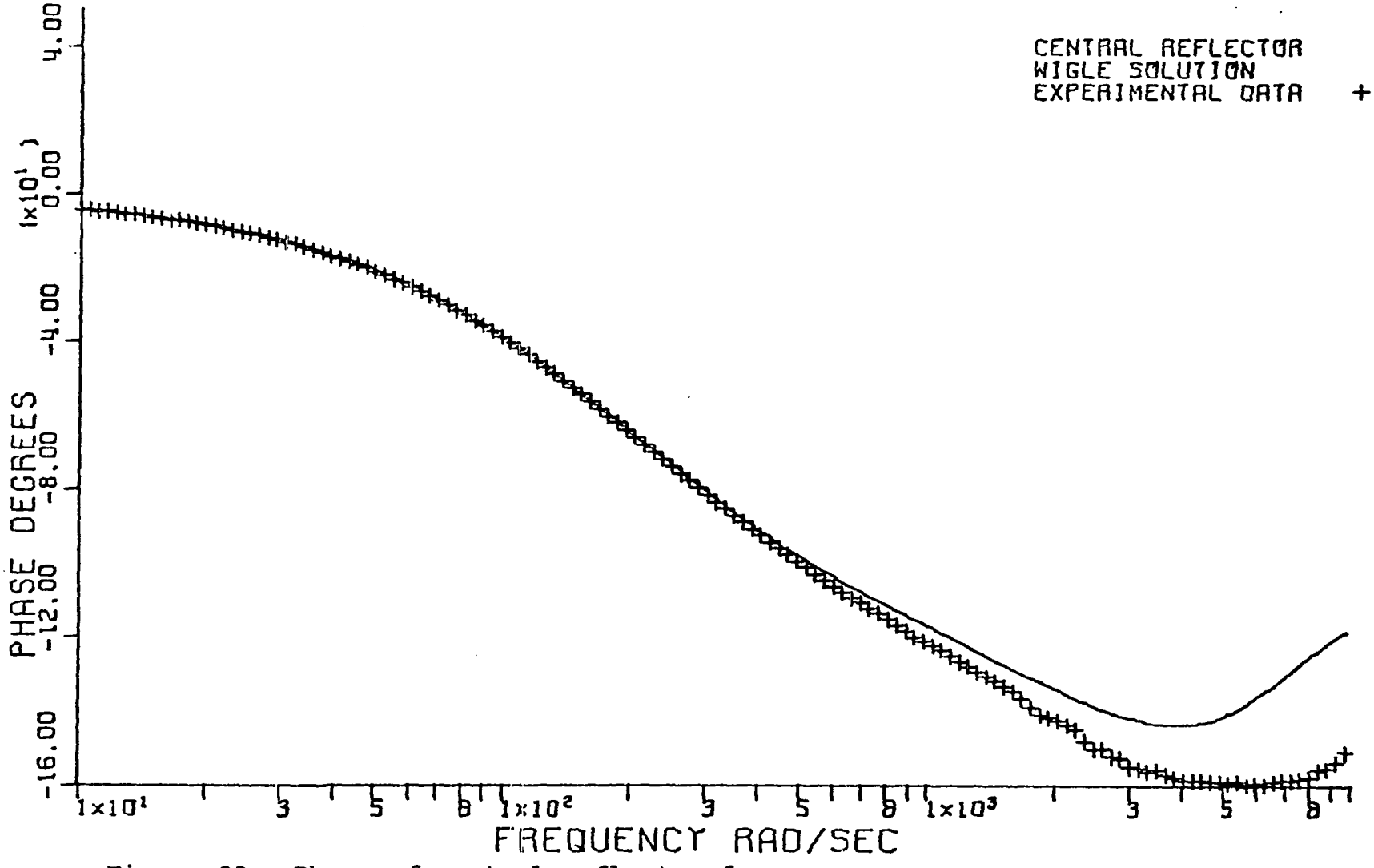

Figure 33. Phase of central reflector frequency response

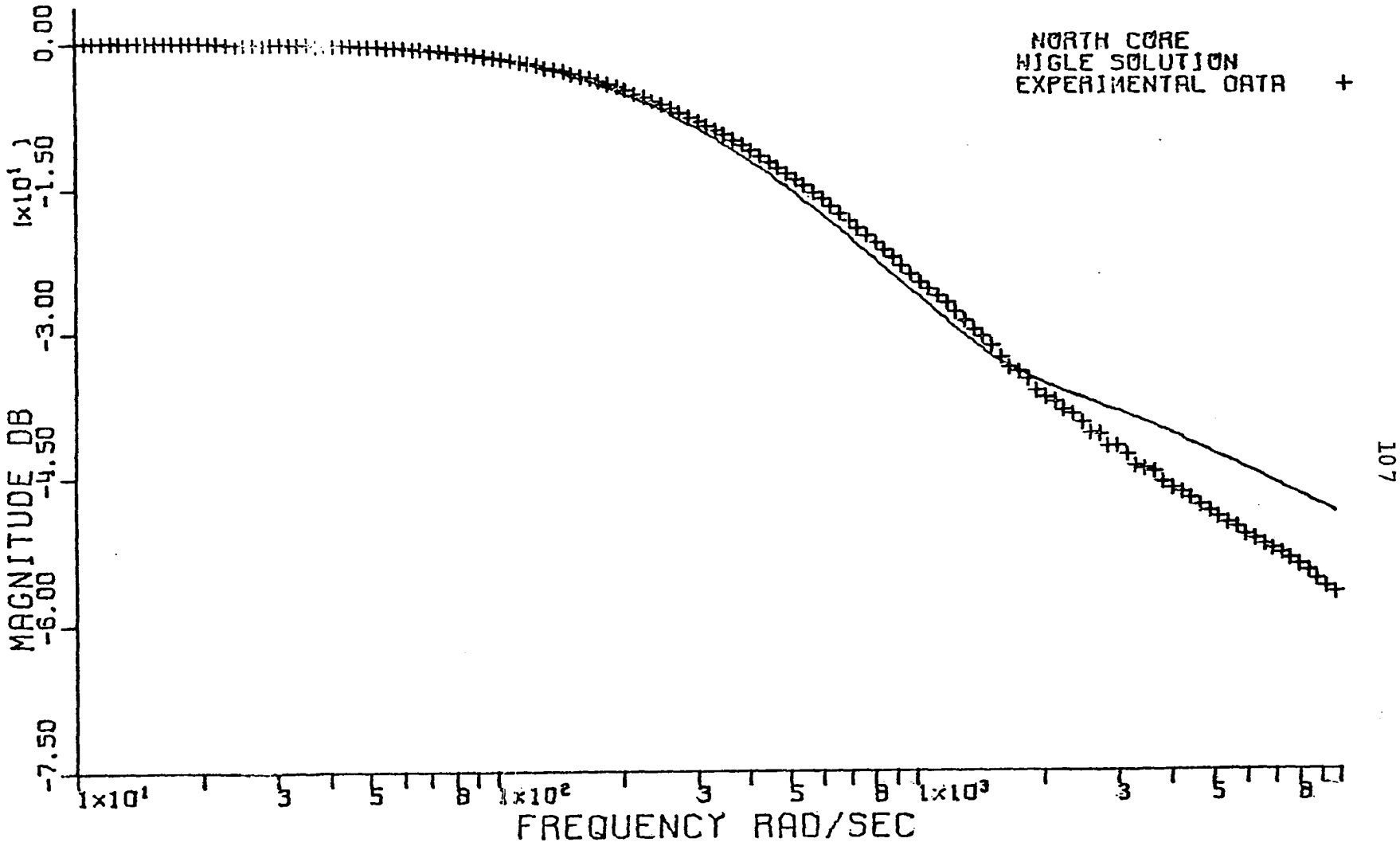

Figure 34. Magnitude of north core frequency response

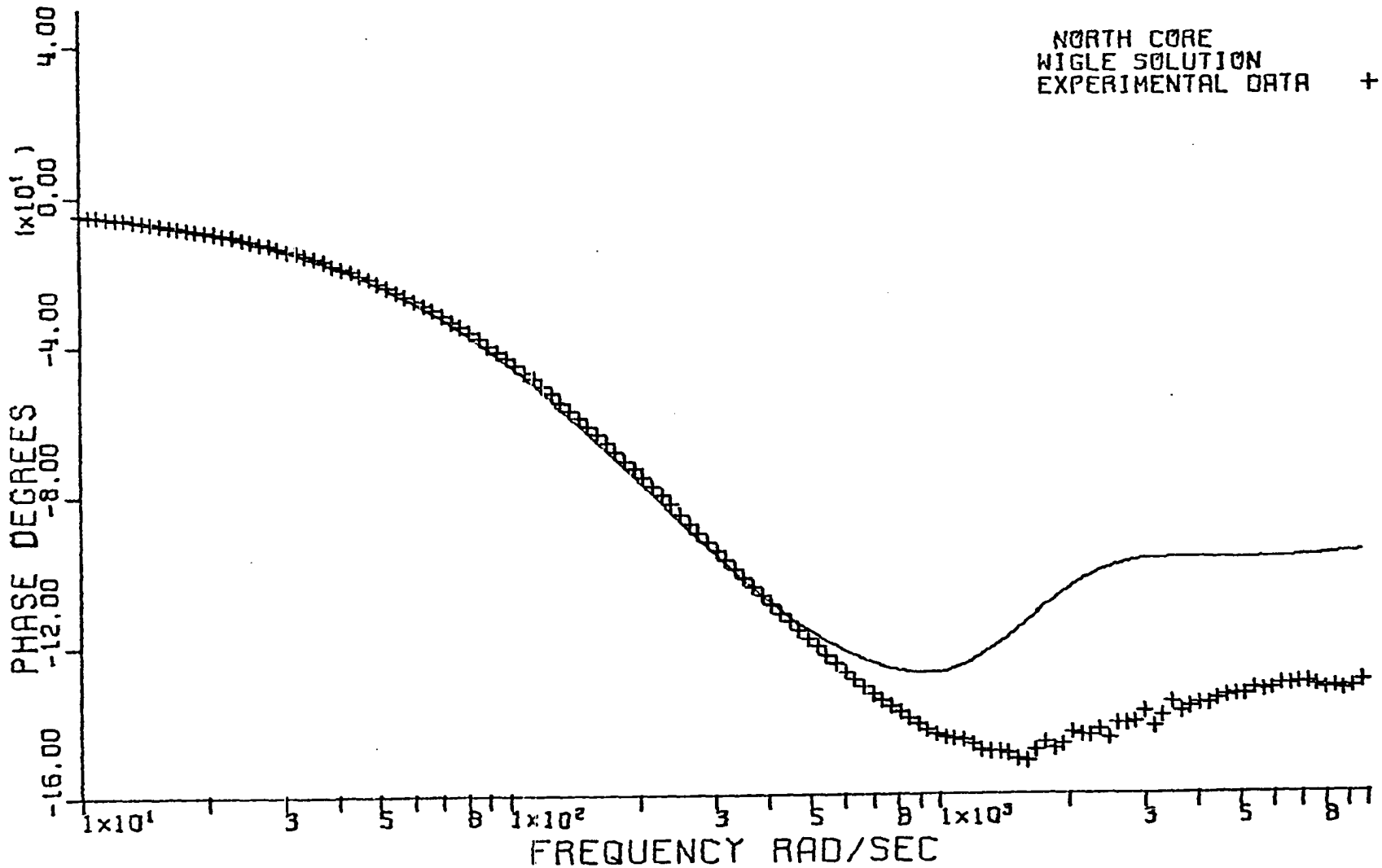

Figure 35. Phase of north core frequency response

IX. SUMMARY AND CONCLUSIONS

It was stated in the Introduction that the purpose of this thesis was to provide an experimental frequency response comparison with the mathematical models of Merritt [41], Betancourt [8], and Nodean [43], as well as with the WIGLE code [11]. As the experiment evolved, it became apparent that a quantitative comparison with Merritt's model would be of uncertain meaning but that a qualitative comparison relating to the existence or non-existence of the sink that Merritt reported at 2000 rad/sec could be made. With the experimental configuration used, the sink would be expected to appear in the north core. Neither the experiment nor the other models (as used here) show any evidence of the sink as such. However, there is definitely an inflection point in the north core magnitude curve at about 2000 rad/sec along with a corresponding upswing in the phase. As discussed in Section III, such behavior is completely compatible with the wave cancellation mechanism Merritt proposed to explain the sink. It is suggested here that Merritt's model was able to sense the phenomenon but for some unknown reason exaggerated it to the point of making it appear to be a sink.

Quantitative comparisons were achieved with the models of Betancourt (the NMA) and Nodean and also with the WIGLE code. These results have been described in Sections VI, VII, and

VIII respectively. Nodean's model most successfully predicted the shape of the frequency response curves at high frequencies. While all three models are based on the two group diffusion equations, Nodean's model is the only mathematically exact solution and this fact may be responsible for the above result. With regard to the numerical value of the functions, however, Nodean's method first departed from experimental results at lower frequencies than either the NMA or WIGLE. This result is thought to be due to the fact that both the NMA and WIGLE were made to model the spatial distribution of the source term whereas Nodean's method inherently assumes a localized perturbation.

Because of their ability to describe the source term, the NMA and WIGLE are thought to have the greatest potential for accurate frequency response calculations. In its present form, however, the NMA suffers from the early time convergence problem discussed in Section VI and is consequently inferior to either Nodean's method or WIGLE.

In terms of overall accuracy in frequency response calculations, WIGLE provided the best solution. The "exactness" of a WIGLE solution is limited only by the sizes of the space grid and the time steps. As these sizes are made very small, the WIGLE solution approaches an exact solution and in the limit, its accuracy is dependent only on 1) the degree of accuracy in modeling the source, and 2) the inherent limita-

tions of one-dimensional two-group diffusion theory. The work of Masters and Cady [40] suggests that the results should not be extremely sensitive to the space dependence of the source and the present success of Nodean's method supports this conclusion. In the limit, then, it is thought that WIGLE represents the best that one dimensional two group diffusion theory can provide. It should be pointed out, however, that WIGLE solutions with very small mesh sizes will also be very expensive to run.

Overall, the pulsed neutron technique for determining frequency response was certainly successful in providing the foregoing comparisons. The method is not without its difficulties - the present effort disclosed both equipment and data processing problems which had to be overcome. However, these problems were adequately solved for present purposes and the solutions could likely be improved upon in future work. The pulsed neutron technique is thought to have good potential for further frequency response measurements in a low power reactor such as the UTR-10 or in a newly assembled "cold" core. In a core that has been operating at high flux levels, the background radiation level might be too high to allow adequate resolution of response to the pulsed source.

X. SUGGESTIONS FOR FURTHER WORK

As a result of this investigation, several areas suitable for further study can be outlined. The list below includes ideas relating to the models and also ideas relating to the experiment itself.

1) The NMA model shows potential for describing the pulsed neutron experiment but suffers from the previously discussed convergence problem. This problem should be solved if the NMA is to achieve its highest degree of usefulness.

2) Nodean's model does a very commendable job of describing the frequency response trends but is limited by the inherent assumption of a localized perturbation. It might be productive to study the problem of extending Nodean's method to include a spatially dependent source.

3) It would be interesting to experiment with WIGLE using different source functions and perhaps different grid sizes. If such an experiment should show a sufficient degree of sensitivity to the source function, it would then be worthwhile to look at ways of possibly improving the source function of Appendix C.

4) To achieve a more exact calculated frequency response

at high frequencies, it may be necessary to depart from the two group diffusion equations and implement models based on more sophisticated theory. Ohanian, Booth, and Perez [45] modeled a neutron wave experiment in a moderating medium with an energy-dependent diffusion theory in which the energy dependence was expressed by an eigenvalue expansion. Duderstadt [18], however, warns of errors due to Bragg diffraction in polycrystaline media, continuous eigenvalue spectra, and other causes. Describing the UTR-10 by a related method (or with a transport theory formulation) would certainly be a challenging task but one which, if successful, could represent a major advance in descriptive ability.

5) The methods used to process experimental data for this thesis worked well. However, they are likely not the most efficient methods and not necessarily the best. Further studies could easily be made in this area. Specifically, it is suggested that convolution in the frequency domain be investigated as a possible method of data smoothing.

XI. LITERATURE CITED

1. AMERICAN STANDARD COMPANY, Advanced Technology Laboratories Division, Operating Manual for the UTR-10 Reactor, Mountain View, Calif., Author (1959).

2. ARGONNE NATIONAL LABORATORY, "Reactor Physics Constants," ANL-5800, 2nd ed., U.S. Govt. Print. Off., Washington D.C. (1963).

3. R. AVERY, Proc. Intern. Conf. Peaceful Uses At. Energy, Geneva, 12 182 (1958).

4. G. C. BALDWIN, Nucl. Sci. Eng., 6 320 (1959).

5. S. J. BALL, "A Digital Filtering Technique for Efficient Fourier Transform Calculations," ORNL-TM-1778, Oak Ridge National Laboratory (1967).

6. M. BECKER and K. S. QUISENBERRY, Univ. of Arizona Symp. Neutron Dynamics and Control, U. of Ariz. (1965).

7. R. E. BELLMAN, R. E. KALABA, and J. LOCKETT, Numerical Inversion of the Laplace Transform, American Elsevier Publishing Co., New York (1966).

8. J. M. BETANCOURT, "Analysis of Coupled Core Reactors Using the Natural Mode Approximation," PhD Dissertation, Iowa State University (1968).

9. S. R. BIERMAN, K. L. GARLID and J. R. CLARK, Nucl. Appl., 2 515 (1966).

10. R. B. BLACKMAN and J. W. TUKEY, The Measurement of Power Spectra, Dover Publications, Inc., New York (1959).

11. W. R. CALDWELL, A. F. HENRY, and A. J. VIGILOTTI, "WIGLE - A Program for the Solution of the Two-Group Space-Time Diffusion Equations in Slab Geometry," WAPD-TM-416, Westinghouse Electric Corp., Atomic Power Division, Pittsburgh, Pa. (1964).

12. N. CARTER, "Solution of Space-Time Kinetic Equations for Coupled-Core Nuclear Reactors," PhD Dissertation, Iowa State University (1967).

13. N. CARTER and R. DANOFSKY, Conf. Coupled Reactor Kinetics, C. G. Chezem and W. H. Kohler, Eds., pp. 249-269, The Texas A & M Press, College Station, Texas (1967).

14. R. A. DANOFSKY, Nucl. Sci. Eng., 36 28 (1967).

15. R. A. DANOFSKY, Personal Communication (June 1971).

16. H. T. DAVID, Personal Communication (Dec. 1970).

17. D. E. DOUGHERTY and C. N. SHEN, Nucl. Sci. Eng., 13 141 (1962).

18. JAMES J. DUDERSTADT, Nucl. Sci. Eng., 33 119 (1968).

19. L. R. FOULKE and E. P. GYFTOPOULOS, Nucl. Sci. Eng., 30 419 (1967).

20. EDWARD GARELIS, Nucl. Sci. Eng., 18 242 (1964).

21. EDWARD GARELIS and JOHN L. RUSSELL, JR., Nucl. Sci. Eng., 16 263 (1963).

22. M. W. GOLAY and K. B. CADY, Nucl. Sci. Eng., 43 303 (1971).

23. TSAHI GOZANI, "The Theory of the Modified Pulsed Source Technique," EIR-Bericht Nr. 79, Eidg. Institut für Reaktorforschung Würenlingen Schweiz (1965).

24. J. M. HARRER, R. E. BOYAR, and D. KRUCOFF, Nucleonics, 8, 10 32 (1952).

25. R. A. HENDRICKSON, "Cross-Spectral Density Measurements in a Coupled-Core Reactor," PhD Dissertation, Iowa State University (1966).

26. F. B. HILDEBRAND, Methods of Applied Mathematics, 2nd Ed., p. 229, Prentice-Hall Inc., Englewood Cliffs, N.J. (1965).

27. J. C. HOOTMAN, Personal Communication (April 1971).

28. IBM TECHNICAL PUBLICATIONS DEPT., System/360 Scientific Subroutine Package (360A-CM-03X) Version III Programmer's Manual, White Plains, New York, Author (1968).

29. KAMAN SCIENCES CORP., Kaman Nuclear Division, Instruction Manual for Model A-800/801 Neutron Generator, Colorado Springs, Col., Author (ca. 1969).

30. Y. KANEKO, F. AKINO, R. KUROKAWA, and K. SUMITA, J. Nucl. Sci. Technol., 3 301 (1966).

31. S. KAPLAN, Naval Reactor Physics Handbook, Vol. 1, A Radkowsky, Ed., pp. 955-977, U.S. Govt. Print. Off., Washington, D.C. (1964).

32. S. KAPLAN, A. F. HENRY, S. G. MARGOLIS, and J. J. TAYLOR, Proc. Intern. Conf. Peaceful Uses At. Energy, Geneva, 4 41 (1964).

33. N. C. KAUFMAN, "A Computer Program for the Analysis of Data from a Pulsed-Neutron Experiment," IN-1085, Idaho Nuclear Corp. (1967).

34. G. R. KEEPIN, Physics of Nuclear Kinetics, Addison-Wesley Publishing Co., Reading, Mass. (1965).

35. C. D. KYLSTRA and R. E. UHRIG, Nucl. Sci. Eng., 22 191 (1965).

36. JOHN R. LAMARSH, Introduction to Nuclear Reactor Theory, Addison-Wesley Publishing Co., Reading, Mass. (1966).

37. A. W. LANGILL, JR., Automatic Control Systems Engineering, Vol. 1, Prentice-Hall, Inc., Englewood Cliffs, N.J. (1965).

38. B. E. LEONARD, Univ. of Arizona Symp. Neutron Dynamics and Control, U. of Ariz. (1965).

39. J. LEWINS, J. of Nuc. Energy, Part A 12 108 (1960).

40. CHRISTOPHER F. MASTERS and K. B. CADY, Nucl. Sci. Eng., 29 272 (1967).

41. I. W. MERRITT, "Spatially Dependent Frequency Response of Coupled-Core Reactors," PhD Dissertation, Iowa State University (1968).

42. P. MICHAEL and M. N. MOORE, Proc. of the Symp. on Neutron Thermalization and Reactor Spectra, Ann Arbor, Michigan, International Atomic Energy Agency (1968).

43. W. C. NODEAN, "The Response of a Coupled Core Reactor to a Localized Oscillation of the Absorption Cross Section," PhD Dissertation, Iowa State University (1969).

44. M. J. OHANIAN and N. J. DIAZ, "Final Report on Research on Neutron Pulse Propagation in Multiplying Media for Idaho Nuclear Corp.," Contract Nos. 0-281 and 0-635, University of Florida (1969).

45. M. J. OHANIAN, R. S. BOOTH, and R. B. PEREZ, Nucl. Sci. Eng., 30 95 (1967).

46. R. T. OVERMAN and H. M. CLARK, Radioisotope Techniques, McGraw-Hill, New York (1960).

47. R. B. PEREZ, R. S. BOOTH, R. S. DENNING, and R. H. HARTELY, Trans. Am. Nucl. Soc., 7 49 (1964).

48. R. B. PEREZ and R. E. UHRIG, Univ. of Florida Symp. Neutron Noise, Waves and Pulse Propagation, U. of Fla. (1967).

49. C. A. PRESKITT, "Solutions to the Age Equation in Finite Systems with an Application to Pulsed Neutron Experiments," ORNL-TM-765, Oak Ridge National Laboratory (1963).

50. W. ROTTER, Symp. Pulsed Neutron Research, Karlsrube, Germany, Vol. II, International Atomic Energy Agency (1965).

51. J. L. RUSSELL, JR. and W. ROTTER, Nucl. Sci. Eng., 32 417 (1968).

52. DONALD G. SCHULTZ and JAMES L. MELSA, State Functions and Linear Control Systems, p. 118, McGraw-Hill, New York (1967).

53. ROBERT E. UHRIG, Univ. of Arizona Symp. Reactor Kinetics and Control, U. of Ariz. (1964).

54. L. E. WEAVER, System Analysis of Nuclear Reactor Dynamics, Rowman and Littlefield, New York (1963).

55. L. E. WEAVER, Reactor Dynamics and Control, American Elsevier Publishing Co., New York (1968).

56. A. N. WEINBERG and H. C. SCHEINLER, Physical Review, 74 851 (1948).

57. C. R. WYLIE, JR., Advanced Engineering Mathematics, 2nd ed., p. 283, McGraw-Hill, New York (1960).

XII. ACKNOWLEDGMENTS

In carrying out the work described in the foregoing pages, the author is indebted to the U.S. Atomic Energy Commission for providing an A.E.C. Special Fellowship, to the National Science Foundation for providing Dr. Danofsky with funds which were used in conjunction with the project, to the engineering staff of Ames Laboratory for loans of and assistance with equipment, and to the members of his graduate committee. Special thanks go to Dr. R. A. Danofsky for his enlightening guidance and many helpful discussions, and to Dr. H. T. David for consultation on statistical matters.

Finally, the author is indebted to a good friend, Miss Ann Kapaun, for her continuing encouragement and inspiration.

XIII. APPENDIX A: DESCRIPTION OF THE UTR-10 AND ITS PARAMETERS

The UTR-10 (University Training Reactor-10) is a light water moderated and cooled, graphite reflected, slab geometry reactor which is licensed to operate at power levels of up to 10 kilowatts. The reactor is fueled with about 3 kilograms of fully enriched uranium (greater than 93% U-235) which is approximately evenly divided between two physically separated core tanks positioned as shown in Figure A.1. Each core is itself subcritical and criticality is achieved only by exchange of neutrons through the graphite central reflector. Each core contains 6 fuel elements consisting of 12 aluminum clad fuel plates per element. Control of the reactor is accomplished by varying the vertical position of 4 boral rods (2 safety rods, 1 shim rod, and 1 regulating rod) which are located in the graphite reflector adjacent to the core tanks.

For a complete description of the UTR-10, the reader is referred to reference [1]. A simplified description depicting the reactor as modeled along with the detector and source locations is provided by Figure A.1. The outer boundaries ($x = 0$ and $x = 285$ cm) shown in Figure A.1 are not the exact physical boundaries of the reactor. Rather, previous experience has shown that setting the flux to zero

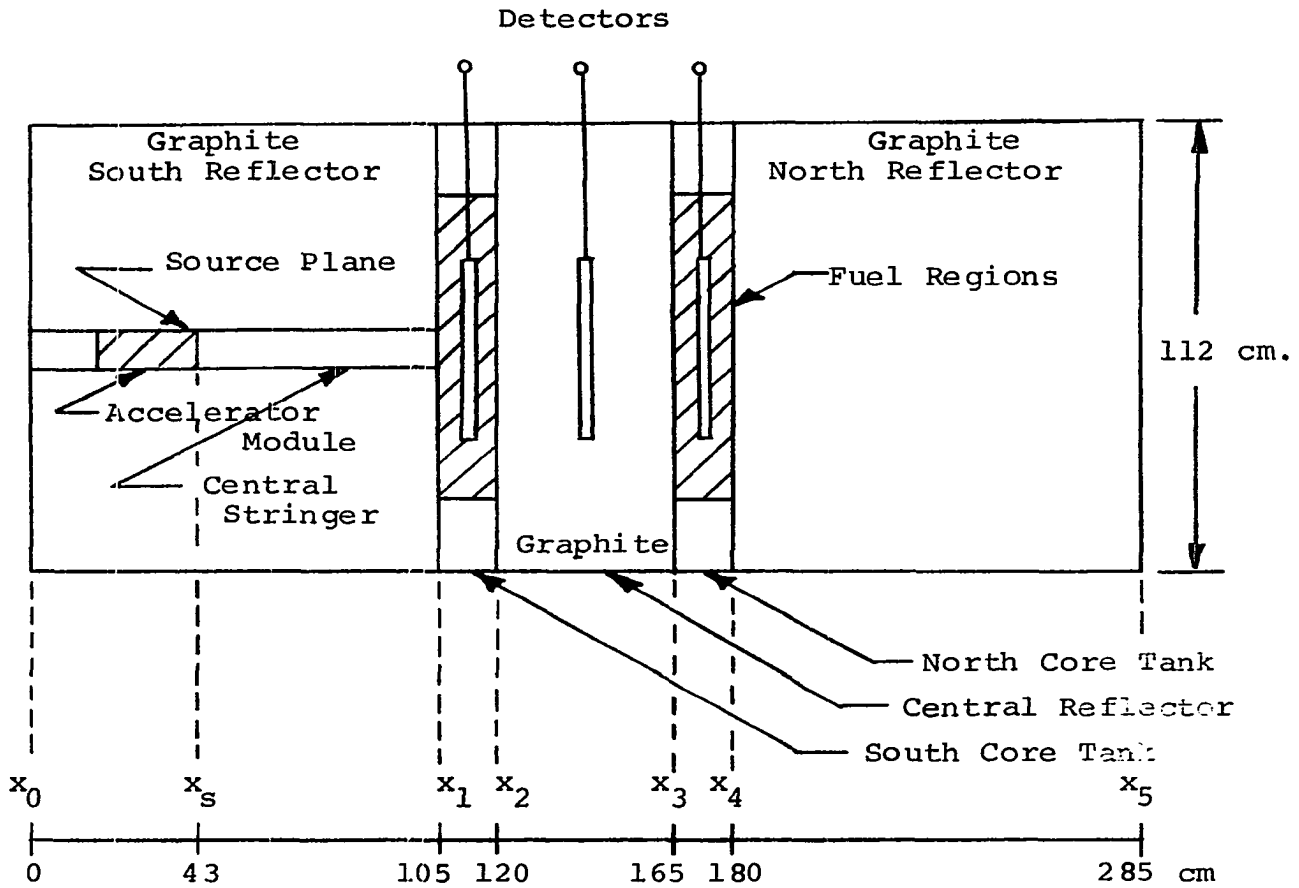

Figure A.1. Schematic diagram of the UTR-10

at these locations results in a realistic description of the reactor over the regions of significant flux magnitude [15].

For purposes of analysis, the UTR-10 was divided into the following 5 regions:

Region 1 - x = 0 to x = 105 cm

Region 2 - x = 105 to x = 120 cm

Region 3 - x = 120 to x = 165 cm

Region 4 - x = 165 to x = 180 cm

Region 5 - x = 180 to x = 285 cm

Note that regions 1, 3, and 5 are reflector whereas regions 2 and 4 are the core tanks. Within the ith region, the one dimensional two energy group, one delayed neutron group diffusion equations can be written as

$$D_{F_i} \nabla\phi_{r_i}(x,t) - \Sigma_{R_i}\phi_{F_i}(x,t) + \nu\Sigma_f(1-)\phi_{S_i}(x,t) + \lambda C_i(x,t) = \frac{1}{V_F}\frac{\partial\phi_F(x,t)}{\partial t} \quad \text{(A.1a)}$$

$$D_{S_i}\nabla\phi_{S_i}(x,t) - \Sigma_a\phi_{F_i}(x,t) + \Sigma_{R_i}\phi_{F_i}(x,t) = \frac{1}{V_S}\frac{\partial\phi_S(x,t)}{\partial t} \quad \text{(A.1b)}$$

$$\beta\nu\Sigma_{f_i}\phi_{S_i}(x,t) - \lambda\bar{C}_i(x,t) = \frac{\partial C_i(x,t)}{\partial t}$$

where

ϕ_F = fast neutron flux

ϕ_S = slow (thermal neutron flux

Σ_R = fast removal cross section

Σ_f = slow fission cross section

Σ_a = slow absorption corss section

C = precursor density

β = delayed neutron fraction = 0.0064

λ = decay constant for delayed neutrons = 0.08 sec^{-1}

ν = average number of neutrons produced per thermal fission

V_F = fast group speed = 4.36×10^8 cm/sec

V_S = slow group speed = 2.2×10^5 cm/sec.

In writing the above equations, it has been assumed that fast group absorption is negligible and that only slow neutrons produce fissions. Note that in the reflector regions, the equations will simplify because $\nu\Sigma_f$ becomes zero. In the multiplying regions, $\nu\Sigma_f$ may be adjusted as described in Section VI to model the desired degree of subcriticality. Table A.1 shows the accepted values for the other UTR-10 parameters [43].

Table A.1. UTR-10 parameters

Parameters	Region				
	north reflector	north core	central reflector	south core	south reflector
D_F (cm)	1.016	1.23	1.016	1.23	1.016
D_F (cm)	0.840	0.1894	0.840	0.1894	0.840
Σ_r (cm^{-1})	0.00276	0.0267	0.00276	0.0267	0.00276
Σ_a (cm^{-1})	0.00024	0.09079447	0.00024	0.09079447	0.00024

Equations (A.1) describe a one dimensional reactor only - as they stand, they do not account for leakage in the y and z directions. Transverse leakage can be accounted for by assuming that for a fixed x, the y and z direction fluxes can be described by fundamental solutions to the wave equations

$$\frac{d^2\phi(y)}{dy^2} + B_y^2\phi(y) = 0 \qquad \text{(A.2a)}$$

and

$$\frac{d^2\phi(z)}{dz^2} + B_z^2(y) = 0 \ . \qquad \text{(A.2b)}$$

In the y direction, leakage, L_y is recognized to be of the form

$$L_y = D\frac{d^2\phi}{dy^2}$$

and thus,

$$L_y = -DB_y^2\phi(y) \ .$$

But, in the experiment to be described, the y coordinate is fixed so that L_y may be expressed as a function of x and t by

$$L_y(x,t) = -DB_y^2\phi(x,t) \ . \qquad \text{(A.3a)}$$

Similarly, in the z direction,

$$L_z(x,t) = -DB_z^2\phi(x,t) \ . \qquad \text{(A.3b)}$$

Combining Equations (A.3a) and (A.3b), the transverse leakage L_T, can be expressed by $L_T = -DB_T^2\phi$ where $B_T^2 = B_x^2 + B_y^2$. The functional dependence has been dropped for simplicity of notation. For the UTR-10, the transverse buckling was determined experimentally by Merritt [41] and found to be equal to 0.00325 cm^{-2}. After simplifying the notation, Equations (A.1) may be re-written to account for transverse leakage as

$$D_F\nabla^2\phi_F - (\Sigma_R+D_FB_T^2)\phi_F + \nu\Sigma_f(1-\beta)\phi_S+\lambda\phi_F = \frac{1}{V_F}\frac{\partial\phi_F}{\partial t} \qquad (A.4a)$$

$$D_S\nabla^2\phi_S - (\Sigma_a+D_SB_T^2)\phi_S + \Sigma_R\phi_F = \frac{1}{V_S}\frac{\partial\phi_S}{\partial t} \qquad (A.4b)$$

$$\beta\nu\Sigma_f\phi_S - \lambda C = \frac{\partial C}{\partial t} \qquad (A.4c)$$

In the steady state, the right sides of Equations (A.4) become zero and the reference reactor operator, $[H_0(x)]$, for the natural mode approximation becomes

$$[H_0(x)] = \begin{bmatrix} [D_F\frac{d^2}{dx^2} - (\Sigma_R+D_FB_T^2)]V_F & \nu\Sigma_f(1-\beta)V_F & \lambda V_F \\ \Sigma_RV_S & [D_S\frac{d^2}{dx^2} - (\Sigma_a+D_SB_T^2)]F_S & 0 \\ 0 & \beta\nu\Sigma & -\lambda \end{bmatrix}.$$

The adjoint operator is thus given by

$$[H_0^*(x)] = \begin{bmatrix} [D_F \frac{d^2}{dx^2} - (\Sigma_R + D_F B_T^2)]V_F & \Sigma_R V_S & 0 \\ \nu\Sigma_f(1-\beta)V_F & [D_S \frac{d^2}{dx^2} - (\Sigma_a + D_X B_T^2)]V_S & \beta\nu\Sigma_f \\ \lambda V_F & 0 & -\lambda \end{bmatrix}.$$

Since the natural modes $\underline{\psi}_{mk}(x)$ are defined to be the eigenvectors of the equation $[H_0(x)]\underline{\psi}_{mk}(x) = \omega_{mk}\underline{\psi}_{mk}(x)$, it follows that the space modes will be the solutions to the equations

$$D_F \frac{d^2\psi^1_{mk}}{dx^2} - (D_F B_T^2 + \Sigma_R + \frac{\omega_{mk}}{V_F})\psi^1_{mk} + \nu\Sigma_f(1-\beta+\frac{\beta}{\lambda+\omega_{mk}})\psi^2_{mk} = 0 \quad \text{(A.5a)}$$

$$D_S \frac{d^2\psi^2_{mk}}{dx^2} - (D_S B_T^2 + \Sigma_a + \frac{\omega_{mk}}{V_S})\psi^2_{mk} + \Sigma_R\omega^1_{mk} = 0 \quad \text{(A.5b)}$$

$$\psi^3_{mk} = \frac{\beta\nu\Sigma_f}{\lambda+\omega_{mk}}\psi^2_{mk} = 0. \quad \text{(A.5c)}$$

Similarly, the adjoint space modes will be defined by the equations

$$D_F \frac{d^2}{dx^2}\psi^{*1}_{mk} - (\Sigma_R + D_F B_T^2 + \frac{\omega_{mk}}{V_F})\psi^{*1}_{mk} + \Sigma_R \frac{V_S}{V_F}\psi^{*2}_{mk} = 0 \quad \text{(A.6a)}$$

$$D_S \frac{d^2}{dx^2}\psi^{*2}_{mk} - (\Sigma_a + D_S B_T^2 + \frac{\omega_{mk}}{V_S})\psi^{*2}_{mk} + \nu\Sigma_f \frac{V_F}{V_S}\psi^{*1}_{mk} = 0 \quad \text{(A.6b)}$$

$$\psi^{*3}_{mk} = V_F\psi^{*1}_{mk}. \quad \text{(A.6c)}$$

Note that the $[H_0(x)]$ and $[H_0^*(x)]$ operators change parameter values when crossing a region interface. Thus, Equations (A.5) and (A.6) must be solved in the 5 separate regions of the reactor subject to appropriate boundary conditions. For a complete discussion of this operation, the reader is referred to reference [8].

XIV. APPENDIX B: DERIVATION OF THE ANALYTIC CONTINUATION FOR FOURCO

Consider the problem of Fourier transforming the function f(t). From the defining integral, the transform is given by

$$F(\omega) = \int_{-\infty}^{+\infty} f(t)e^{-j\omega t}\, dt \ . \qquad (B.1)$$

In the pulsed neutron experiment, f(t) is zero for negative time and hence the lower limit on the integral can be replaced by zero. Further, consider the integral to be split into the two parts

$$F(\omega) = \int_{0}^{T} f(t)e^{-j\omega t}\, dt + \int_{T}^{\infty} f(t)e^{-j\omega t}\, dt \qquad (B.2)$$

and assume T represents a time after which f(t) can be represented by a pure exponential of the form $f(t) = Ae^{-\alpha t}$. Letting $F_1(\omega)$ represent the first integral and $F_2(\omega)$ the second,

$$F(\omega) = F_1(\omega) + F_2(\omega)$$

where

$$F_2(\omega) = A\int_{T}^{\infty} e^{-(\alpha+j\omega)t}\, dt.$$

The function $F_1(\omega)$ can be computed numerically by the FOURCO algorithm [5] and the task at hand is to carry out the integration for $F_2(\omega)$. By the usual integration formula,

$$F_2(\omega) = \frac{A(\alpha-j\omega)}{\alpha^2+\omega^2} e^{-\alpha T} e^{-j\omega T}. \qquad (B.3)$$

Substituting the identity

$$e^{-j\omega T} = \cos\omega T - j\sin\omega T$$

into Equation (B.3) and simplifying yields

$$F_2(\omega) = \frac{Ae^{-\alpha t}}{\alpha^2+\omega^2}[\alpha\cos\omega T - \omega\sin\omega T - j(\alpha\sin\omega T + \omega\cos\omega T)] \qquad (B.4)$$

The real and imaginary parts of $F_2(\omega)$ are thus respectively

$$\text{Real } F_2(\omega) = \frac{Ae^{-\alpha T}}{\alpha^2+\omega^2}[\alpha\cos\omega T - \omega\sin\omega T] \qquad (B.5a)$$

$$\text{Imag } F_2(\omega) = -\frac{Ae^{-\alpha T}}{\alpha^2+\omega^2}[\alpha\sin\omega T + \omega\cos\omega T]. \qquad (B.5b)$$

In the program, the channel at which the transition to analytic continuation is to be made is known as NTRUNC and the numerical value of f(t) evaluated at the transition point is FO(NTRUNC). NTRUNC is input as data and the corresponding time, T, is computed. FO(NTRUNC) and T are then related by

$$FO(NTRUNC) = Ae^{-\alpha T} \qquad (B.6)$$

Since both FO(NTRUNC) and T are known, Equation (B.6) may be solved for A and substituted into Equations (B.5) to yield

$$\text{Real } F_2(\omega) = \frac{FO(NTRUNC)}{\alpha^2+\omega^2}[\alpha\cos\omega T-\omega\sin\omega T] \qquad \text{(B.7a)}$$

$$\text{Imag } F_2(\omega) = -\frac{FO(NTRUNC)}{\alpha^2+\omega^2}[\alpha\sin\omega T+\omega\cos\omega T]. \qquad \text{(B.7b)}$$

The structure of FOURCO is such that it was easy to compute the real and imaginary parts of $F_2(\omega)$ from Equations (B.7) and add them respectively to the real and imaginary parts of $F_1(\omega)$ to form the complete $F(\omega)$.

XV. APPENDIX C: DERIVATION OF THE SPACE DEPENDENT SOURCE FUNCTION

Assume that within a given region of the UTR-10, neutron slowing down is described by the continuous slowing down equation without capture. From Lamarsh [36], this equation may be written as

$$\frac{D(u)}{\xi\Sigma_s(u)} \frac{d^2}{dx^2} q(x,u) = \frac{\partial q(x,u)}{\partial u} \tag{C.1}$$

where all symbols have their standard meanings. Further, assume that the lethargy dependent coefficient $\frac{D(u)}{\xi\Sigma_s(u)}$ can be replaced by an average value of the form

$$\overline{\frac{D(u)}{\xi\Sigma_s(u)}} = \frac{\int_0^{u_f} \frac{D(u)}{\xi\Sigma_s(u)}\, du}{\int_0^{u_f} du} . \tag{C.2}$$

The numerator, $\int_0^{u_f} \frac{D(u)}{\xi\Sigma_s(u)}\, du$, is recognized to be the Fermi age, τ_f, of neutrons having the lethargy of interest, u_f. Since the present problem is to find a fast group source function for the two group diffusion equations, u_f was taken as 2.18 which corresponds to the lethargy of neutrons that were born at 14.3 Mev but have slowed to 1.6 Mev. Equation (C.2) can be written

$$\overline{\frac{D(u)}{\xi\Sigma_s(u)}} = \frac{\tau_f}{u_f} \tag{C.3}$$

and Equation (C.1) thus becomes

$$\frac{\tau_f}{u_f}\frac{d^2}{dx^2}q(x,u) = \frac{\partial q(x,u)}{\partial u} . \qquad (C.4)$$

Equation (C.4) may be Laplace transformed with respect to u to obtain

$$\frac{\tau_f}{u_f}\frac{d^2}{dx^2}Q(x,s) = SQ(x,s) - q(x,0) . \qquad (C.5)$$

Consider the simplified picture of the UTR-10 shown in Figure C.1. In the non-source regions (2, 3, 4, and 5) $q(x,0) = 0$ so that Equation (C.5) becomes

$$\frac{d^2}{dx^2}Q(x,s) - \frac{u_f}{\tau_f}SQ(x,s) = 0 . \qquad (C.6)$$

In the ith region, the solution to Equation (C.6) is recognized to be

$$Q_i(x,s) = A_i(s)e^{-K_i x} + B_i(s)e^{+K_i x} \qquad (C.7)$$

where

$$K_i^2 = \frac{S u_f}{\tau_{fi}}$$

Since there are 4 non-source regions, Equations (C.7) contain 8 coefficients (A_i and B_i) which must be determined from boundary conditions, if a solution is to be obtained. At an internal interface, the flux and current density must be continuous at the interface [36]. In terms of slowing down

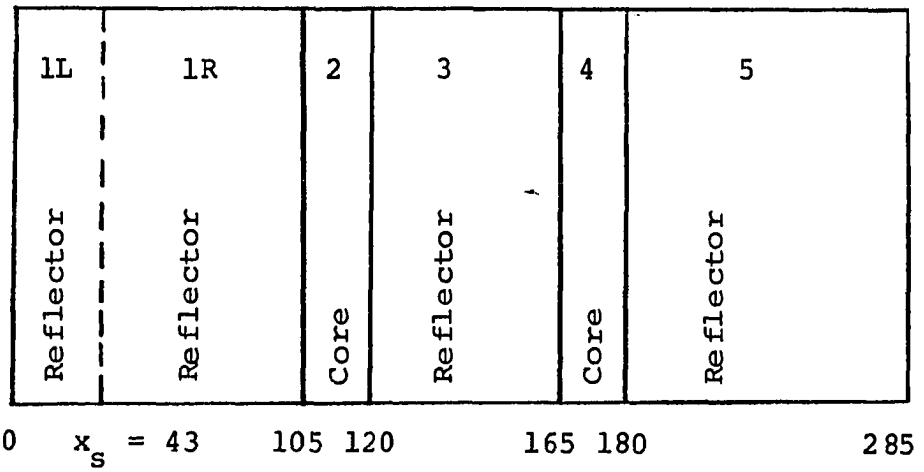

Figure C.1. Simplified diagram of UTR-10

density, the flux and current conditions become respectively

$$\left(\frac{1}{\xi\Sigma_s}\right)_i Q_i(x_I^-,s) = \left(\frac{1}{\xi\Sigma_s}\right)_{i+1} Q_{i+1}(x_I^+,s) \qquad (C.8a)$$

$$\left(\frac{D}{\xi\Sigma_s}\right)_i \frac{d}{dx} Q_i(x_I^-,s) = \left(\frac{D}{\xi\Sigma_s}\right)_{i+1} \frac{d}{dx} A_{i+1}(x_I^+,s) \qquad (C.8b)$$

where x_I represents the coordinate of the interface between region i and region i+1. Since Σ_s is only weakly dependent on lethargy, the coefficient $\left(\frac{1}{\xi\Sigma_s}\right)_i$ may be assumed constant and further, the coefficient $\left(\frac{D}{\xi\Sigma_s}\right)_i$ may again be replaced by its average value, $\frac{\tau_{fi}}{u_f}$. The non-source regions contain 3 internal interfaces and thus Equations (C.8) provide a total of 6 boundary conditions. A 7th condition is provided by setting the slowing down density equal to zero at the outer boundary (x = 285) but to complete the solution for Q(x,s) in the non-source regions, Equation (C.5) must simultaneously be solved in region 1.

In region 1, the source may be represented by $q(x,0) = C\delta(x-x_s)$ where C is an arbitrary amplitude constant that may be set equal to 1 for convenience. Equation (C.5) thus becomes

$$\frac{d^2}{dx^2} Q(x,s) - \frac{su_f}{\tau_f} Q(x,s) + \frac{u_f}{\tau_f} \delta(x-x_s) . \qquad (C.9)$$

In terms of the x variable, Equation (C.9) is of the same form as Equation (38) and can thus be solved by the Green's function approach outlined in Section VII. Following Section VII,

$$Q(x,s) = \frac{u_f}{\tau_f} G(x,s) \qquad (C.10)$$

where G(x,s) is the Green's function. By the first condition on the Green's function, $G_L(x,s)$ must satisfy the homogeneous equation

$$\frac{d^2}{dx^2} Q(x,s) - \frac{su_f}{\tau_f} Q(x,s) = 0 \qquad (C.11)$$

for $0 \leq x < x_s$ and $G_R(x,s)$ must satisfy the same equation for $x_s \leq x < 105$ cm. In regions 1L and 1R, G(x,s) is therefore given respectively by

$$G_L(x,s) = A_{1L}(s)e^{-K_1 x} + B_{1L}(s)e^{+K_1 x} \qquad (C.12a)$$

and

$$G_R(x,s) = A_{1R}(s)e^{-K_1 x} + B_{1R}(s)e^{+K_1 x} . \qquad (C.12b)$$

Combining Equations (C.12) with Equation (C.10) yields

$$Q_{1L}(x,s) = \frac{u_f}{\tau_{f1}} [A_{1L}(s)e^{-K_1 x} + B_{1L}(s)e^{+K_1 x}] \qquad (C.13a)$$

$$Q_{1R}(x,s) = \frac{u_f}{\tau_{f1}} \left[A_{1R}(s)e^{-K_1 x} + B_{1R}(s)e^{+K_1 x}\right] . \qquad (C.13b)$$

Equations (C.13) in conjunction with Equations (C.7) form a set of 6 equations which, for a given s, may be solved simultaneously for Q(x,s) if a total of 12 boundary conditions can be found. Seven boundary conditions have already been discussed, two more result from applying the interface conditions between regions 1 and 2, and a 10th condition is provided by the requirement that $Q(0,s) = 0$. The remaining two boundary conditions are supplied by applying conditions 3 and 4 of the Green's function requirements. From Green's function requirement 3, $G_L(x_s,s) = G_R(x_s,s)$ and hence

$$Q_{1L}(x_s,s) = Q_{1R}(x_s,s) . \qquad (C.14a)$$

From Green's function requirement 4, $\frac{d}{dx} G_R(x_s,s) - \frac{d}{dx} G_L(x_s,s) = -1$ so that

$$\frac{d}{dx} Q_{1L}(x_s,s) - \frac{d}{dx} Q_{1R}(x_s,s) = - \frac{u_f}{\tau_{f1}} . \qquad (C.14b)$$

A total of 12 boundary conditions are indeed available and for any value of s desired, Equations (C.7) and (C.13) can be solved for Q(x,s). The remaining problem is to inverse transform Q(x,s) to obtain q(x,u). The inversion was accomplished numerically using the method of Bellman,

Kalaba, and Lockett [7] - hereafter to be referred to as Bellman's method. Bellman introduces a change of variable into the Laplace transform to redefine the limits of integration and then replaces the integral by a numerical quadrature formula in terms of the shifted Legendre polynomials. In terms of the present problem variables, this procedure is equivalent to approximating the lethargy dependence of $q(x,u)$ with a polynomial. Assume that the approximating polynomial is chosen to be of degree N. Bellman shows how to derive an NxN matrix B (referred to as Bellman's matrix) such that

$$\text{Col}[q(x,u_1),\ q(x,u_2),\ \ldots\ q(x,u_N)]$$

$$= B\,[\text{Col}\ Q(x,1),\ Q(x,2),\ \ldots\ Q(x,N)]$$

where the u_i are lethargy values equal to the negative logarithms of the zeros of the shifted Legendre polynomials. Further, Bellman tabulates B matrices for N = 3, 4, ... 15 so that at any fixed x, a series of points of the $q(x,u)$ function may be obtained simply by computing the corresponding $Q(x,s)$ series and multiplying by the correct B matrix. Bellman also shows how to perform scaling operations such that one of the u_i can always be made to equal 2.18. Since $Q(x,s)$ is readily available from previous derivation, the method provides a simple means of approximating $q(x, 2.18)$.

Theoretically, the accuracy of approximation would be expected to increase as N gets larger. Bellman, however, points out that the B matrix is derived by inverting a matrix which grows more ill-conditioned as N becomes larger and thus, large N may lead to numerical inaccuracy. In the present problem, calculations were run with different N values and the solutions compared. While the solutions were in reasonable agreement throughout regions where slowing down density was of significant magnitude, N values greater than 3 predicted negative q(x, 2.18) in regions far removed from the source plane. Consequently, the N = 3 approximation was chosen as the source for the NMA and WIGLE calculations. This function is shown in the region between the source plane and the far edge of the north core by Figure C.2. Beyond the north core, the function is down over 3 orders of magnitude and rapidly becomes negligible. The magnitudes shown in Figure C.2 are those directly from the computer program that implemented the calculations described in this appendix. As previously pointed out, however, the magnitude is arbitrary. When actually using the function described here as a source, a scale factor of 10^{11} was introduced for convenience in subsequent calculations.

In carrying out the foregoing computation, the Fermi age of 1.6 Mev neutrons (starting from 14.3 Mev) was assumed

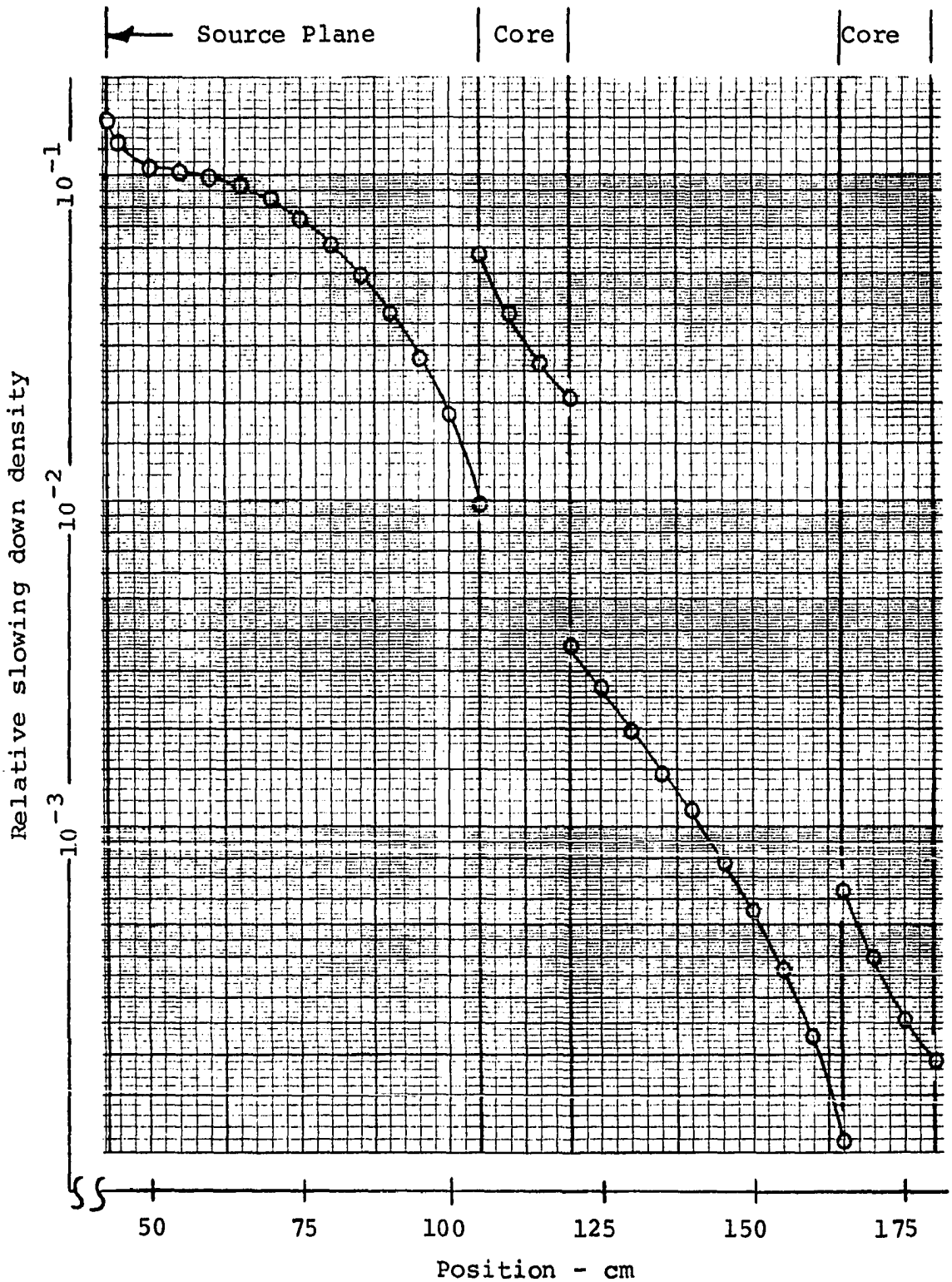

Figure C.2. Space dependent 1.6 Mev source

to be 532 cm^2 in graphite and 130 cm^2 in the core regions. The first age was based on reference [49] and the second was estimated from data found in reference [2].

XVI. APPENDIX D: DESCRIPTION OF SMODAT-IX

The source listing of SMODAT-IX is as follows:

```
      SUBROUTINE SMODAT(BKGND,FO,IBSMO,ICSMO,NSMO,DT01,DT02)
      IMPLICIT REAL*8(A-H,O-Z)
      DIMENSION FO(1),BKGND(1)
      NSTART=6
      NSTOP=NSMO
      NPNT=11
      IF(ICSMO.GT.1) NSTOP=10
      CALL PLSQ(BKGND,FO,IBSMO,DT01,DT02,NSTART,NSTOP,SPNT)
      IF(ICSMO.LE.1) GO TO 2
      NSTART=11
      NSTOP=NSMO
      NPNT=21
      IF(ICSMO.GT.2) NSTOP=15
      CALL PLSQ(BKGND,FO,IBSMO,DT01,DT02,NSTART,NSTOP,NPNT)
      IF(ICSMO.LE.2) GO TO 2
      NSTART=16
      NPNT=31
      CALL PLSQ(BKGND,FO,IBSMO,DT01,DT02,NSTART,NSTOP,NPNTS)
    2 RETURN
      END
```

The meanings of the input parameters are:

BKGND - At the point within FOURCO where SMODAT is called, the array BKGND contains the set of points to be smoothed.

FO - FO is the array which will contain the smoothed function.

IBSMO - IBSMO is a parameter which determines how the first five points of the array FO are to be determined. If IBSMO is read into FOURCO as zero, no smoothing will be applied to the first five points. If IBSMO is other than zero, smoothed values for the first five

points will be computed from a least squares parabola fit to the first 11 points.

ICSMO - ICSMO is a parameter which controls the number of points in each parabolic fit once the routine has advanced far enough into the function for a sufficient number of points to be available on either side of the point being estimated. ICSMO should be read into FOURCO as 1, 2, or 3 to obtain respectively 11, 21, or 31 points per parabola.

NSMO - NSMO is the number of points to be smoothed. If N is the number of points per fit being used, NSMO must be no greater than the total number of points in the function minus (N-1)/2.

DT01 - DT01 is the time step for the first point.

DT02 - DT02 is the time step for all points after the first.

In the experiment reported in this thesis, the first time step in the observed function differed from all remaining time steps by $\frac{1}{2}$ of the time analyzer channel width. This distinction was incorporated into the modified FOURCO and hence was carried into SMODAT. As SMODAT has evolved, however, the distinction is really superfluous. Subroutine PLSQ (parabolic least squares) which is called by SMODAT simply does a series of 2nd degree least squares fits to sets of points which are equally spaced in time. Since time zero

is never used as a data point, it is immaterial if the point sets are translated along the time axis. All that gets returned to FOURCO is a set of points which FOURCO will orient properly with respect to time.

As an illustration of SMODAT operation, consider the case of IBSMO = 0 and ICSMO = 2. These parameter values were the ones actually used when processing experimental data. On the first call to PLSQ, the "smoothed" value for point 6 will be computed from a parabola fitted to points 1 through 11, the smoothed value for point 7 from points 2 through 12, and so on until smoothed point number 10 has been computed. Since IBSMO = 0, the first 5 points are left unaltered. Beginning with point number 11, PLSQ will put 21 points in each fit so that point 11 will be computed from a parabola fit to points 1 through 21 etc. Since ICSMO has been assumed to be 2, NSTOP will now remain equal to NSMO and the sequential fitting will continue in this fashion until the desired fraction of the time function has been smoothed. Note that if the analytic continuation option in FOURCO is in use, there is no advantage to smoothing beyond the point where the transition to analytic continuation is to be made.

XVII. APPENDIX E: DETERMINATION OF COUNTING SYSTEM RESOLVING TIME CORRECTION

The usual formula for relating observed count rate, N_o, to true count rate, N_T, is

$$N_T = \frac{N_o}{1-N_o t_r} \tag{E.1}$$

where t_r is the system resolving time. Equation (E.1) is the formula used by GRIPE-II [32] and hence the formula applied in the present work. However, Bierman, Garlid and Clark [9] point out that Equation (E.1) is correct only if the counting system is of the non-paralyzable type. For a paralyzable system, the corresponding formula is [9]

$$N_o = N_T e^{-N_T t_r} . \tag{E.2}$$

Bierman, Garlid and Clark also point out that physical counting systems are seldom truly of either type but rather, behave as some combination thereof. In the present experiment, for example, the RIDL analyzer is definitely paralyzable but the preceding electronics are thought to be an excellent approximation of a non-paralyzable system. Fortunately, the distinction between the two types is important only at very high count rates. In the experiment, the maximum observed count rate was approximately 10^5 cps. Setting $N_o = 10^5$ and using the estimated resolving time of 1 microsecond in Equations (E.1)

and (E.2) yields true count rates which differ by less than 2 percent. Therefore, the use of Equation (E.1) to characterize the complete system is justified provided that the estimated resolving time is approximately correct. An experiment to measure the resolving time will next be described.

The approach used was to locate the system detector near a variable intensity neutron source and to locate a monitor detector in the same neutron field but at a position of relatively low count rate. At low source intensities, neither the system being studied nor the monitor has significant resolving time errors and if system count rate is plotted versus monitor count rate, the result will be a straight line. At high source intensities, however, resolving time errors will cause a departure from linearity. If the monitor detector is so located that its resolving time errors may still be assumed negligible, the departure from linearity may be used to compute resolving time for the system under study. Two attempts were made at implementing this method. The first attempt used the UTR-10 reactor as a neutron source, the second used a Texas Nuclear Corp. neutron generator. It was difficult, however, to achieve sufficient experimental accuracy and the resolving time estimates ranged from 0.1 to 1.3 microseconds. The 0.1 microsecond value is clearly impossible because the system incorporates 0.5 microsecond wide logic pulses. Although these experiments failed to

produce an accurate resolving time estimate, they were valuable in that they indicate 1 microsecond to be at least of the right order of magnitude. Further, they showed conclusively that at a count rate of 10^5 cps, the system was still working well and showed no tendency to saturate.

Since the foregoing experiments did not yield an accurate resolving time estimate, the 1 microsecond value selected was deduced by considering individual elements in the system. The slowest element in the system was known to be the RIDL analyzer which is a paralyzable type device. If a paralyzable system is excited with a periodic pulse train, the maximum pulse rate at which the device can function is given by [9]

$$\max N_T = t_r^{-1} \quad . \tag{E.3}$$

By driving the analyzer with a periodic pulse generator and observing the pulse rate at which the analyzer began to falter, analyzer resolving time could be computed via Equation (E.3). Using this method, the analyzer resolving time was found to be 0.85 microseconds. Although the analyzer is responsible for the largest fraction of lost counts, some losses will be due to other elements in the system as well. The extent of these other losses is not known exactly but oscilloscope observations, the experiments described previously in this appendix, and a series of experiments performed with a random noise pulser

all indicate they are small. As pointed out in Section IV, the resolving time corrections themselves were small and hence it was allowable to relax the accuracy requirements on the resolving time. In view of the foregoing data, the best estimate of system resolving time was judged to be 1 microsecond.